ELECTRON-BEAM PUMPED SEMICONDUCTOR LASERS

ELECTRON-BEAM PUMPED SEMICONDUCTOR LASERS

by

B. S. KAWASAKI, B.Sc.

A Thesis

Submitted to the Faculty of Graduate Studies

in Partial Fulfilment of the Requirements

for the Degree

Doctor of Philosophy

McMaster University

August 1972

DOCTOR OF PHILOSOPHY
(Physics)

McMASTER UNIVERSITY
Hamilton, Ontario

TITLE: Electron-Beam Pumped Semiconductor Lasers

AUTHOR: Brian Susumu Kawasaki, B.Sc. (Maths. and Phys., University of Toronto)

SUPERVISOR: Professor J. Shewchun, Professor B. K. Garside

NUMBER OF PAGES: ix, 159

SCOPE AND CONTENTS:

The major purpose of the work described in this thesis has been the development of an analytical model for the electron-beam pumped semiconductor laser system consistent with the main dynamic effects observed experimentally in the stimulated emission. The lasing materials used in this study were single crystals of CdS, CdSe and GaAs. The choice was made on the basis of the availability of high purity single crystals and for representation of both II-VI and III-V materials in the study.

Generally, the light output from a pulse-excited semiconductor laser changes in both wavelength and far-field pattern as a function of time during the excitation pulse. The effects investigated divide naturally into two parts. The first part deals with the tuning of the peak output of the stimulated emission toward lower energies during the excitation pulse. The second part deals with a deviation of

the far-field radiation pattern of the spatial laser mode with respect to the cavity axis and the changes of this angle with time during the pump pulse.

In parallel with these investigations, a theoretical model of the semiconductor laser was developed. This model takes into account spatial variations in the gain and refractive index in the semiconductor material and changes in these profiles with time. The analysis, in terms of the experimental parameters, leads to a prediction of angular tuning of the far-field mode and can account for certain features of faster-than-bandgap wavelength tuning in a number of disparate laser materials. A particularly significant consequence of the model is the prediction of dramatic variations in cavity loss as a function of time. The major consequences of this effect for laser dynamics are discussed.

ACKNOWLEDGMENTS

I wish to express my appreciation to my supervisors, Dr. J. Shewchun and Dr. B. K. Garside, for their guidance and support in this work.

TABLE OF CONTENTS

FIGURE CAPTIONS

CHAPTER I

1. Introduction

The study of semiconductor lasers, first initiated in 1962, has left unanswered a number of questions concerning their dynamic properties. For example, there have been observations of rapid shifts of the lasing wavelength [1,2,3,4] which could not be accounted for in terms of bandgap shifts. Moreover, features such as time delays between the start of pumping and onset of lasing [5,6,7,8], and the variation of lasing threshold with temperature [9,10,11] have not been clearly defined or explained. These questions reflect the lack of adequate models to characterize semiconductor lasers.

A major purpose of the work described in this thesis has been to develop an analytical model of a simple semiconductor laser system which can account for the main dynamic effects observed in the stimulated emission. The choice of the electron-beam pumped semiconductor laser as the system to be analyzed was dictated by this purpose. As discussed in the next section, this system is the simplest to parametrize, and it can be used with a broad range of materials. The lasing materials used in this study were single crystals of CdS, CdSe and GaAs. The choice was made on the basis of the availability of high purity single crystals and for

representation of both II-VI and III-V materials in the study.

Generally, the light output from an electron-beam pulse-excited semiconductor laser changes in both wavelength and spatial far-field pattern as a function of time during the excitation pulse. The effects investigated in this work divide naturally into two parts. The first part deals with the tuning of the peak output of the stimulated emission toward lower energies during the excitation pulse. The second part deals with a deviation of the far-field radiation pattern of the spatial laser mode with respect to the cavity axis and the changes of this angle during the excitation pulse. Effects of the first type will hereafter be termed "wavelength tuning", and those of the second type, "angular tuning".

In parallel with these experimental investigations, a theoretical model of the semiconductor laser was developed. This model takes into account spatial variations in the gain and refractive index in the semiconductor material and changes in their profiles with time. The analysis, in terms of the experimental parameters, leads to a prediction of angular tuning and can account for certain features of faster-than-bandgap wavelength tuning in a number of disparate laser materials. A particularly significant consequence of the model is the prediction of dramatic variations in cavity loss as a function of time. The major consequences of this effect for laser dynamics are discussed in later sections.

In order to place the research work into perspective, a brief description of the general principles of semiconductor laser operation will be provided. This description is given in the next section, and is followed by the practical reasons which dictated the experimental set-up and procedures.

2. General Principles of Operation of Semiconductor Lasers

There are several good basic reviews on the semiconductor laser in the literature [12,13,14,15] and consequently the following description is brief and stresses those aspects of such lasers which relate most directly to this work.

All lasing action is dependent upon the existence of gain between two energy levels or bands but there are certain aspects, unique to semiconductor lasers, which make them very versatile. Among these are: (1) semiconductor lasers are based upon inversion between energy bands rather than atomic or molecular levels and hence can, in principle, be easily tuned over a considerable range of wavelengths, (2) there are several methods of achieving sufficient gain to produce lasing in these materials and (3) these lasers have small physical dimensions (of the order of 100 microns to the side).

Figure 1 illustrates the basic operation of semiconductor lasers. Fig. 1(a) shows an intrinsic semiconductor at zero temperature where the completely filled electronic states of the valence band (assumed parabolic) are separated from the empty conduction band by an energy gap. If electrons are excited from the valence band to the

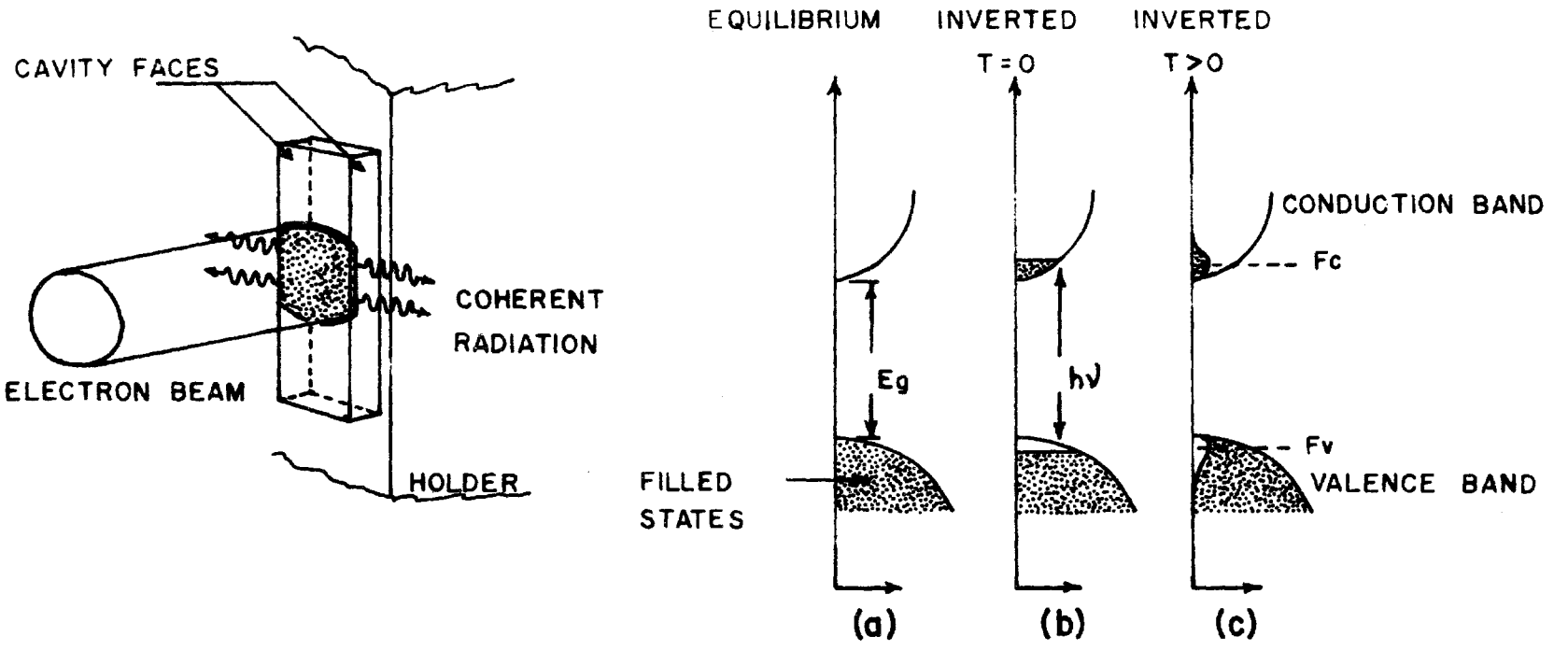

Fig. 1. Idealized band diagram of a direct bandgap semiconductor before and after pumping. Diagram of electron beam creating a thin gain region in laser crystal.

conduction band they will rapidly thermalize in a time $\lesssim 10^{-10}$ sec. [16] to equilibrium distributions governed by the Fermi-functions for probability of occupation:

$$f_c = 1/(1 + \exp(E-F_c)/kT)$$

$$f_v = 1/(1 + \exp(F_v-E)/kT)$$

where F_c, F_v are quasi-Fermi levels and k is Boltzmann's constant. The distribution is shown for T = 0°K (Fig. 1(b)) and T > 0°K (Fig. 1(c)).

In a more general case, the semiconductor may be doped and the band shapes may not be parabolic. Consideration will be given to such cases subsequently. In particular, the differences between exciton-controlled and band-to-band controlled transitions and their effects upon gain and loss mechanisms will be treated.

In Figure 1, a direct semiconductor has been illustrated, i.e., a semiconductor in which the lowest conduction band minimum and highest valence band maximum are at the same value of crystal momentum. There has been a claim that laser action was observed in SiC [17], an indirect bandgap material. However, the evidence in support of this claim is somewhat limited and has been criticized in detail by Hall [18]. It has been generally concluded that the original workers have not proved their case and in the

opinion of Thornton [19] much better experiments are necessary to substantiate such a claim. In light of these arguments all work in this thesis has been performed employing direct band-gap semiconductors.

The method used for achieving a condition of gain in the semiconductor sample was electron-beam pumping. This method was first suggested by Basov at the Second Quantum Electronics Conference in 1961. A high energy beam of electrons, usually greater than 20 kV., is directed at an appropriate surface of a sample. The electrons lose their energy within a few microns of the surface for the materials and beam voltages [20] used here. The beam generates low energy electron-hole pairs with rather poor efficiency (approximately 30%) because of momentum conservation considerations. For the materials and voltages used here about 10^4 pairs are created per incident electron. These carriers relax by radiationless processes to the respective band edges and produce a region of gain near the surface of the laser sample at wavelengths close to the band edge.

As noted previously, a feature of semiconductor laser systems is the variety of means of achieving population inversion. The two methods used besides electron-beam pumping are: optical pumping using a separate source laser, and electrical injection by means of p-n or hetero-junction. There is a considerable amount of literature on these methods [21,22], and therefore, the comments here will be

limited to a comparison between these methods and that of electron-beam pumping.

In terms of simplicity of both experimental set-up and operation, the use of junction injection is more desirable than electron-beam pumping; there is no need for the vacuum chamber that the electron-beam requires, and the pulsing circuits are simpler. The use of junction injection would, however, put unacceptable limits on the type of experiments which can be performed and render the analysis more complex and less controlled. The presence of impurity profiles would confuse interpretation of observations. Also, and probably more importantly, it is often difficult, if not sometimes impossible to produce the heavily doped, spatially narrow, well-defined junctions that the injection method requires. This limitation likely holds for CdS and CdSe. As a consequence, electron-beam pumping can be used on a far broader range of materials.

Optical pumping, upon first consideration, appears to offer advantages over electron-beam pumping in terms of both simplified experimental set-up and efficiency of pumping (with the resulting lower associated crystal heating). However, in order to achieve efficient pumping with a laser source, the source wavelength must be matched to the band-gap of the sample material. The number of such sources is somewhat limited. It will also become clear as a result of the work reported in this thesis, that optical

pumping will generally have much higher thresholds in watts/cm^2 even when efficiently coupled. Other major considerations are that it is difficult to control pump pulse shape sufficiently well by the optical pump method and the fact that the depth of penetration of the pump radiation for a pump energy near the band-gap is generally a rapidly varying function of wavelength. Both of these factors add considerable complexity and uncertainty to the analysis of results. In electron-beam pumping, the current density of the pulse of electrons can be shaped very accurately in time, and the penetration depth of the electrons can be controlled by beam voltage.

For these principal reasons, the method of electron-beam pumping was chosen for this work. Details of this method will be presented in the section concerning Apparatus.

In the description of various aspects of the experimental observations several parameters were used. Some parameters (actually system characteristics) were determined by the nature of the experimental set-up. In this category are: (1) temperature change due to heating of the crystal by the incident electron-beam, and (2) cavity loss due to surface and bulk imperfections in individual cavity samples used. Other parameters could be deliberately varied. In this category are: (1) excitation region thickness (controlled at least in part by the incident

electron-beam voltage), and (2) band-gap of the material (controlled by choice of semiconductor type).

CHAPTER II

THEORETICAL

1. Theoretical Model of the Electron-Beam Pumped System

(a) Solution of field equations

The far-field radiation patterns of modes from electron-beam pumped lasers are to a good approximation given by the Fourier transforms of the laser mode fields at the output end of the laser cavity. Consequently, to predict the far-field radiation patterns it is necessary to develop a suitable theory for the spatial variation of the eigenmodes of an appropriately specified laser cavity. In addition, as shown in the later development of the theory, it is necessary to allow for spatial variations in the refractive index. In general, the calculations must be applied to the situation in which the laser is operating well above threshold. Formally, this requires a self-consistent solution for the laser cavity field and the spatially dependent gain (possibly including the spatially varying refractive index). Values of the carrier generation rate, the spatial variation of the laser cavity temperature and several cavity parameters including cavity reflectivity losses and the losses in the unpumped region of the laser cavity define the solution. This problem is excessively

complex. It can be circumvented to some extent if we can make a judicious guess at the spatial dependence of the saturated gain, but it is unrealistic to attempt this over any significant range of control parameters. Under these circumstances we have chosen to analyze the simplest possible model in which the crystal (Fig. 2) is taken to be a semi-infinite slab bounded by the plane x=o (pumped surface) and the reflecting plane surfaces at z=o and z=ℓ. The electrons from the beam are assumed to lose their energy uniformly in a depth d from the pumped surface to create a region of gain. Further into the crystal, the unpumped region has a loss α_s at the oscillator frequency. In fact, this gain region width will be determined only in part by the depth of penetration of the incident beam. The carriers also diffuse and thus widen the gain region. The extent of this effect is dependent on the material used and will be calculated where appropriate.

One way to estimate how well this model relates to experiment is by comparing its results with the predictions of a model employing a different spatial dependence of the gain. This comparison is appropriate because our model does not take into account the potentially important "tailing-off" of the gain into the unpumped region which is implied both by carrier diffusion and the form of spatial energy loss of the beam in Klein's model [20] for kilovolt electron beams. Fortunately, another model has been presented [23]

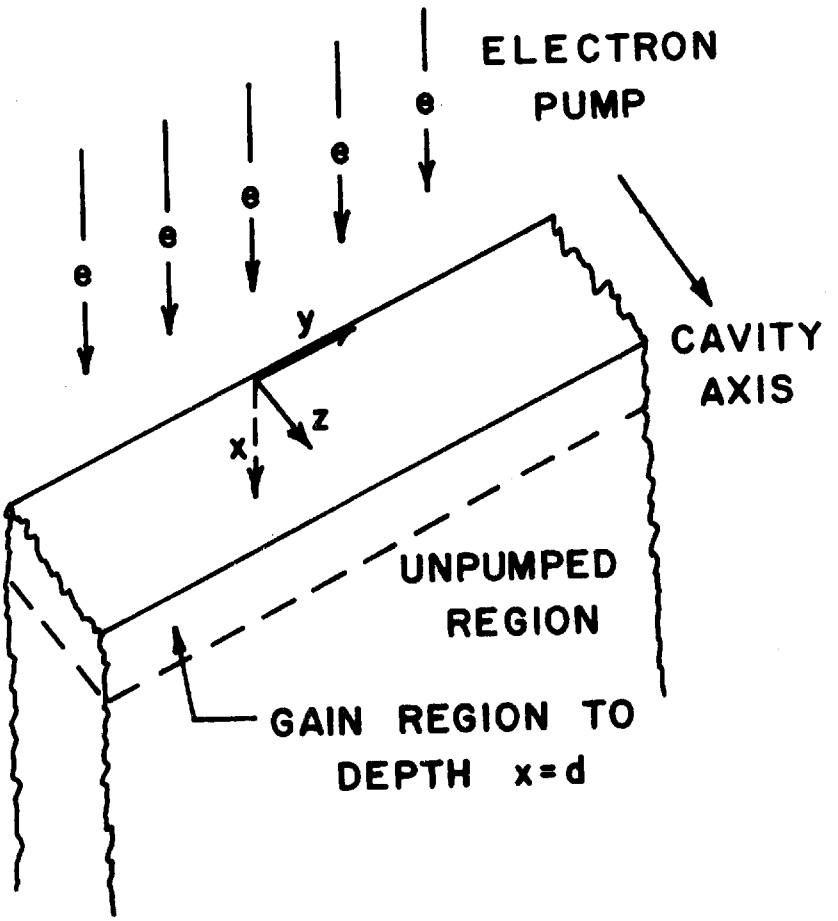

Fig. 2. Mathematical model of semiconductor laser. The cavity axis is z and a gain region uniform to depth d is assumed.

which can be used for comparison. In this model the gain and index profiles analyzed are of the form:

$$A \operatorname{sech}^2 Bx \qquad (A,B)\text{real} \quad .$$

In a subsequent part of this chapter we will describe how this model was developed and how we extended it to make a number of comparisons between the results of the two theories for diffraction losses and angular tuning. At this point it will suffice to say that the results obtained are reasonably close over the range of parameters of experimental interest. Consequently, we have generally employed the simple model presented here for two basic reasons. Firstly, it has the virtue of conceptual simplicity, which is reflected in the mathematical analysis. The equations describing the eigenmodes and eigenvalues can be expressed in a parametric form which greatly reduces the number of computations necessary in the analysis of the experimental results. It has the added virtue that the parametric representation permits the extraction of the approximate functional dependence of diffraction losses on cavity parameters. Secondly, the computation of both the near- and far-field patterns is greatly simplified using this model. Consequently, the demands on computation time are again reduced over that required using the "sech^2" model of ref. 23. The derivation of our simplified model is given below.

Since the time to set up equilibrium conditions of light intensity in the crystal (time required for light to travel the length of the crystal a few times) is very short with respect to the time of any frequency or gain changes, a constant instantaneous frequency is assumed in the solution. The equation to be solved is given by (Appendix A):

$$\frac{\partial A}{\partial t} = \frac{c^2}{2i\omega_o\varepsilon}\left[-\frac{\partial^2 A}{\partial t^2} + k^2 A - \frac{\omega_o^2\varepsilon}{c^2} A\right] \quad . \tag{2.1}$$

We seek a solution of the general form

$$E(x,t) = A(x,t)\sin\frac{\pi n z}{\ell}\, e^{i\omega_o t} \quad . \tag{2.2}$$

Since there is an index change in the gain region, the permittivity is taken to be of the form:

$$\begin{aligned} &\varepsilon_o' + \delta\varepsilon_o''(x,t) - i\varepsilon_o'' + i\varepsilon_g'' && \text{in } (0,d) \\ &\varepsilon_o' \qquad\qquad - i\varepsilon_o'' - i\varepsilon_\ell'' && \text{in } (d,\infty) \quad . \end{aligned} \tag{2.3}$$

ε_o' is the basic contribution to index. $\delta\varepsilon_o''(x,t)$ is the spatial change in the permittivity due to the presence of gain or of a temperature change. ε_o'' describes the non-resonant radiation losses consisting of cavity reflectivity losses together with the absorption at the laser frequency

(impurities, etc.). ε_g'' (ε_ℓ'') describes the negative (positive) absorption of the laser radiation in the pumped (unpumped) regions of the laser cavity.

The eigenmodes of the laser will have amplitudes stable in time, and therefore, the solutions must fulfil the condition: $\partial A/\partial t = 0$. Subject to this and the appropriate boundary conditions at x=d (Appendix A), the solutions we seek are of the general form:

$$\begin{aligned} A &= \sin px \qquad \text{in } (0,d) \\ A &= A_o \exp(-qx) \qquad \text{in } (d,\infty) \end{aligned} \tag{2.4}$$

where p,q are complex. Substitution of these solutions into the wave equations give:

$$-p^2 = (k^2 - \frac{\omega^2 \varepsilon_o'}{c^2}) - \frac{i\omega^2 \varepsilon_g''}{c^2} - \frac{\omega^2}{c^2} \delta\varepsilon_o'' + i\varepsilon_o'' \tag{2.5}$$

$$q^2 = (k^2 - \frac{\omega^2 \varepsilon_o'}{c^2}) + \frac{i\omega^2 \varepsilon_\ell''}{c^2} - i\varepsilon_o'' \quad . \tag{2.6}$$

Subtracting (2.5) from (2.6)

$$p^2 + q^2 = \frac{i\omega^2}{c^2} (\varepsilon_g'' + \varepsilon_\ell'') + \frac{\omega^2}{c^2} \delta\varepsilon_o''$$

or

$$p^2 + q^2 = i(\alpha+\beta) + \frac{\omega^2}{c^2} \delta\varepsilon_o'' \tag{2.7}$$

where $\alpha = \frac{\omega^2}{c^2}\varepsilon''_g$ and $\beta = \frac{\omega^2}{c^2}\varepsilon''_\ell$.

The requirement that the field and its derivative be continuous at x=d leads to $p/q = -\tan(pd)$ (2.8)

$$\left.\begin{aligned} \therefore\quad p^2 &= \left[\frac{\omega^2\delta\varepsilon''_o}{c^2} + i(\alpha+\beta)\right]\sin^2 pd \\ q^2 &= \left[\frac{\omega^2\delta\varepsilon''_o}{c^2} + i(\alpha+\beta)\right]\cos^2 pd \end{aligned}\right\} . \tag{2.9}$$

From (2.9)

$$-2ip^2 = \frac{-2i\omega^2\delta\varepsilon''_o}{c^2}\sin^2 pd + 2(\alpha+\beta)\sin^2 pd \tag{2.10}$$

Now if $p = p' + ip''$ an identity is:

$$-2ip^2 = [(p' + p'') - i(p' - p'')]^2 \tag{2.11}$$

$$\begin{aligned} \therefore\ (p' + p'') - i(p' - p'') &= \sqrt{2}\sin pd\{(\alpha+\beta) - i\frac{\omega^2\delta\varepsilon_o}{c^2}\}^{1/2} \\ &= \sqrt{2}\sin pd\,\{(\gamma' + i\gamma'')^2\}^{1/2} \\ &= \sqrt{2}\sin pd\,\{(\gamma'^2 - \gamma''^2 \\ &\quad + 2i\gamma'\gamma'')\}^{1/2} \end{aligned} \tag{2.12}$$

where $\gamma'^2 - \gamma''^2 = \alpha + \beta$

$$\gamma'\gamma'' = \frac{-\omega^2 \delta \varepsilon''_o}{2c^2} \tag{2.13}$$

therefore, we have

$$(p' + p'') - i(p' - p'')$$

$$= \sqrt{2} \sin pd(\gamma' + i\gamma'')$$

$$= \sqrt{2}\ (\gamma' + i\gamma'')[\sin p'd \cosh p''d + i \cos p'd \sinh p''d]$$

$$= \sqrt{2}\ [(\gamma' \sin p'd \cosh p''d - \gamma'' \cos p'd \sinh p''d)$$

$$+ i(\gamma' \cos p'd \sinh p''d + \gamma'' \sin p'd \cosh p''d)] \tag{2.14}$$

$$\therefore \quad \frac{p' - p''}{p' + p''} = \frac{\gamma' \cos p'd \sinh p''d + \gamma'' \sin p'd \cosh p''d}{\gamma'' \cos p'd \sinh p''d - \gamma' \sin p'd \cosh p''d} \cdot \tag{2.15}$$

Now letting $p'd = u$ and $p''d = ku$

$$\frac{1-k}{1+k} = \frac{\gamma' \cos u \sinh ku + \gamma'' \sin u \cosh ku}{\gamma'' \cos u \sinh ku - \gamma' \sin u \cosh ku}$$

$$= \frac{-\cot u \tanh ku + \gamma''/\gamma'}{1 - (\gamma''/\gamma') \cot u \tanh ku}$$

$$= \frac{\cot u \tanh ku - E_p}{1 + E_p \cot u \tanh ku} \tag{2.16}$$

where $E_p = \gamma''/\gamma'$ is a measure of the index step.

We can use this equation to solve for (u,k) pairs for given index steps. For small E_p the solution for the different order modes will be:

u lies in $(\pi/2, \pi)$ gives 0 order mode

u lies in $(3\pi/2, 2\pi)$ gives 1st order mode

etc.

We now wish to put the expression in a form which we can relate to the cavity parameters. From (2.14)

$$p' + p'' = \sqrt{2}\,[\gamma' \sin p'd \cosh p''d - \gamma'' \cos p'd \sinh p''d]$$

$$u + ku = d\sqrt{2}\,\gamma'^2\,[\sin u \cosh ku + E_p \cos u \sinh ku] \quad . \quad (2.17)$$

Now $\gamma'^2 - \gamma''^2 = \alpha + \beta$

$$\therefore \quad \gamma'^2\,[1 - E_p^2] = \alpha + \beta \quad . \quad (2.18)$$

Substitute into (2.17)

$$u + ku = \frac{d\sqrt{2(\alpha+\beta)}}{\sqrt{1-E_p^2}}\,[\sin u \cosh ku + E_p \cos u \sinh ku] \quad (2.19)$$

but from the imaginary part of (2.5)

$$2p'p'' = \alpha \qquad \text{or} \qquad 2ku^2 = \alpha d^2 \quad . \tag{2.20}$$

Substitute into (2.19)

$$u + ku = \frac{d\sqrt{2(2ku^2/d^2)+\beta}}{\sqrt{1-E_p^2}} [\sin u \cosh ku + E_p \cos u \sinh ku]$$

$$u^2(1+k^2)(1-E_p^2) = 2d^2\left(\frac{2ku^2}{d^2} + \beta\right)[\sin u \cosh ku + E_p \cos u \sinh ku]^2$$

$$u^2(1+k^2)(1-E_p^2) = [4ku^2 + 2d^2\beta][\sin u \cosh ku + E_p \cos u \sinh ku]^2 \tag{2.21}$$

$$2d^2\beta = \frac{u^2(1+k)^2(1-E_p^2)}{[\sin u \cosh ku + E_p \cos u \sinh ku]^2} - 4ku^2. \tag{2.22}$$

Now from lemma 1, Appendix A

$$\alpha = \frac{\omega n}{c} g = \frac{2\pi n}{\lambda} g \tag{2.23}$$

and $$\beta = \frac{\omega n}{c} \alpha_s = \frac{2\pi n}{\lambda} \alpha_s$$

$$\therefore \quad \frac{2\pi nd^2\alpha_s}{\lambda} = \frac{u^2(1+k^2)(1-E_p^2)}{2[\sin u \cosh ku + E_p \cos u \sinh ku]^2} - 2ku^2 \tag{2.24}$$

or

$$\frac{\alpha_s}{g_o} = \frac{1}{2} f(k,u)$$

where $g_o = \lambda/2\pi nd^2$

and

$$f(k,u) = \frac{u^2(1+k^2)(1-E_p^2)}{[\sin u \cosh ku + E_p \cos u \sinh ku]^2} - 4ku^2 \tag{2.25}$$

similarly

$$\frac{g}{g_o} = 2ku^2 \qquad \text{(from (2.20))} \quad . \tag{2.26}$$

It should be noted here that g corresponds to the diffraction loss discussed in the Introduction which proves to be a critically important parameter in the analysis.

The method of solution now proceeds as follows. A range of (u,k) pairs is first generated by computer from (2.16) for a given range of u. For each set, the corresponding values of cavity parameters are generated by the expressions (2.24) and (2.26). Solutions corresponding to given experimental conditions can then be chosen.

From the chosen sets of (u,k) the field amplitude can be calculated as shown in the following section.

(b) Display of Solutions as a Function of x

In this section we will derive the laser mode fields assuming that we have solved the field equations for given input parameters (α_s, g, d) and have sets of (u,k) corresponding to the solutions.

From the original conditions:

in (0,d)

$$A = \pm \sin [(u + iku)x/d] \tag{2.27}$$

(± since sign of p',p" can be chosen provided both are the same)

$$A = \mp \frac{1}{2i} [\exp(i(u+iku)x/d) - \exp(-i(u+iku)x/d)]$$

$$= \mp [\sin u(\tfrac{x}{d}) \cosh ku(\tfrac{x}{d}) + i \cos u(\tfrac{x}{d}) \sinh ku(\tfrac{x}{d})] \; . \tag{2.28}$$

From this it may be shown that:

$$|A|^2 = \sinh^2 ku(\tfrac{x}{d}) + \sin^2 u(\tfrac{x}{d}) \tag{2.29}$$

in (d,∞)

$$A = A_o \exp(-qx) \quad .$$

Also we know $p/q = -\tan pd$. If we write $q = q' + iq''$, substitute and take real and imaginary parts, we obtain:

$$q'd = -\frac{u}{2}\left(\frac{\sin 2u + k \sinh 2ku}{\sin^2 u + \sinh^2 ku}\right) \tag{2.30}$$

and

$$q''d = -\frac{u}{2}\left(\frac{\sinh 2ku - k \sin 2u}{\sin^2 u + \sinh^2 ku}\right) \quad .$$

Now

$$|A|^2 = C \exp\left(-q'd\left(\frac{x}{d}\right)\right)^2 \tag{2.31}$$

where C is to be determined by boundary conditions

$$\therefore \quad |A|^2 = C \exp(-2q'd(x/d)) = C \exp(-2\sigma(x/d)) \tag{2.32}$$

where

$$\sigma = q'd = -\frac{u}{2}\left(\frac{\sin 2u + k \sinh 2ku}{\sin^2 u + \sinh^2 ku}\right) \quad .$$

By matching solution (2.32) with the solution in (0,d) it may be shown that:

$$|A|^2 = (\sin^2 u + \sinh^2 ku)\exp\left[-2\sigma\left(\frac{x}{d} - 1\right)\right] \quad . \tag{2.33}$$

We now have expressions for the amplitude and phase of the laser modes in terms of the cavity parameters.

(c) The far-field mode patterns

In this section, diffraction theory will be used to generate the far-field mode patterns from the near-field patterns.

The field at the cavity face can be expressed as:

$$E(\alpha) = |E(\alpha)|\exp(i\phi(\alpha)) \quad \text{where} \quad \alpha = \frac{x}{d} \quad . \tag{2.34}$$

This represents the portion of A(x) transmitted from the crystal edge. It may be show (Appendix B) by standard methods that, to a good approximation, the far-field pattern is given to within a constant by:

$$E'(\theta) \propto \int |E(\alpha)|\ e^{i\phi(\alpha)}\ e^{ik\theta\alpha}\ d\alpha \quad . \tag{2.35}$$

$E(\alpha)$ is defined separately in the two zones $(0,d)$ and (d,∞).

In the region $(0,d)$

$$|E(\alpha)| = [\sinh^2 ku\alpha + \sin^2 u\alpha]^{1/2} \tag{2.36}$$

and $$\phi(\alpha) = \tan^{-1} [\cot u\alpha \tanh ku\alpha] \quad . \tag{2.37}$$

In the region (d,∞)

$$|E(\alpha)| = [\sin^2 u + \sinh^2 ku]^{1/2} \exp(\sigma(\alpha-1)) \qquad (2.38)$$

where $\sigma = \frac{u}{2} \left(\frac{\sin 2u + k \sinh 2ku}{\sin^2 u + \sinh^2 ku}\right)$

and $\phi(\alpha) = \frac{u\alpha}{2} \left(\frac{\sinh 2ku - k \sin 2u}{\sin^2 u + \sinh^2 ku}\right)$. (2.39)

The integration for the far-field pattern was done numerically for the (0,d) portion and analytically for the (d,∞) region. The analytic calculation is shown in Appendix C.

2. Another Model of the Electron-Beam Pumped Laser

As stated previously, the model we have just developed is necessarily only an approximation of the experimental conditions; that is, the gain profile assumed is not the true gain profile which would reflect carrier diffusion and gain saturation. To determine the extent to which this approximation affects the predicted results we can examine another gain profile, preferably one which would be in error in the opposite direction to our previous model. The stepped gain model which we developed probably overestimates the gain at x=d since the gain should decrease smoothly across this region. On the other hand, the "$sech^2$" model developed by Bogdankevich et al. [23], which we will now examine, likely underestimates the gain at x=d. This occurs for two reasons. Firstly, the "$sech^2$" model is parametrized to be equivalent in half-height width of gain to the truncated gaussian shape of differential energy loss (dE/dx) of the electron beam [20]. The gain shape thus does not reflect the profile broadening effects of gain saturation. Secondly, this model also lacks the profile broadening which would be caused by carrier diffusion. This model does, however, include a tailing-off of gain toward the unpumped region, a factor which could be of importance. Hence a comparison of the results from the

two models should give us a reasonable picture of the extent of the discrepancies introduced by our approximation.

The model developed by Bogdankevich et al. [23] is, like ours, based upon an active medium with a spatially varying complex permittivity, which includes the spatial change in gain and refractive index. The gain and index profiles are chosen to permit a 1-region analytic solution of the field equations.

The complex permittivity is used in the form:

$$\varepsilon(x,t) = \varepsilon_o + \delta\varepsilon_o(x) + i\varepsilon''_o - i\varepsilon''(x,t) \qquad x \geq 0$$

$$= 1 \qquad x < 0$$

where $\delta\varepsilon_o(x)$ describes the change in dielectric constant due to the inhomogeneous distribution of electrons and holes

ε''_o describes the non-resonant radiation losses and $\varepsilon''(x,t)$ describes the negative or positive absorption of the laser radiation due to radiative recombination or the formation of electron-hole pairs.

Using a field of the form:

$$E(x,t) = U(x)e^{-i\Omega t}$$

the equation for the determination of the eigenfunction U(x) is:

$$\frac{d^2U}{dx^2} + \left(\frac{\omega_o^2}{c^2}\right)\left[i\varepsilon''_o - i\varepsilon''(x) - \delta\varepsilon_o(x) + \frac{2\Omega\varepsilon_o}{\omega_o}\right]U = 0 \quad . \qquad (2.40)$$

This equation can be solved analytically for gain and index profiles of the form:

$$\varepsilon''(x) = \frac{\varepsilon''_m + \varepsilon''_\infty}{\cosh^2 px} - \varepsilon''_\infty \qquad (2.41)$$

where ε''_m is the value of $\varepsilon''(x)$ at x=o and ε''_∞ is the value at large x for laser frequency ω_o.

$$p = 1/(2d\ \ell n(3 + 2\sqrt{2}))$$

where d is the width of the distribution at its mid-height coordinate.

$$\delta\varepsilon_o(x) = \frac{-\delta\varepsilon_o}{\cosh^2 px} \quad , \quad \delta\varepsilon_o = \frac{4\pi ne^2}{m^*\varepsilon_o\omega_o^2}$$

where n and m* are, respectively, the density and effective mass of the carriers.

The solutions of (2.40) will then be:

$$U(x) = \cosh^{-K}(px)\cdot F\left[K + \tfrac{1}{2} + P,\ K + \tfrac{1}{2} - P\,|K+1|\tfrac{1}{2}(1 - \tanh px)\right] \qquad (2.42)$$

where F is the hypergeometric function,

$$K^2 = (k^2/p^2)\cdot\frac{1}{\varepsilon_o}\left[\frac{2\Omega\varepsilon_o}{\omega_o} + i(\varepsilon_\infty'' + \varepsilon_o'')\right]$$

$$P^2 - \frac{1}{4} = (k^2/p^2)\cdot\frac{1}{\varepsilon_o}\left[-\delta\varepsilon_o + i(\varepsilon_m'' + \varepsilon_\infty'')\right] \qquad (2.43)$$

with the constraints

$$K + \frac{1}{2} - P = -n \quad , \quad n = 1, 3, 5, \text{ etc.}$$

and $\mathrm{Re}(K) > 0$.

The second constraint limits the solutions to

$$U_n \sim \cosh^{P + \frac{1}{2} + n}(px) P_n(\tanh px) \qquad (2.44)$$

where P_n is a polynomial of order n. The first constraint for the lowest order mode (n=1) leads to the following equation for eigenvalues of ε_m'' at threshold:

$$\frac{\varepsilon_m'' - \varepsilon_o''}{\varepsilon_o} = \frac{3}{2}\frac{p^2}{k^2}\left\{\frac{1}{2}\left[\left(1 + \frac{4k^2}{p^2}\frac{\delta\varepsilon_o}{\varepsilon_o}\right)^2 + \left(\frac{4k^2}{p^2}\frac{(\varepsilon_m'' + \varepsilon_o'')}{\varepsilon_o}\right)^2\right]^{1/2}\right.$$

$$\left. + \frac{1}{2}\left(1 + \frac{4k^2}{p^2}\frac{\delta\varepsilon_o}{\varepsilon_o}\right)^{1/2}\right\} \quad . \qquad (2.45)$$

Computer programs have been written to solve for the eigenvalues of ε_m'' and to generate the far-field patterns for the lowest order laser mode,

$$U_1 = \cosh^{P + \frac{3}{2}}(px)\tanh(px) \quad .$$

The latter was accomplished employing Fast Fourier transform methods developed by Cooley and Tukey [24].

A comparison of typical results from the two models will be made subsequently.

3. General Determination of Parameters in the Model

(a) General

In this section, some general results of the models will be presented together with a discussion of the possible variations of the input parameters.

If a comparison of theoretical and experimental results for the far-field patterns for semiconductor lasers is to be made, the two parameters which can be most readily considered are the far-field mode width and deviation angle from the cavity axis. A comparison of the predicted results given by the two models now available enables us to investigate the extent to which the predicted values of these variables is theory-dependent. These considerations were based on the calculated variations of the field patterns with input parameters and fits to experimental data. The specifics of the choice will be deferred to Chapter 4. At this point it will suffice to say that the deviation angle of the peak of the spatial far-field mode, θ_p, from the cavity axis was chosen as the most suitable parameter for analysis of the experimental data.

Figure 3 shows the far-field laser mode patterns generated from the stepped gain model using parameters

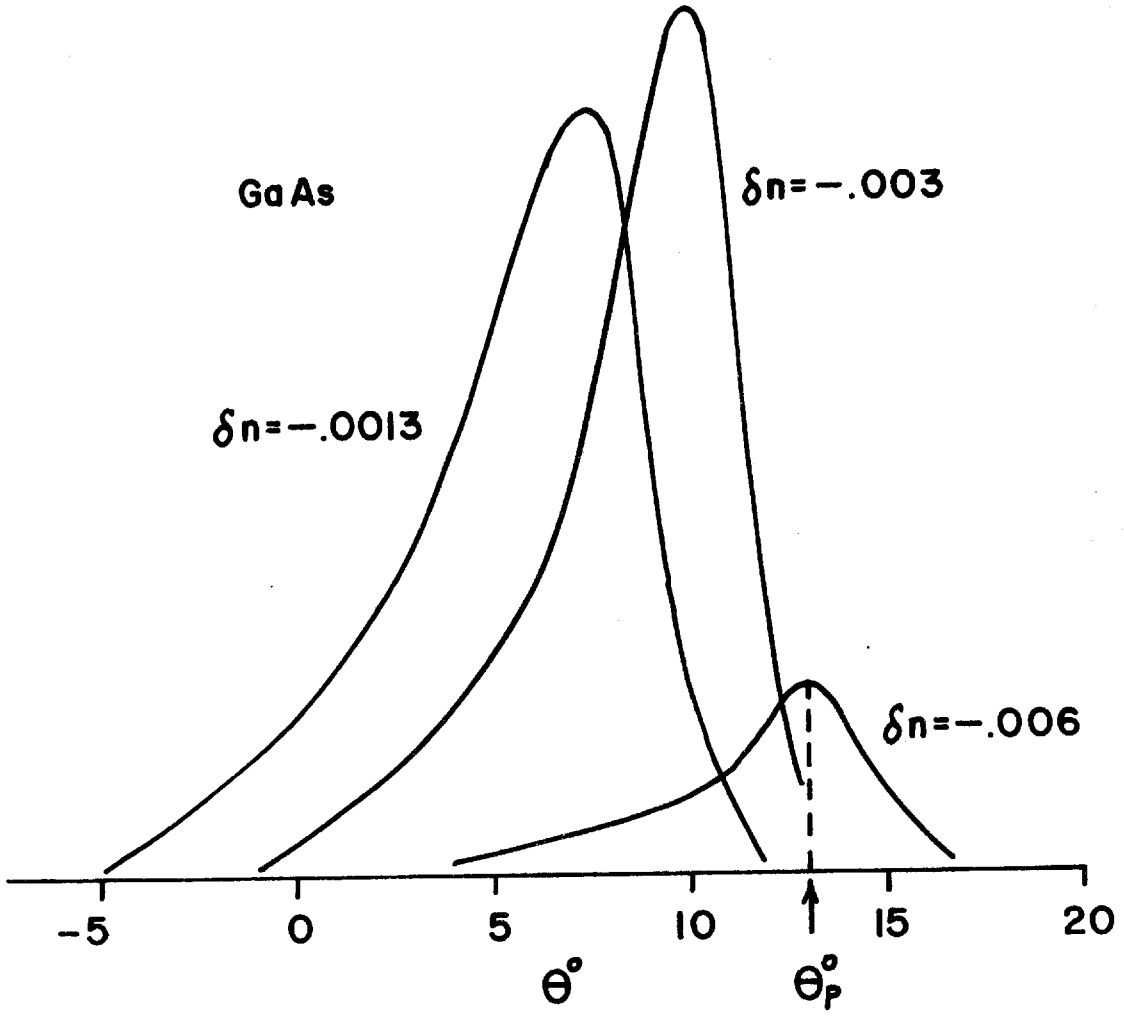

Fig. 3. Theoretically generated far-field modes for GaAs laser assuming a gain region width of 3.2 microns, α_s=170 cm^{-1} and three values of (negative) index step in the gain region.

typical for GaAs electron-beam pumped lasers. Values of the index step required to give far-field mode deviations of the degree observed experimentally are of the order 10^{-2}. The values of the index step indicated are negative which is found to be appropriate for GaAs. The intensity normalization is intended to facilitate comparison with the experimental curves for GaAs shown later. Index changes of the order 10^{-2} are quite large - at least an order of magnitude greater than can be produced in lasing GaAs by mechanisms considered by earlier investigators, viz. free carriers [4,23]. However, there do exist mechanisms which can and do produce changes of this size as discussed later in this chapter.

The mechanism cited to produce the changing of the angular deviation of the far-field mode (angular tuning) in the previous diagram was a change in the index difference between the pumped and unpumped regions of the laser. A continuous change of this index step during the pump pulse results in angular tuning of the far-field mode. Subsequent calculations will show that this mechanism satisfactorily explains our experimental observations, but, for the sake of completeness, we should also consider another mechanism which could result in such angular tuning. This second mechanism is a variation in time of d, the width of the gain region. The theoretical model predicts a dependence of the angular deviation of the far-field mode upon d in the

approximate form: $\theta_p d \cong$ constant if the index of refraction does not change.

The experimental data presented later illustrates that an explanation for angular tuning of θ_p in terms of d changes requires d to increase by approximately one order of magnitude in times of about 100 nanoseconds.

Since d is determined at least initially by the penetration of the beam electrons into the semiconductor, d will depend upon beam voltage and material type [20]. Assuming that we hold beam voltage, material type and pump current density constant, the ways in which d can change with time are limited to:

1. diffusion of electrons (assumed to diffuse faster than holes)
2. creation of electron-hole pairs further into the unpumped region of the crystal by the spontaneous and stimulated photon fields.

The treatment of these two factors is presented in Appendix D, and the following conclusions are reached.

1. d changes due to carrier diffusion cannot account for the observed angular tuning because the changes in d are too small and they stop within a few nanoseconds,
2. d changes due to reabsorption of radiation merely change the shape of the tail of the pump profile into the unpumped region and do not occur over periods of time sufficiently long to account for the experimental observations.

(b) Possible Variations in Index Step in Gain Region

There are two factors which can produce effective index changes between the gain region and the unpumped region large enough to cause significant changes in the far-field radiation pattern. One factor relates to the temperature variations near the gain region resulting from heating by the inefficient pumping (approx. 30% efficiency [20]) and subsequent thermal diffusion. The index of refraction is a function of temperature and therefore, a temperature difference between two spatial points will result in a corresponding difference in index.

Another factor which can cause relatively large index variations is directly related to the presence of gain. For a given wavelength of light, the pumped and unpumped regions represent different values of optical "loss". Since loss and index of refraction are related through Kramers-Kronig relations [25], there will exist a difference in index of refraction between the two regions at this wavelength. Moreover the value of index difference will be a function of wavelength because the absorption edge of a semiconductor, near which the laser operates, is a region of rapidly-varying absorption. It is a direct consequence of the dispersion relations that this rapid rise in absorption leads to changes

in the index of refraction difference. Similar changes in index of refraction have been considered by Ashkin et al.[26] in laser pumped CdS and index changes of the order 10^{-3} have been observed.

The values of these index changes for GaAs and CdSe are estimated in Appendix E. It is interesting to note that of the two proposed sources of index change, namely spatial variations of temperature and gain, the former is the dominant mechanism in CdSe and the latter in GaAs over most of the ranges of wavelength and temperature variation occurring in the experiments. The experimental observations reflect this difference.

CHAPTER III

EXPERIMENTAL

1. Experimental Set-Up

The apparatus used in this work was constructed specifically for these experiments. Those portions of the apparatus which could be obtained commercially were purchased. The other portions which were not commercially available, or which could not be reasonably incorporated into the system, were fabricated.

The former will be indicated by name and manufacturer, and the latter will be described in some detail.

(a) General description of system

A block diagram of the system is shown in Fig. 4. The major components of the system are as follows: the electron gun with its associated H.V. power supply, beam pulse control electronics; an electron-beam focusing coil; the sample housing chamber with fitted liquid helium dewar, viewing ports, and electrical feedthrough; the spectrometer with its imaging system; the data recovery section consisting of sample current detector, sampling oscilloscope and chart recorder.

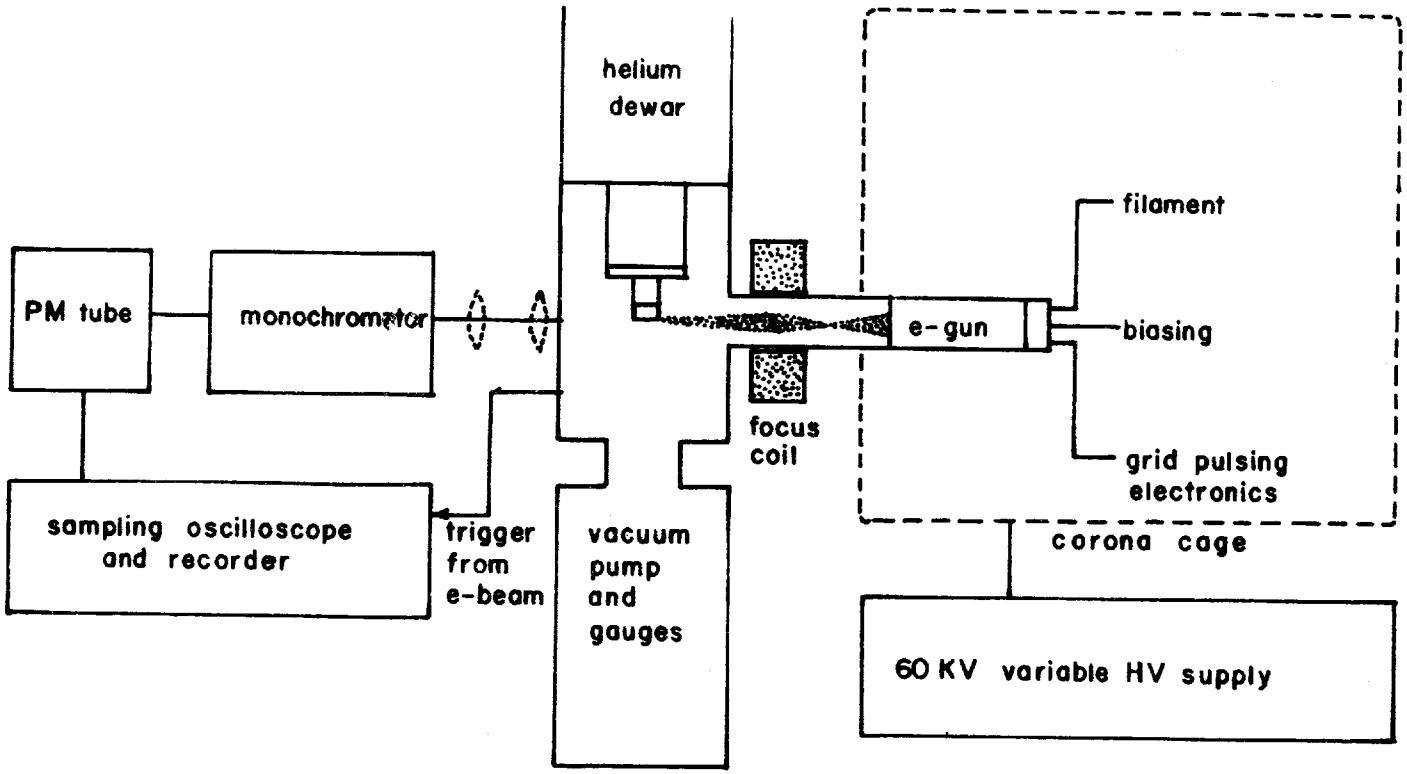

Fig. 4. Block diagram of experimental system.

The components used in the system in an unmodified form are described in Table 1. The other portions of the apparatus will now be described individually.

(b) Electron-beam generation

The electron gun is a modified SE-5AZP (Superior Electronics Corporation) radar gun. Figure 5 illustrates the electrode lay-out and typical voltages on these electrodes during operation. The electron source is an indirectly-heated oxide-coated cathode. Grid 1 encloses the cathode and .050" diameter hole in it determines the initial beam diameter. This grid is pulsed from negative voltage (with respect to the cathode) to ground in order to gate the flow of electrons down the tube. Grids 2 and 3 serve dual purpose as accelerating the electrostatic focusing electrodes. The final accelerating electrode is not an integral part of the gun; it is a tubular shaped portion of the vacuum connection between the beam tube to the sample chamber and the electron gun sleeve. The power supplies for the heater filament and grids 1 and 2 were standard transformer and diode full-wave rectifier circuits with capacitor-inductor filtering. The high voltage for grid 3 was obtained by tapping down on the main high voltage supply (Fig. 6).

Table 1

Instrument	Manufacturer and Designer
1. Research Dewar	Sulfrian Cryogenics model 749
2. Chart Recorder	hp model 7100B
3. Monochometer	Jarrell-Ash 0.5 meter Ebert
4. Photomultiplier Tubes	RCA 7102 and RCA 6199
5. Sampling Oscilloscope	hp 140A frame, 1425A sampling time base, 1410 sampling vertical amplifier
6. High Voltage Supply	Del Electronics Corp. 60 RHPT-1.5-1
7. Constant Voltage Supply	Sola 23-25-210
8. Isolation Transformer	Del Electronics Corp. 3-CTR-60-11
9. Focus Coil	Constantine Eng. Labs AF 334-340
10. P.M. tube precision power supply	Fluke 412-B
11. Coil micropositioner	Line Tool Co. model C

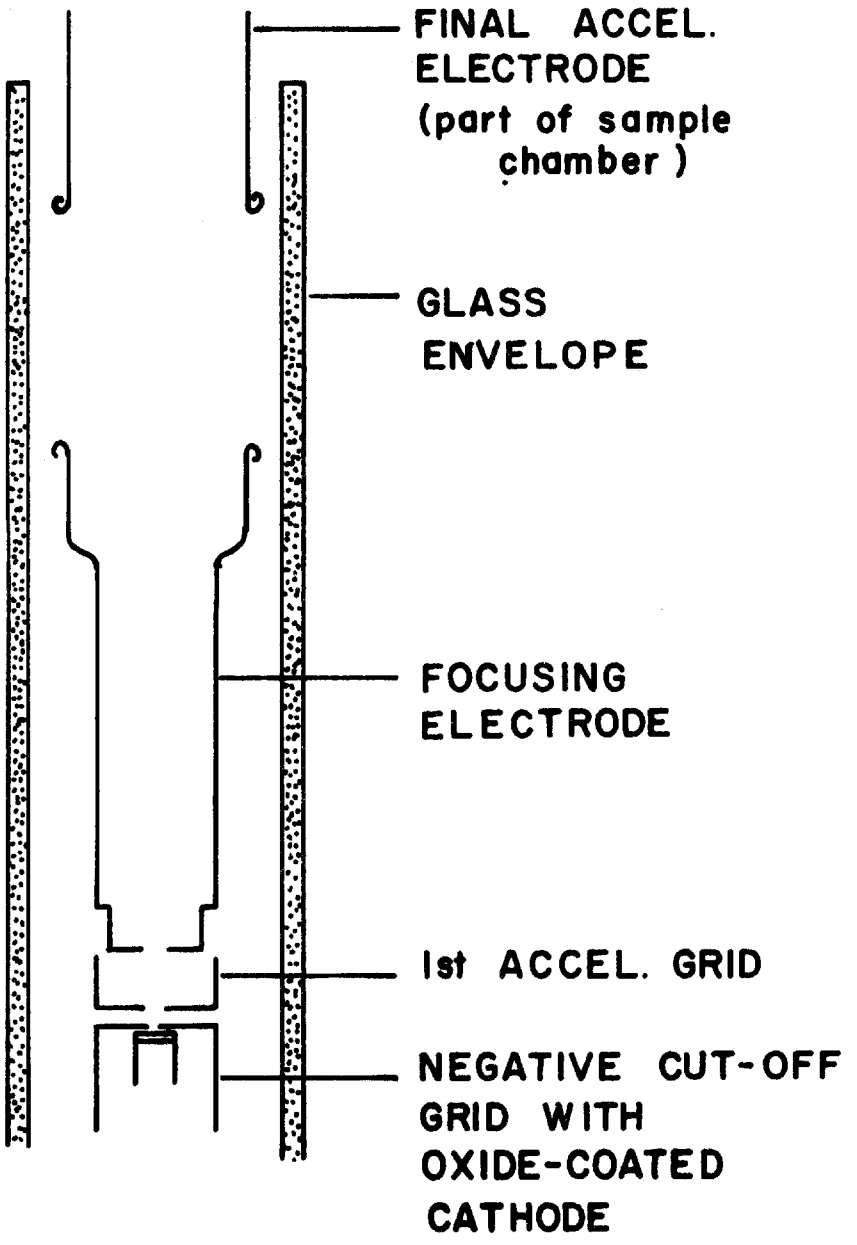

Fig. 5. Electron gun assembly.

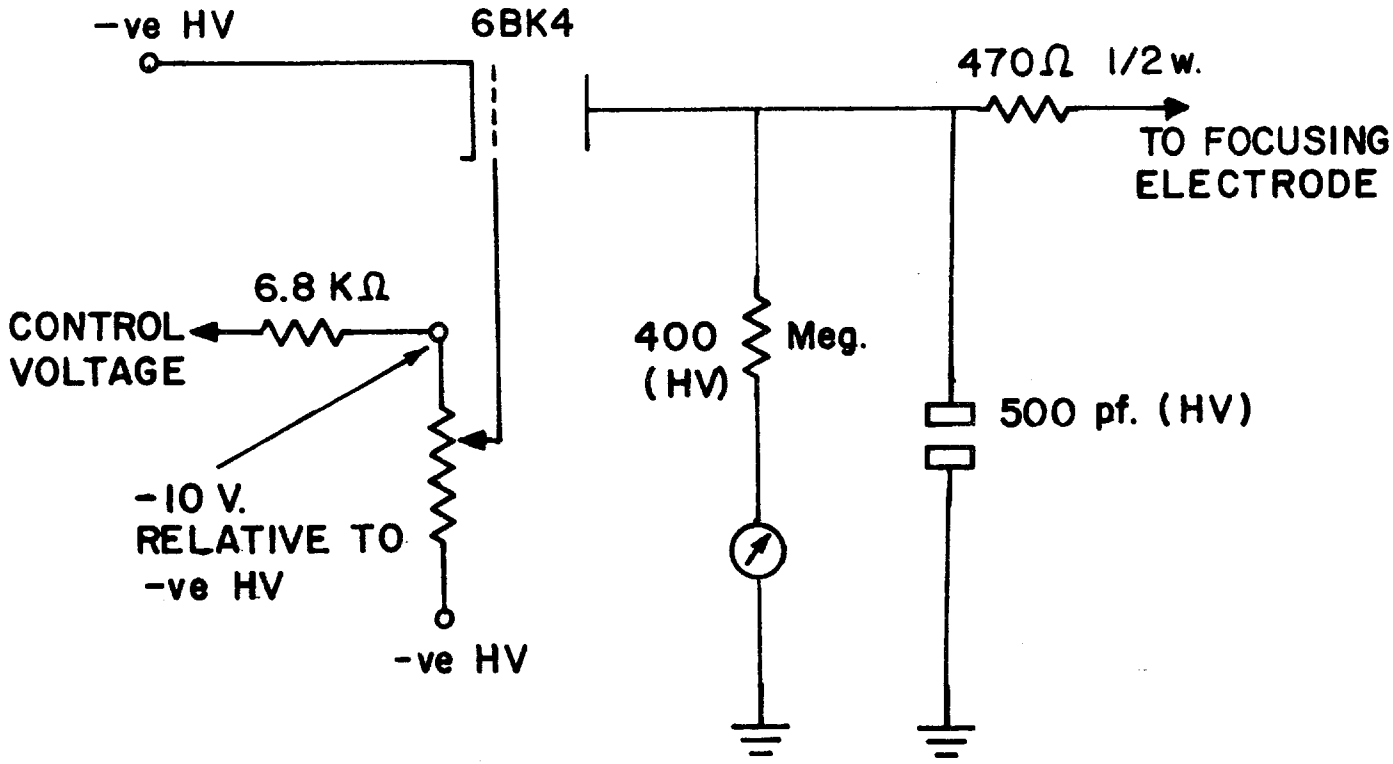

Fig. 6. Schematic for focusing anode supply.

The glass housing of the electron gun is connected to the beam tube by a quick-disconnect "O"-ring vacuum seal, and the beam tube is connected in a similar way to the sample chamber. Final focusing of the electron beam is by a magnetic focus coil around the beam tube (Table 1). The focusing coil is mounted on an X-Z micromanipulator to provide a means of accurate positioning of the beam on the sample (± 5 microns could be repeated). With this arrangement of focusing, the electron gun is capable of producing current densities greater than 20 A/cm^2 at 40 kV for a .010" focused beam diameter.

The grid 1 pulser is a coaxial line pulser (Fig. 7) triggered by a mercury-wetted reed switch (Hamlin HRC-1). The switch is housed in a 3/8" bore brass tube fitted with BNC connectors, and matching of the line discontinuities introduced by the switch is achieved by use of quarter-wave stubs (BNC, open-ended).

The electron beam pulse produced by these circuits had to be very well defined because events separated in time by only a few nanoseconds were often investigated. A 220 ns. long electron beam pulse with rise and fall times of approximately 1 ns. and less than 10% overshoot ringing and droop (produced by resonance tuning and pulse shaping circuits on the electron beam gating signal) was employed in the experiments reported in this thesis.

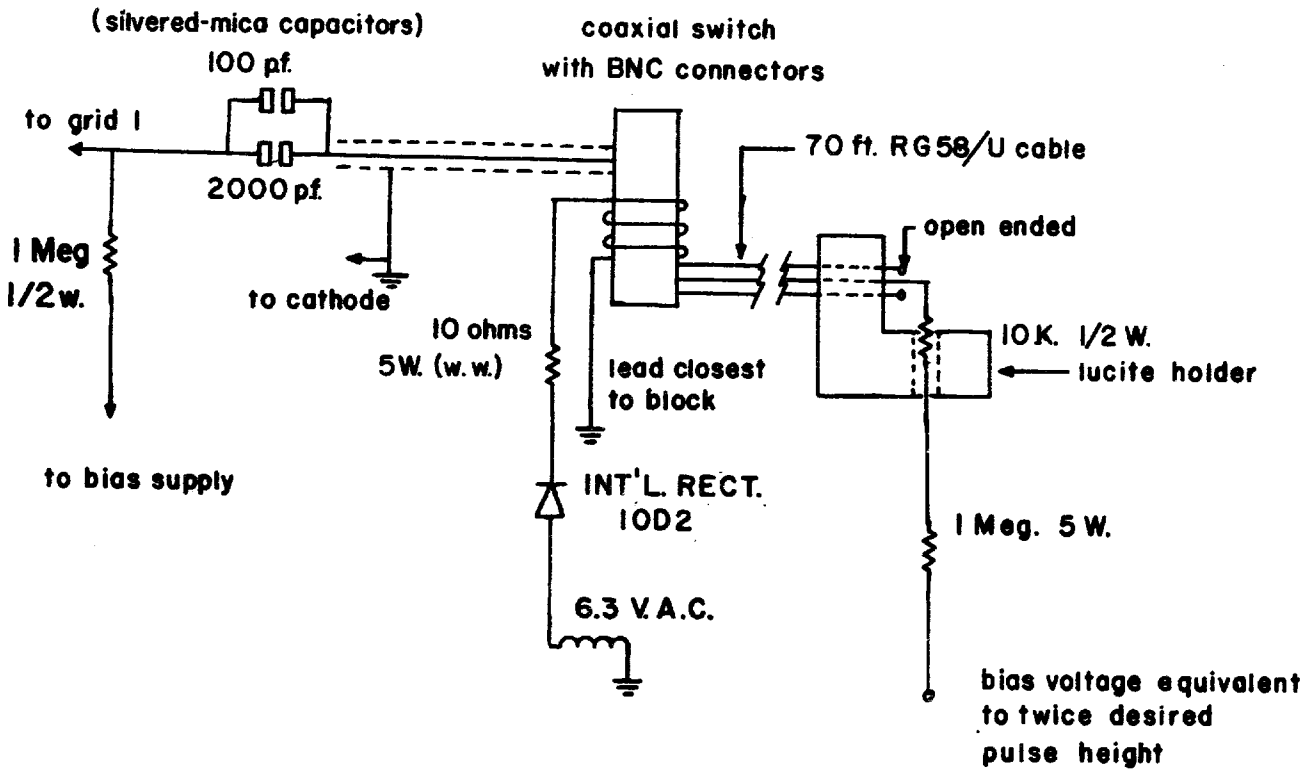

Fig. 7. Schematic of Cable Pulser.

All the electronics for the electron gun with the exception of the 40 kV accelerating potential is connected to the line through an isolation transformer and constant voltage transformer (Table 1). These circuits are housed in a perspex-shielded corona cage floating at the negative high potential.

(c) The Sample Chamber

The sample chamber was designed with a view to versatility of operation, reliability of vacuum seals, and lack of contamination. The main body of the chamber is a standard 4" Van de Graaf cross of stainless steel. The helium dewar is set on the top port and a 2" oil diffusion pump is fitted to the bottom port with a flange that also serves as a table mount. The two side ports are fitted with 1/4" thick Vycor windows using the standard Van de Graaf connectors. All connectors permit relative rotation of the adjacent parts. This feature permits azimuthal orientation of the sample with respect to the electron beam. The beam-tube vacuum connector is fitted at the 4-fold symmetric axis of the cross and a BNC vacuum feedthrough to one arm serves as the current probe (for triggering coincidence circuits in the data analysis section). The sample itself is mounted with indium solder to a copper block bolted to the dewar cold finger. Location of the beam with respect to

the sample is facilitated by a phosphor-coated brass screen in front of the sample. Small holes drilled in this screen (electrically insulated from the sample block but connected to output current feedthrough) permit estimation of beam current density.

(d) Data Analysis System

The arrangement of the light analysis components depends upon the particular type of measurement undertaken and will be described where necessary in later sections. The major components are (Table 1); a motor-driven monochromator, photomultiplier detector with a housing for cooling by cold nitrogen gas, a lens system to collect and focus the light, a sampling oscilloscope to display the time variation of the light pulse, and a strip-chart recorder for permanent recording of data. Using these components we can make the specialized measurements required. These measurements involve analysis of light signals at specific wavelengths and times after start of the electron-beam pulse cycle.

(e) Sample Preparation

The type of crystal samples that can be used in these experiments is set by several requirements. The size of the cavity length is limited to a few hundred microns (max.) by two conditions: (1) the area that can be illuminated by the focussed electron beam at sufficient beam current densities, and (2) the Fabry-Perot mode separations that can be resolved by the monochrometer (0.2 Å for the model in our system) limit the cavity length to a few hundred microns maximum. The surface of the crystal illuminated by the electron beam must be flat and undamaged to within a small fraction of a micron because the depth of penetration of the electron beam is typically one or two microns. The corners of the crystal at the cavity ends must be very well defined because of the small depth of gain region; i.e., the corners cannot be "rounded" by polishing or by handling damage.

For these reasons, the use of polishing was avoided entirely. Samples were prepared by cleaving three surfaces of the crystal - the cavity faces and the face illuminated by the electron beam. The GaAs used was grown by the float-zone method and was p-type, Zn doped to 1.2-2.4 x $10^{18}/cm^3$. The CdSe was cut from a Harshaw high purity crystal grown from the vapour phase, n-type with impurity concentration of $\sim 10^{16}/cm^3$ (Harshaw specifications).

2. Lasing Threshold Considerations

Since we will be using terms such as "stimulated emission", "lasing" and "lasing threshold", it is appropriate to discuss what is meant by these terms.

A number of authors [3,42-51] have used the following criteria, in various combinations, to indicate the presence of laser action in electron-beam pumped semiconductors:

1) superlinearity of the light output as a function of beam current;
2) spectral narrowing;
3) the appearance of spatial diffraction patterns in the emitted light (spatial coherence);
4) a well-defined (frequency) mode pattern in the emitted radiation;
5) the abrupt appearance of spatial modes or orientation of radiation along the resonator axis (beam narrowing);
6) characteristic intense light spots on the crystal cavity face.

None of the above criteria is a satisfactory indication of lasing action when taken alone. 1), 2) and 3) merely indicate the presence of considerable stimulated emission.

As for 4), under the proper experimental conditions, longitudinal frequency modes can be observed in spontaneous emission [3]. Both 5) and 6) are related to the establishment of spatial modes that could in principle be observed below laser threshold.

However, when several of these criteria are met in simultaneous combination; i.e., abrupt appearance of a single spatial mode in the presence of considerable stimulated emission, then there is a reasonably satisfactory indication of laser action. In the following sections, we will base our claims of lasing action in various materials on these grounds.

The previous criteria have related only to those properties of the light output that might indicate that lasing action is taking place. No consideration has as yet been given to the definition of a threshold beam current density. Evidently, the definition of the threshold current density as that required to turn on the laser after an infinite time is not useful for the pulsed pumping system (with its associated thermal effects) that is being considered here. In this system, the light output varies in wavelength and with time after the start of each pump cycle. Consequently, in whatever manner we choose to specify threshold current density, it will be a function of wavelength and time. In practice we find that the indicators of the presence of lasing action require observation over a range of wavelengths

and/or time; therefore, an operational definition of the threshold current density is required. Since the approach to, and onset of, oscillation takes place over a small range of current density, it matters little what definition of threshold current is used, provided only that it is reproducible. In this work we have used as a definition of laser threshold, that current density at which a single (or small number of) sharply defined Fabry-Perot mode appears suddenly from the spontaneous background when this current corresponds to the upper end of the superlinear region of a log I vs. log current density plot (which hereafter will be termed "intensity curve").

Lasing threshold will, of course, be different for different crystal samples because of unavoidable differences in crystal surface and cleaving accuracy. Indeed the threshold usually varies over parts of a single sample. Because of this uncertainty, each sample must be investigated individually for lasing properties and positioning of the electron beam on the sample must be accurately repeatable. The beam spot size is kept constant by adjustment of the fraction of the beam that passes through a fixed measuring hole in the crystal-locating screen. Positioning of the beam on the crystal could be set within 5 microns through the use of the X-Y micromanipulator on the beam focusing coil.

Certain procedures have been developed to determine whether a particular sample will lase and the current densities

of the electron beam required. For a material in which lasing has been previously observed and approximate wavelength of lasing is known, the first part of the investigation is to make an intensity curve for the sample at a given beam voltage. Figure 8 shows typical intensity curves for a GaAs sample. These plots illustrate the linear increase of light output, integrated over wavelength, at low pumping levels; the onset of a superlinear region indicative of stimulated emission; and high-level saturation. The conditions of view for this data are with the monochrometer aligned along the cavity axis in a plane perpendicular to a cavity face (0° condition) and the radiation sample through a narrow 1° slit. Angular tuning of spatial modes (to be discussed later) affects these measurements but the data shown here is chosen to be consistent with these effects. The intensity curves are measured at given times following the start of the pump pulse due to the variation of the intensity curve with time. This point is discussed in Chapter 4, and this effect is shown to result from the behaviour of diffraction losses with crystal heating.

As mentioned before, a sensitive indicator of lasing action is the striking appearance of a small number (one or more) of sharp Fabry-Perot modes rising out of the spontaneous-mode background. An example of such behaviour appears in Fig. 9, which shows the frequency mode spectrum of a GaAs laser crystal just before and immediately after threshold

Fig. 8. Selected curves of light output intensity integrated over all wavelengths as a function of pumping current density with delay time after the start of the pumping pulse as a parameter. Conditions of view are 0° with 1° slit. Temperature is 77°K and beam voltage is 40 kV.

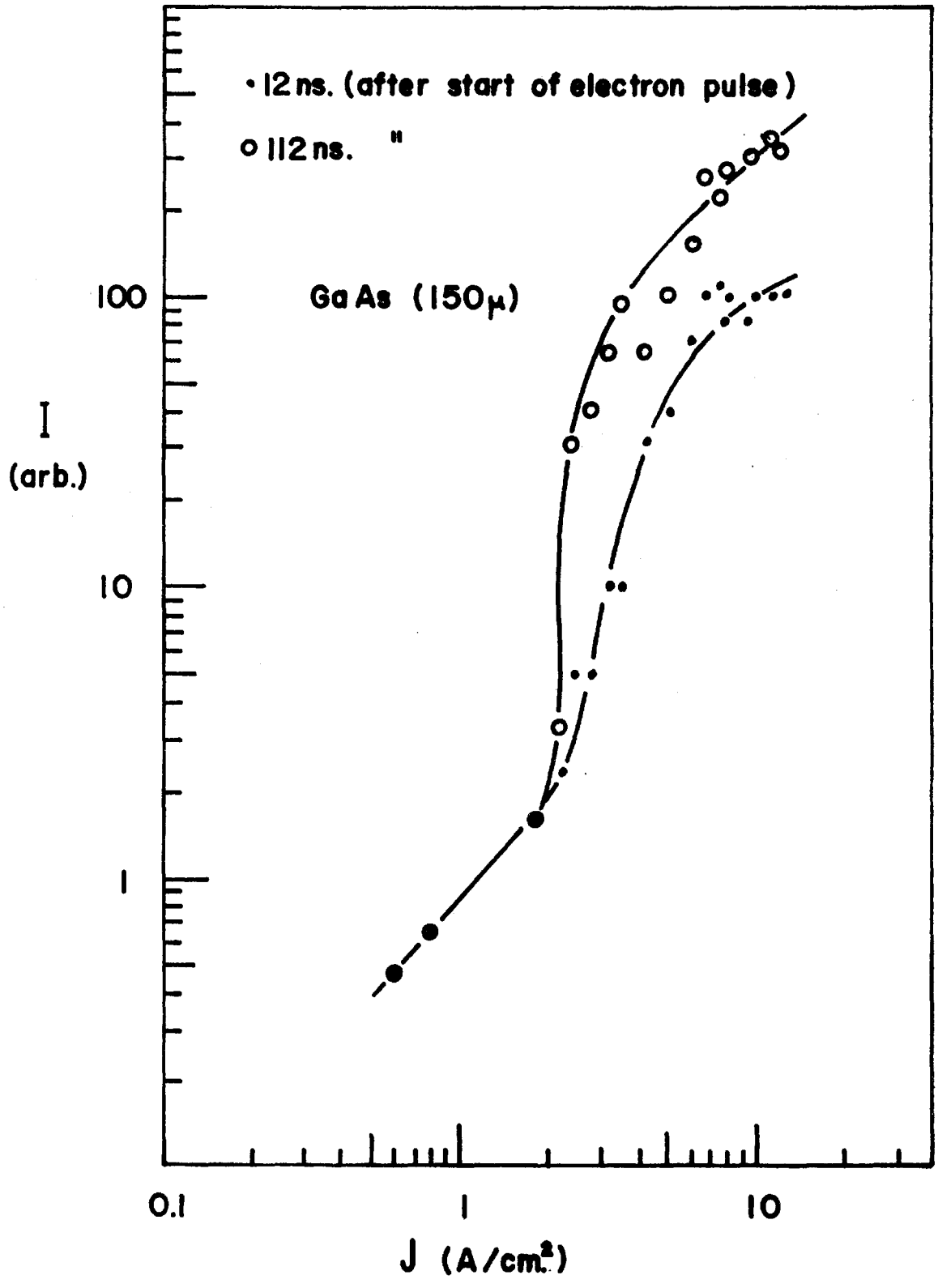
• 12 ns. (after start of electron pulse)
o 112 ns. "
GaAs (150μ)
100
10
1
I
(arb.)
0.1
1
10
J (A/cm²)

Fig. 9. Fabry-Perot modes in GaAs before and after start of lasing. Pumping current density is 6.9 A/cm^2. Temperature is 77°K.

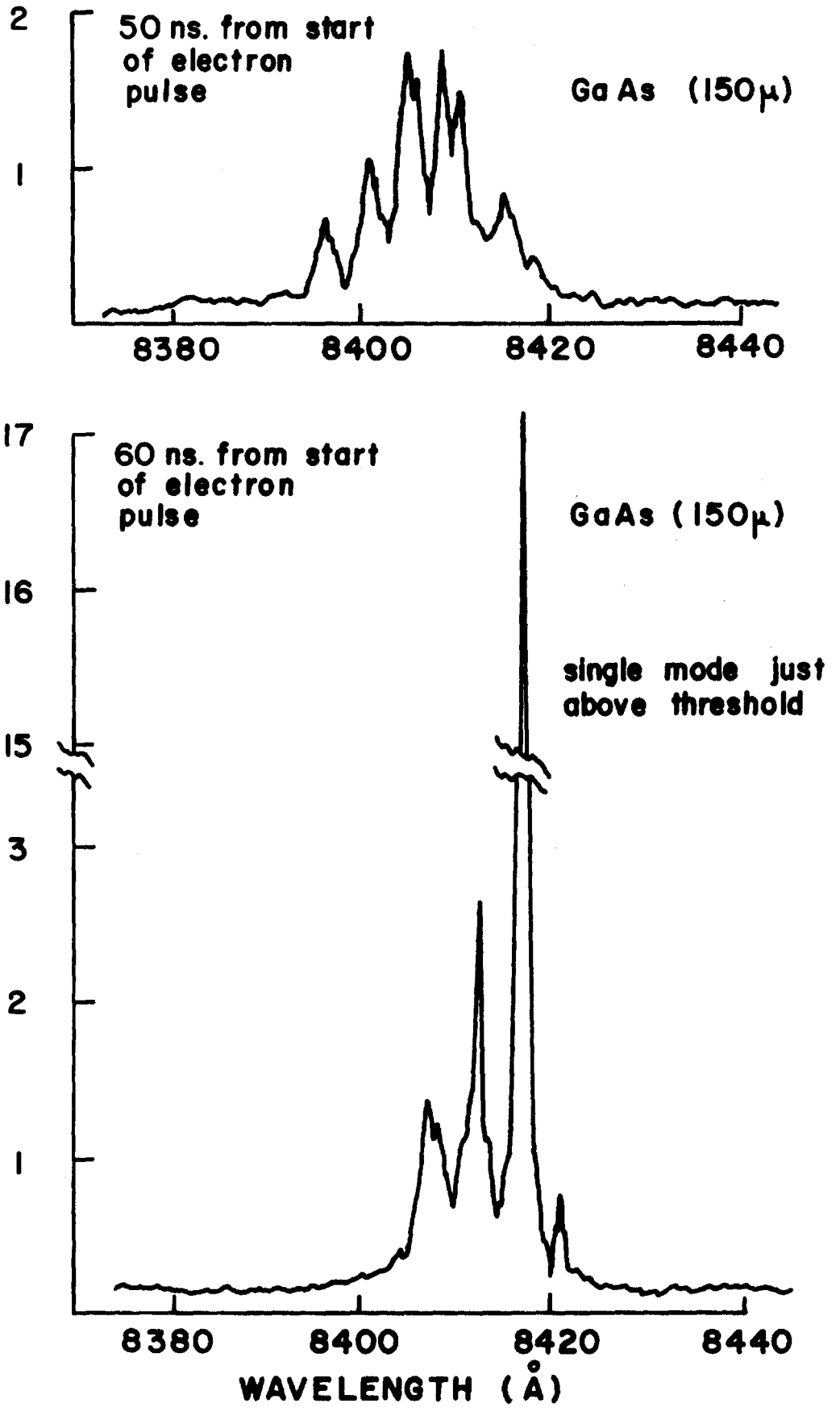
2
1
50 ns. from start of electron pulse
Ga As (150μ)
8380
8400
8420
8440
17
16
15
3
2
1
60 ns. from start of electron pulse
GaAs (150μ)
single mode just above threshold
8380
8400
8420
8440
WAVELENGTH (Å)

has been attained. The nature of the time behaviour of these spectra will be discussed in the next section.

3. Experimental Observations - Wavelength Tuning

In this section the first of the two major parts of the experimental data will be discussed - the tuning of the peak output of the stimulated radiation toward lower energies during the excitation pulse.

(a) General tuning behaviour

When the stimulated light output from pulse-pumped cavities of GaAs, CdS or CdSe is viewed at a given wavelength (using the monochromator) it peaks in time with a half-width of, typically, 10-20 ns. The light intensity peaks at greater delay times, t, from the start of the pump cycle as the wavelength of observation is increased as shown in Fig. 10. The pump current density is held constant. Since a plot of the delay time, t, at the peak of light output versus wavelength shows an approximately linear relationship, a tuning rate, R, in angstroms per nanosecond can be determined for each pump current density. It should be emphasized that this tuning rate relates only to stimulated emission and is usually faster than any shifts of the spontaneous emission.

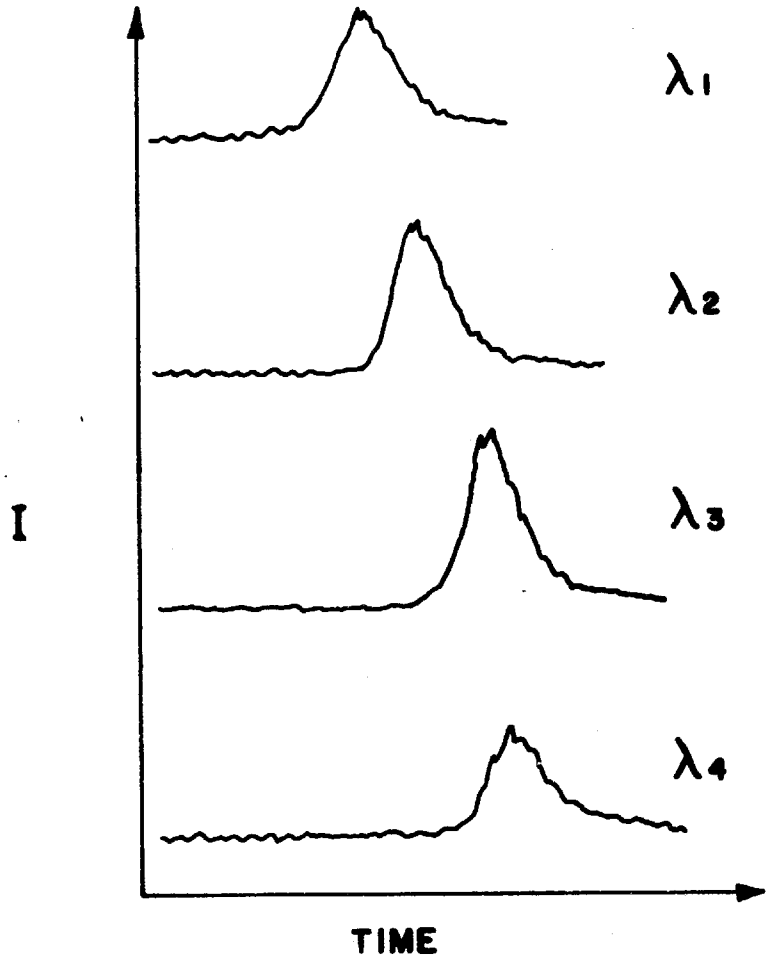

Fig. 10. Light pulses viewed through wavelength window (Typical).

This wavelength tuning consists of a shift of the stimulated emission peak toward longer wavelength which occurs at a faster rate than the band-gap shift due to temperature rise in the pumped region, (which the shift of spontaneous emission presumably reflects), and is found to occur in similar functional form and magnitude in CdS, CdSe and GaAs. Also the behaviour of this tuning with pump current density makes it distinct from the spontaneous emission tuning. In Figs. 11 and 12, the rates of stimulated wavelength tuning are plotted as a function of pump current density for samples of GaAs and CdSe. The important feature to note is that the initial increase in R to longer wavelengths with pump current density is followed by a saturation region. The occurrence of a saturation region well above laser threshold is not consistent with a previously proposed mechanism for wavelength tuning in semiconductor lasers [52]. These authors propose that tuning effects can be caused by a carrier-density dependent decrease in the band-gap energy because of screening of the crystal field by free carriers and because of interactions between carriers. This is discussed at greater length subsequently.

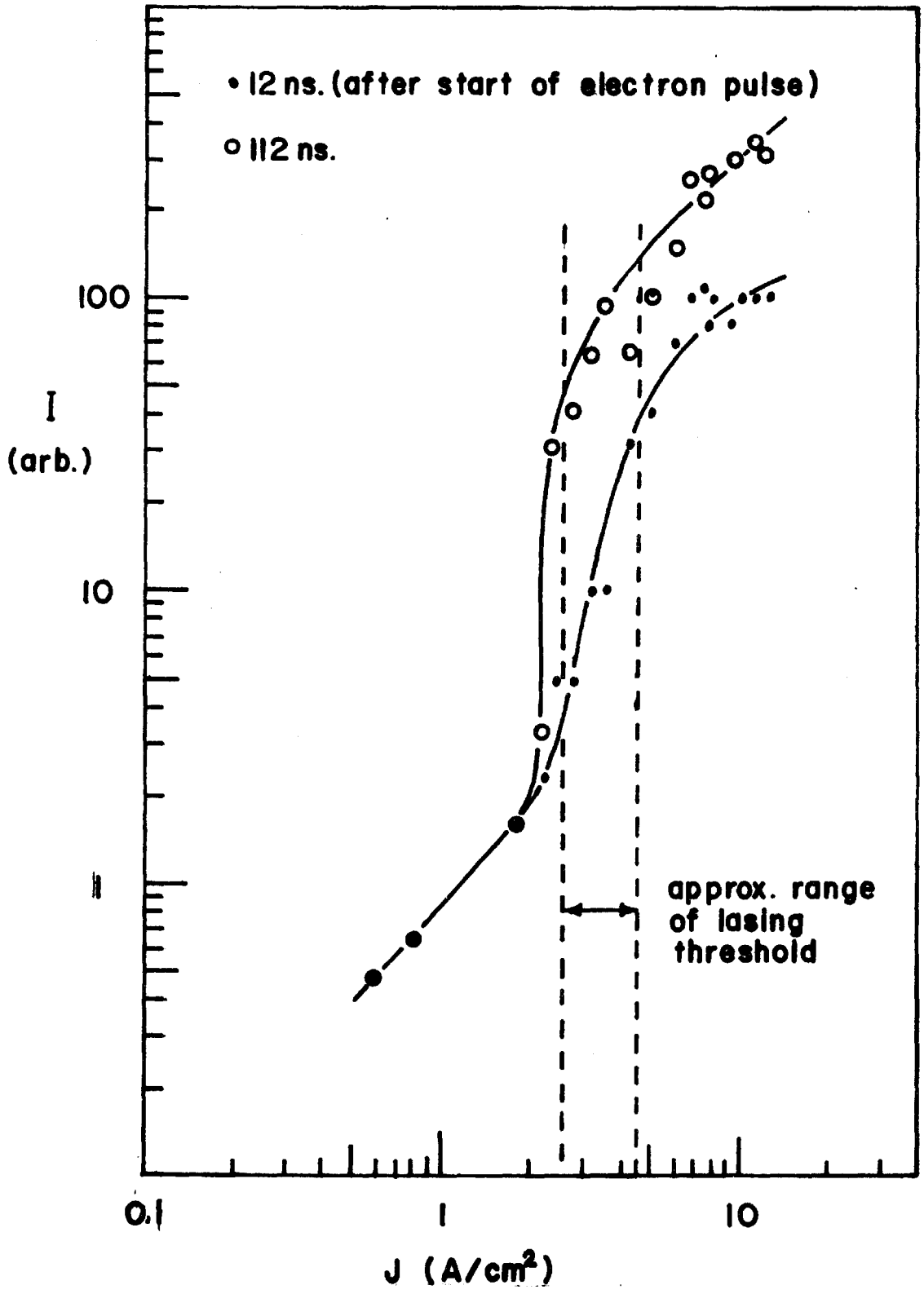

Fig. 11(a) Selected curves of light output intensity integrated over all wavelengths as a function of pumping current density with delay time after the start of the pumping pulse as a parameter. Conditions of view are 0° with 1° slit. Temperature is 77°K and beam voltage 40kV. The dashed lines indicate an operational range for threshold current density.

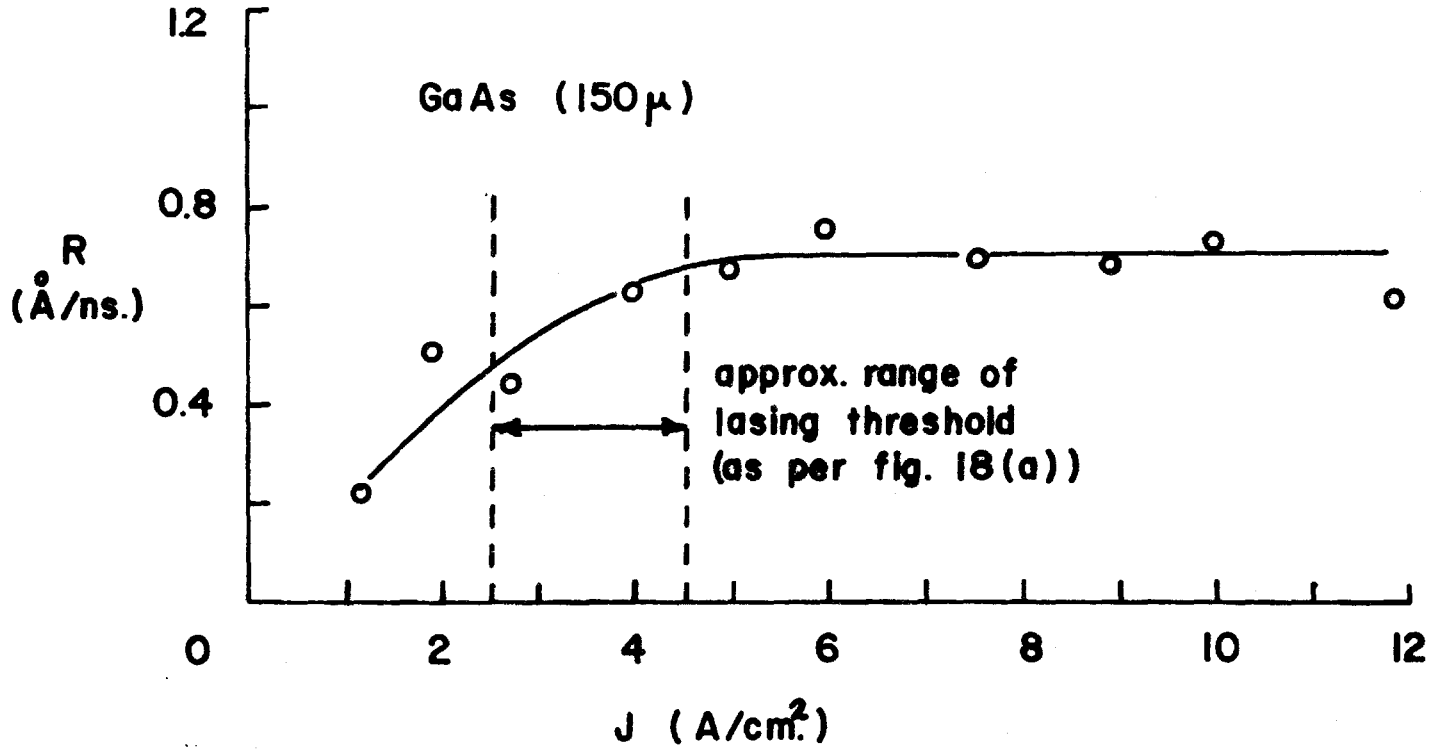

Fig. 11(b) Plot of the tuning rate, R, to longer wavelengths vs. pumping current density for a 150 long GaAs cavity. Beam voltage is 40kV and temperature is 77°K. Conditions of view are 0° with a 1° slit. Note the saturation of R above laser threshold.

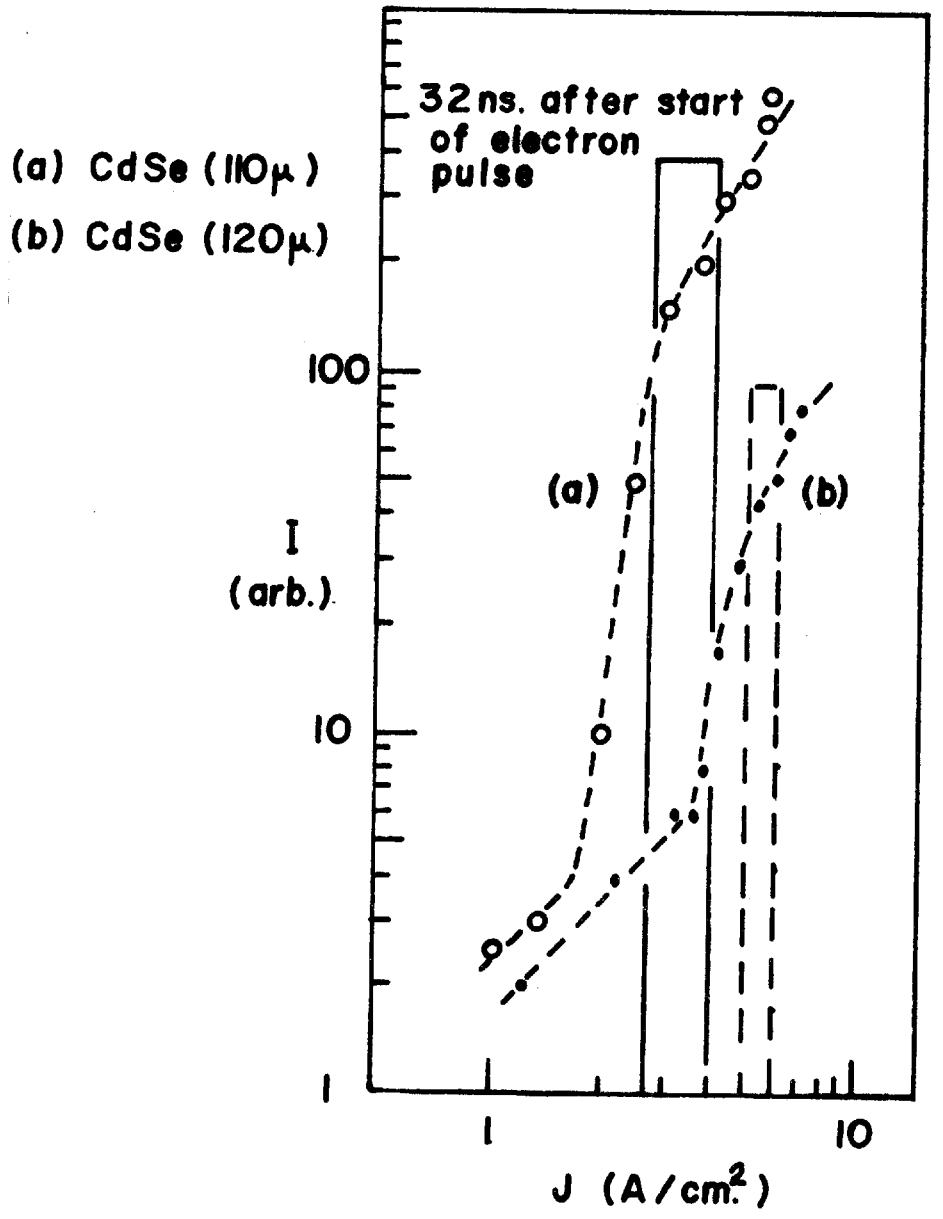

Fig. 12(a) Total light output intensity integrated over all wavelengths vs. pump current density for a delay time of 32 nanoseconds after the start of the pump pulse.

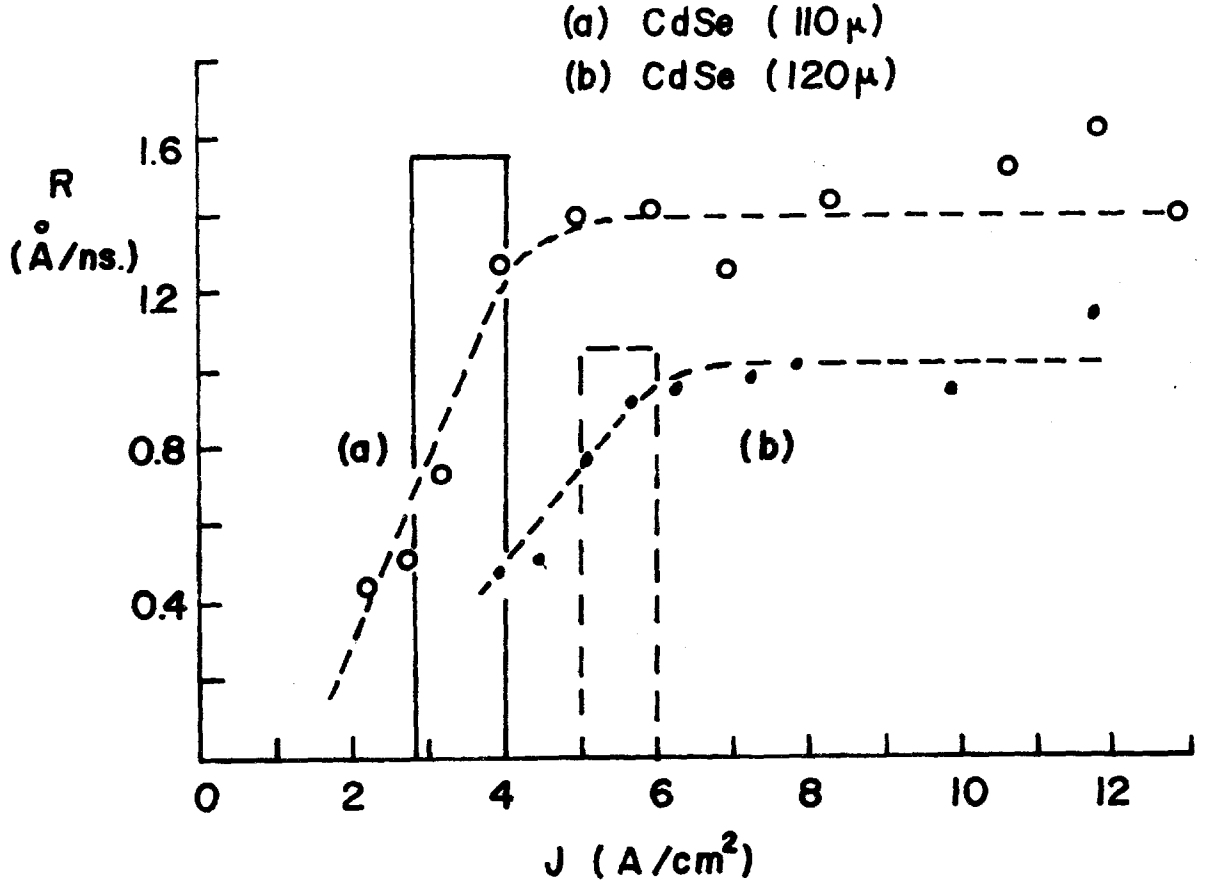

Fig. 12(b) Plot of the tuning rate, R, to longer wavelengths vs. electron pump current density for two CdSe cavities, 110 μ long and 120 μ long. Beam voltage is 40kV and sample holder temperature is 77°K. Conditions of view are 10° with 1° slit. The rectangular boxes indicate the ranges of laser threshold current density. Note that the saturation of R is correspondingly different.

(b) Relationship between Wavelength Tuning and Lasing Threshold

Comparison of the tuning rate R with a plot of light output intensity as a function of beam current density indicates that the saturation region of R is closely related to lasing threshold. Fig. 11(a) shows the intensity vs. beam current density curves for GaAs (150 μ) at two selected delay times following the initiation of pumping. The output light intensity is integrated over all wavelengths. Using the criteria discussed in the previous section on laser threshold, an operational range for threshold current density was established in the region just prior to the second linear region of the intensity curves. As described earlier, lasing threshold is a function of time. For the 150 μ crystal, threshold occurred at lower current densities for longer delay times after initiation of the pumping pulse. Although threshold is a function of time, virtually all of the stimulated emission occurs in a small range of delay time after the start of the pump cycle. This range is approximately bounded in time by the two curves shown in Fig. 11(a). The dashed lines serve to indicate an effective median for each current threshold range corresponding to any given delay-time intensity curve. These effective medians, in turn, serve to identify our operational threshold-current range. It is

apparent that the saturation of the tuning rate R can be associated with the second linear region of the light-output intensity above the lasing threshold-current range. The region over which the tuning rate is changing and approaching saturation is associated, in part, with the threshold current range itself.

Figure 12(a) shows a plot of light output intensity integrated over all wavelengths as a function of pump current density for two CdSe cavities (110 μ and 120 μ). Both curves are plotted for delay time of 32 ns. after the start of the pump pulse. The reasons for delays of this magnitude will become clear in the later analysis. To facilitate presentation of the data,only one curve per sample rather than two as in Fig. 11(a) is shown. The rectangular box regions indicate the ranges of laser threshold-current density and that these are significantly different for the two cavities. The 32 ns. delay curves were selected as typical of those obtained in the threshold-current range. In CdSe the conditions of view were at 10° with a 1° slit. The tuning of the spatial mode in CdSe was significantly different in this respect from GaAs. For the region of delay times over which most of the stimulated emission occurred, the major portion of the radiation was emitted in the region of 10° with respect to the cavity axis. Figure 12(b) also shows the tuning rate R against pump current density for the

corresponding intensity curves. Both samples show the saturation effect but they occur in different regions corresponding to the two different laser threshold-current density ranges.

To investigate the implications of this experimental data, we need three further types of measurement; (1) measurements of tuning rate and intensity curve for a non-lasing crystal; (2) measurements on a single sample in which lasing threshold can be changed; (3) measurements of the rate of spontaneous emission tuning.

(1) Figure 13 shows the results of light intensity and tuning rate measurements on a high cavity loss (non-lasing) GaAs crystal. The intensity plot (Fig. 13(b)) shows only a linear spontaneous emission region and indicates that this crystal did not reach a lasing condition. Furthermore, no well-defined frequency or spatial mode patterns could be observed at the highest pump current densities available. Fig. 13(a) is the corresponding plot of tuning rate R vs. pump current and shows no saturation of the tuning rate. In fact the tuning rate reaches a value twice the saturation value of the previous sample.

(2) Measurements in which the lasing threshold is changed on a single sample can be accomplished by using the electron beam voltage as a parameter. Figure 14(a) shows the light output, integrated over wavelength and time, as a function of electron beam current density for a GaAs crystal

Fig. 13(a) Plot of tuning rate, R, to longer wavelengths vs. pump current density for a 165 μ long GaAs high cavity loss (non-lasing) crystal. Beam voltage is 40 kV and holder temperature is 77°K. Conditions of view are 0° with 1° slit. Note that there is no saturation of R and that R reaches a value twice the saturation value in Fig. 18(b).

Fig. 13(b) Total light output intensity integrated over all wavelengths and all time as a function of pump current density. Conditions of view are 0° with a 1° slit. Beam voltage is 40 kV and holder temperature is 77°K. The plot shows only a linear spontaneous emission region and indicates that a lasing condition was not reached.

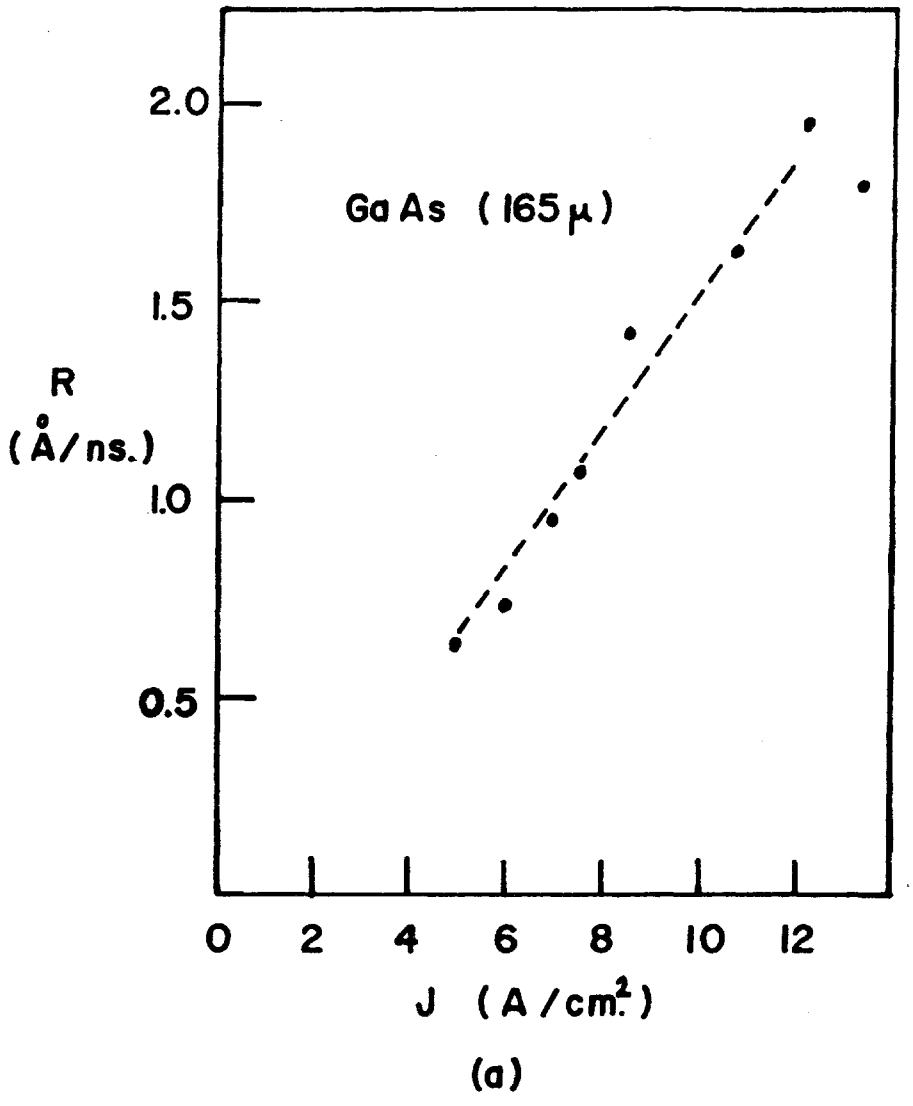
GaAs (165μ)
R
(Å/ns.)
2.0
1.5
1.0
0.5
0
2
4
6
8
10
12
J (A/cm²)

(a)

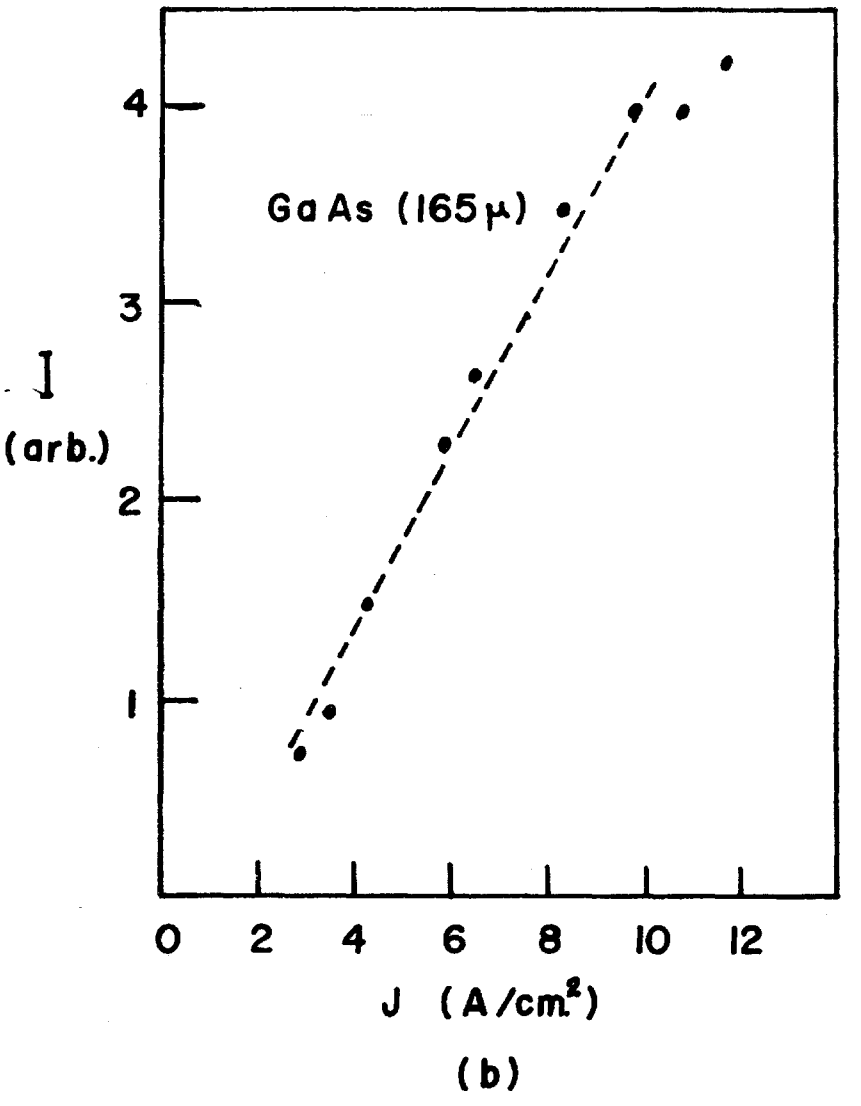
GaAs (165μ)
I
(arb.)
4
3
2
1
0
2
4
6
8
10
12
J (A/cm²)

(b)

Fig. 14(a) Light output, I, integrated over wavelength and time vs. pump current density, J, at three values of beam voltage. The regions of lasing threshold are marked.

Fig. 14(b) Tuning rate, R, vs. J for the three beam voltages. Holder temperature is 77°K.

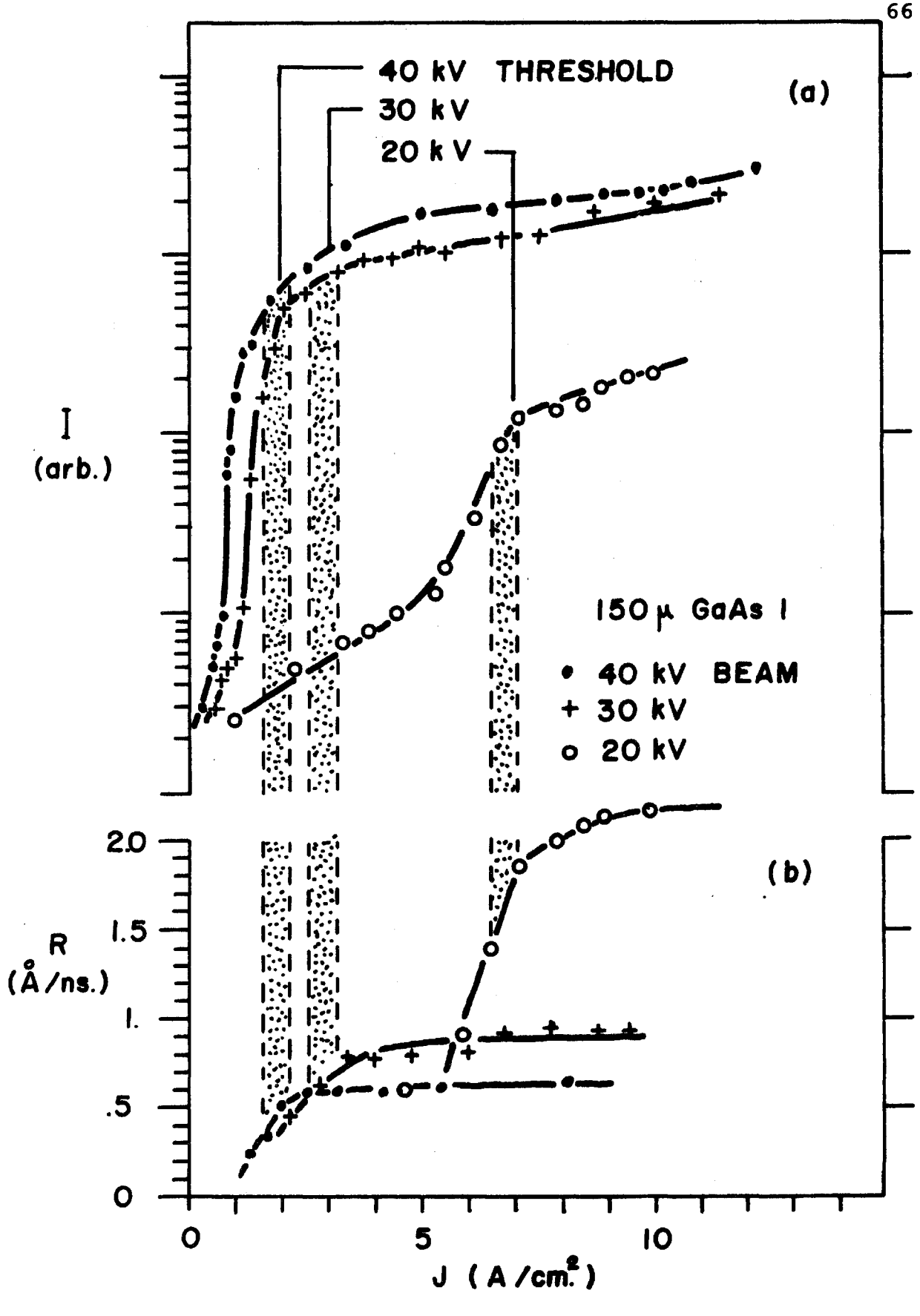
40 kV THRESHOLD
30 kV
20 kV
(a)
I
(arb.)
150 μ GaAs I
• 40 kV BEAM
+ 30 kV
o 20 kV
(b)
R
(Å/ns.)
2.0
1.5
1.
.5
0
0
5
10
J (A/cm²)

at three values of beam voltage. The range of pumping current densities corresponding to lasing threshold was determined by the previously mentioned criteria and is shown at each voltage. To facilitate comparison with the tuning rates the intensity plots are presented in semi-log form. The increase in lasing threshold as the beam voltage is lowered is to be expected due to the consequent change in the width of the gain region in the crystal. This has the effect of increasing the influence of surface losses and emphasizing the importance of losses associated with spreading of the laser beam into loss regions of the crystal. The mean depth associated with electron beam energy dissipation increases by a factor of approximately three [20] as the beam voltage is lowered from 40 to 20 kV. As will be shown in Chapter 4, this change is predicted to cause a large increase in diffraction loss and an associated increased threshold for lasing.

Figure 14(b) shows the rate of tuning of the stimulated emission vs. beam current density for the three values of beam voltage corresponding to Fig. 14(a). These curves all exhibit a linear increase of tuning rate at low currents and a saturation of the tuning rate at higher currents. Comparison of Fig. 14(a) and 14(b) shows the close correspondence between lasing threshold and the onset of saturation in the tuning rate.

Figures 15(a) and 15(b) show the results of the same type of measurements taken on a second crystal with higher lasing threshold current. The same correspondence between lasing threshold and the onset of tuning rate saturation is apparent. Both sets of data show a definite trend between the level at which the tuning rate saturates and the beam voltage. There is an increase in the magnitude of the saturated tuning rate with higher laser threshold. This observation is consistent with the linear increase of tuning rate as a function of beam current density previously observed in non-lasing cavities.

(3) In order to show that thermal tuning of the band edge was not a major contributing effect in this tuning, the rate of tuning of the spontaneous emission was measured. There is very little stimulated emission emerging from lasing crystals of GaAs and CdSe at angles greater than 25° to the cavity axis in the quadrant between the electron beam and the cavity axis. Therefore, by observing the wavelength envelope of the structureless spontaneous emission at 45° with respect to the cavity axis at regularly spaced sets of times following the start of the excitation pulse, the rate of band edge tuning caused by heating could be measured for various electron beam currents. This experimental arrangement is used to obviate the possibility of stimulated emission influencing the observations through angular effects such as those previously mentioned and which will be

Fig. 15(a) Light output, I, integrated over wavelength and time vs. pump current density, J, at three values of beam voltage. The regions of lasing threshold are marked.

Fig. 15(b) Tuning rate, R, vs. J for the three beam voltages. The holder temperature is 77°K.

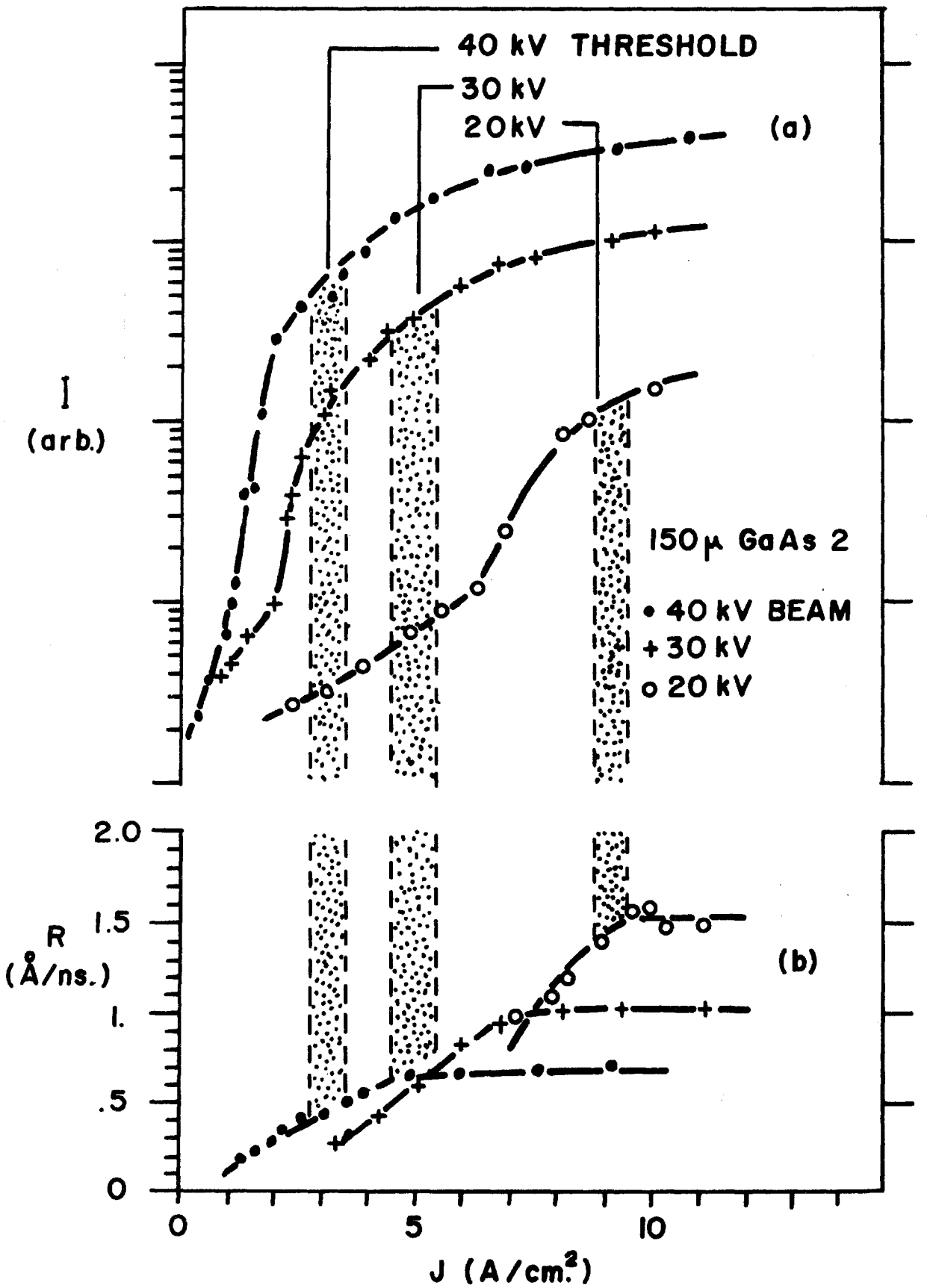
40 kV THRESHOLD
30 kV
20kV
(a)
I
(arb.)
150 μ GaAs 2
• 40 kV BEAM
+ 30 kV
o 20 kV
2.0
1.5
R
(Å/ns.)
1.
.5
0
(b)
0
5
10
J (A/cm.²)

described in detail in the following sections. The rate of tuning of the spontaneous emission was linear with beam current density and was roughly an order of magnitude lower than the tuning rate of the stimulated emission at comparable pumping current densities. For example, in the GaAs sample (150 μ), at a current density of 8.6 A/cm^2., the tuning rate of the spontaneous emission was 0.13 Å/ns. to longer wavelengths. The total shift amounted to approximately 25 percent of the 110 Å half-width of the emission line. Since the stimulated tunes much faster than the spontaneous emission, the stimulated tuning cannot be directly related to a band-gap shift.

In CdSe, for a 120 μ cavity at 8.0 A/cm^2. the spontaneous tuning was measured at 0.18 Å/ns., somewhat higher than that for GaAs. Since the spontaneous tuning rate was linear with beam-current density and was roughly an order of magnitude lower than the tuning rate R of the stimulated emission at comparable pump current densities, the stimulated tuning in CdSe cannot be directly related to a band-gap shift.

It has been consistently observed that the rate of tuning of the stimulated emission peak to longer wavelengths becomes constant for semiconductor lasers of both CdSe and GaAs operated in the regime reasonably well above threshold (this is also true for CdS [53] over the limited range of current densities investigated.) That is, the rate of tuning to long wavelengths is found, within experimental error, to

be constant whenever the laser is operating in the second linear regime of the light output curve against pumping current. Furthermore, it has been observed that this tuning rate does not saturate in poor-quality cavities for which the threshold of laser emission is not attained, but simply continues to increase (approximately linearly) as the pumping current density increases.

Consequently, we conclude that the presence of saturation in the wavelength tuning rate may reasonably be associated with the presence of strong lasing action. Furthermore, in the lasing crystals of CdSe and GaAs examined, there is a good correlation between the onset of saturation in the wavelength tuning rate and the approach to lasing threshold (i.e., the superlinear region of the laser intensity curve) for a given crystal.

Apparently, an explanation of this behaviour requires a mechanism for shifting the peak of the stimulated emission with respect to the band-edge, and the shift must be toward longer wavelengths. In Chapter 4, a mechanism based on wavelength dependent losses in the laser is presented which can account for faster than band-gap tuning of the type observed in non-lasing crystals. The simple analysis presented does not, however, account for above threshold tuning effects.

4. Experimental Observations - Angular Tuning

The spatial inhomogeneity of the non-equilibrium carrier density, and hence the gain, which appears when a semiconductor is excited with an electron beam has a considerable influence on the characteristics of the laser radiation. In particular, the far-field pattern of the radiation from electron-beam-pumped lasers is not symmetrically disposed about the cavity axis, but rather is deviated with respect to the axis at angles up to 30°. Similar, but smaller, angular deviations have been observed previously in GaAs electron-beam-pumped lasers [50] and have been ascribed to spatial variations in the phase-front of the near-field laser cavity modes.

Our experimental observations on GaAs and CdSe reveal a previously unreported feature of this effect. Not only does the angular deviation of the laser mode exist, but it also changes as a function of time during each pump cycle. Typically, the far-field diffraction patterns of the spatial modes have half-widths of 5° - 10°, deviated initially between 10° and 30° from the cavity axis. The deviation angle is found to decrease during each pulse by a factor of two or more. This general behaviour occurs in both II-VI

and III-V materials, but the specific behaviour in each material is dependent upon its optical and thermal properties.

(a) Method of Observation of Far-Field Modes

The method that was adopted for observation of the far-field mode patterns from electron-beam-pumped GaAs and CdSe is shown in Fig. 16. The emitted light in a given radial direction in the plane containing the laser axis and the electron beam path was detected by a photomultiplier tube employing a pinhole aperture. The detector signal was observed using a sampling oscilloscope triggered by a portion of the backscattered electron beam. The oscilloscope display could then be photographed for permanent record. By using the results of several such measurements, the time variation of the laser far-field pattern could be obtained. This measurement technique involves an integration over the wavelengths present in the output. The value of θ_p obtained is less sensitive to this integration than is the width of the far-field mode. This constitutes one reason for using θ_p in the comparison between theory and experiment in addition to those given in Chapter 4.

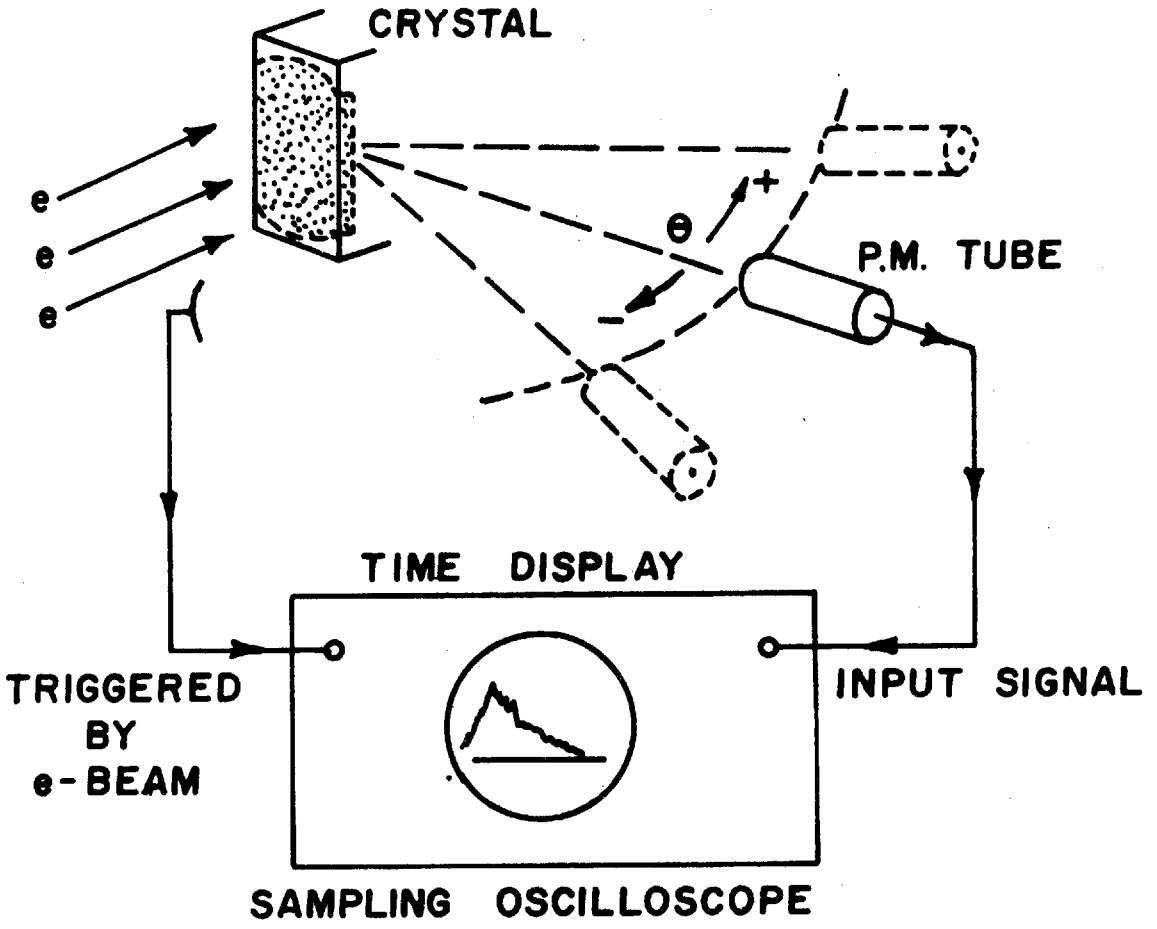

Fig. 16. Diagram of the experimental arrangement used for making angular tuning measurements.

(b) Experimental Observations:

(i) Gallium Arsenide

Figure 17 shows a typical set of spatial mode intensity patterns from GaAs plotted as a function of deviation angle from the cavity axis (0°) observed at different times following the start of the pump pulse. Negative angles represent the quadrant toward the electron beam. The radiation intensity shapes are roughly symmetric with half-widths of 5° to 10°. The important feature to note here is that the deviation angle changes considerably as a function of time during the output pulse. Comparison of Figs. 3 and 17 shows the similarity between the theoretical calculations and experimental observations particularly with respect to the mode asymmetry. The angular tuning of the far-field mode can be interpreted theoretically in terms of a time-varying refractive index step.

The results of a more detailed study of the far-field mode patterns from GaAs, using beam voltage and current density as parameters, are shown in Figs. 18 and 19. Figure 18 shows the relation between the deviation angle of the peak of the radiation pattern and time after the start of the pump cycle at a beam voltage of 30 kV for several values of beam current density. Lasing thresholds at this voltage

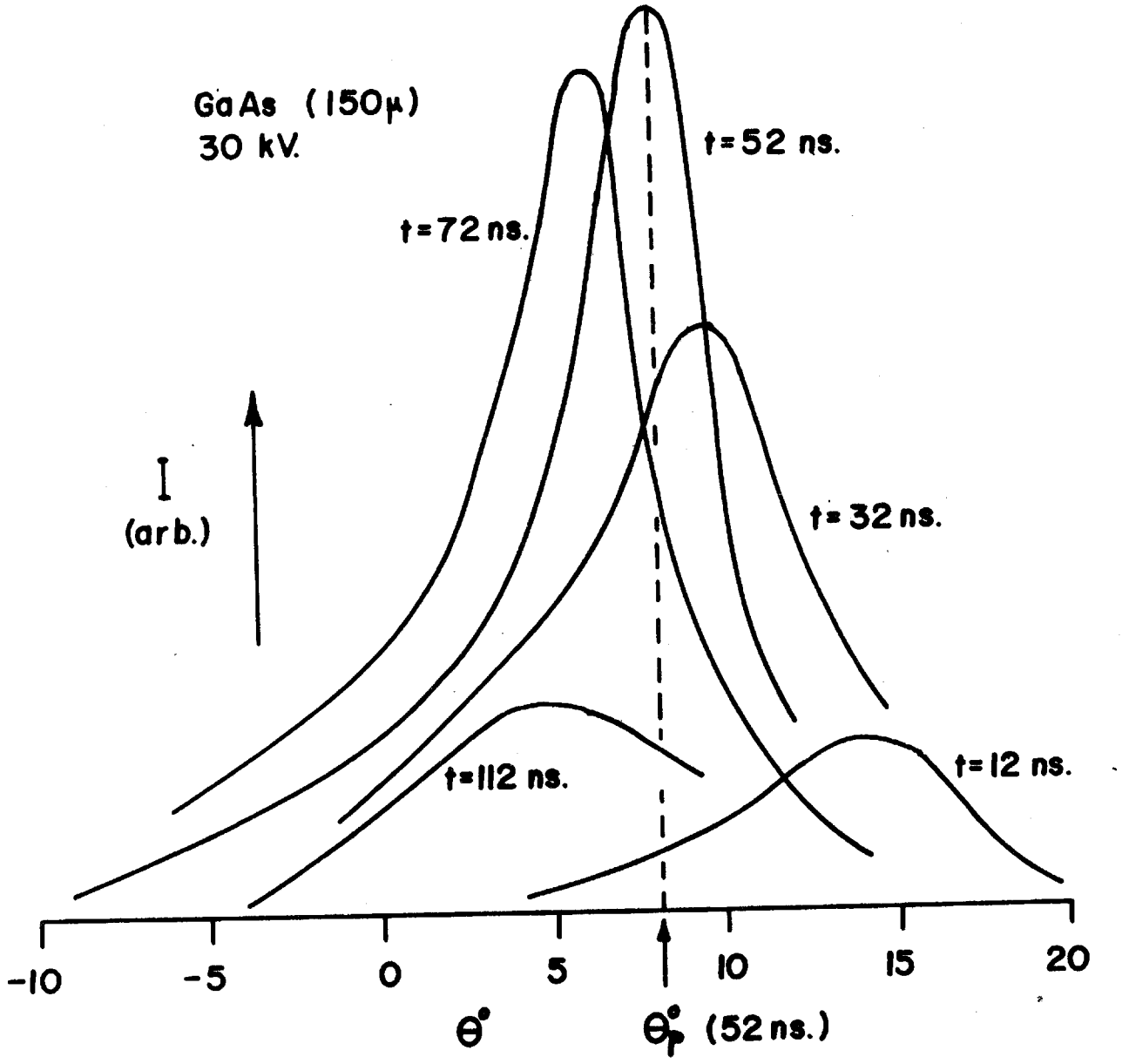

Fig. 17. Experimental observations of far-field radiation pattern from GaAs at a beam voltage of 30kV, current density of 7.0 A/cm^2 and a holder temperature of 77°K. The observations are made at several times following the start of the pump cycle.

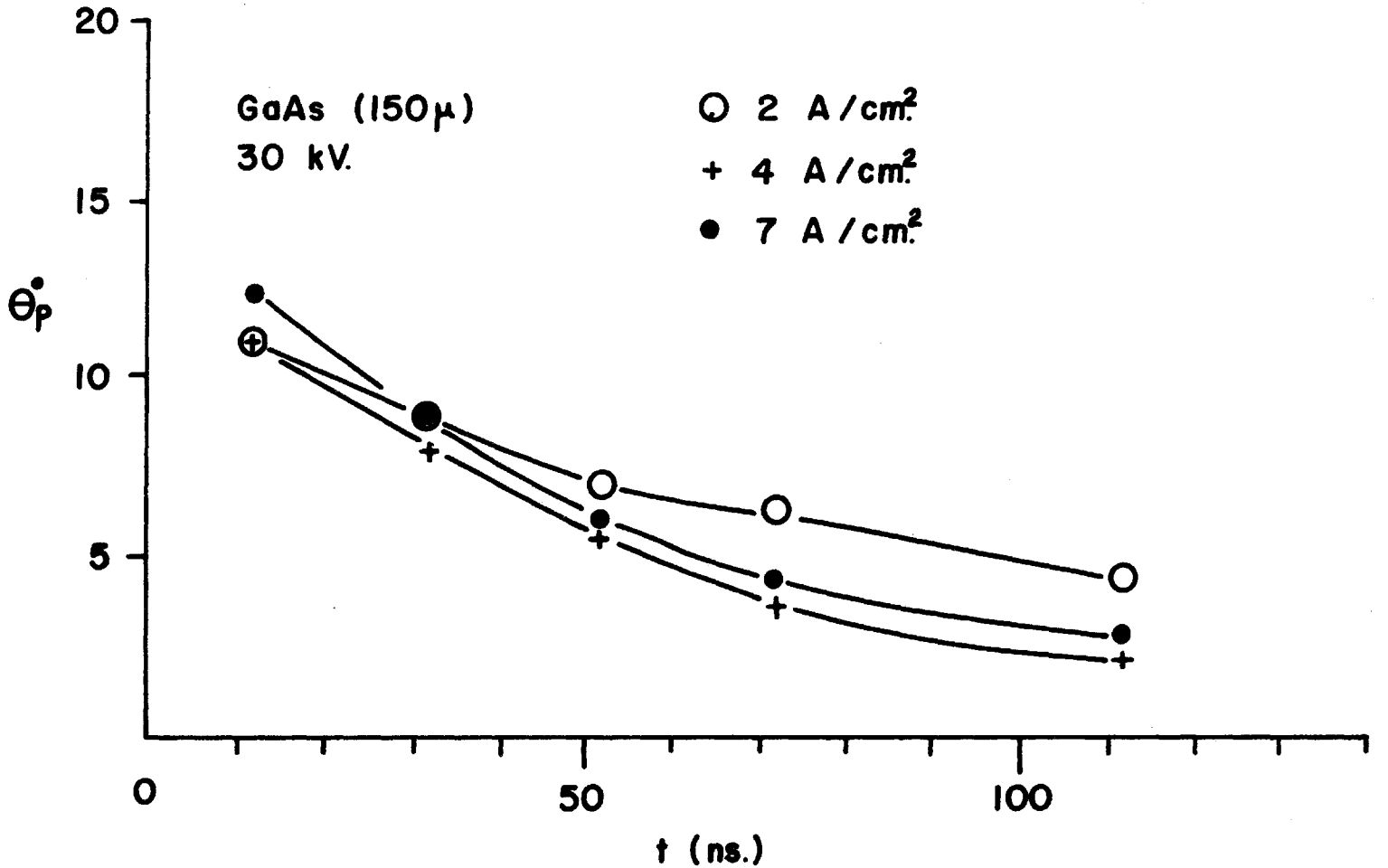

Fig. 18. Experimental observations of the rate of tuning of the deviation angle of the peak of the far field radiation pattern from GaAs, θ_p, at three values of electron beam current. Holder temperature is 77°K.

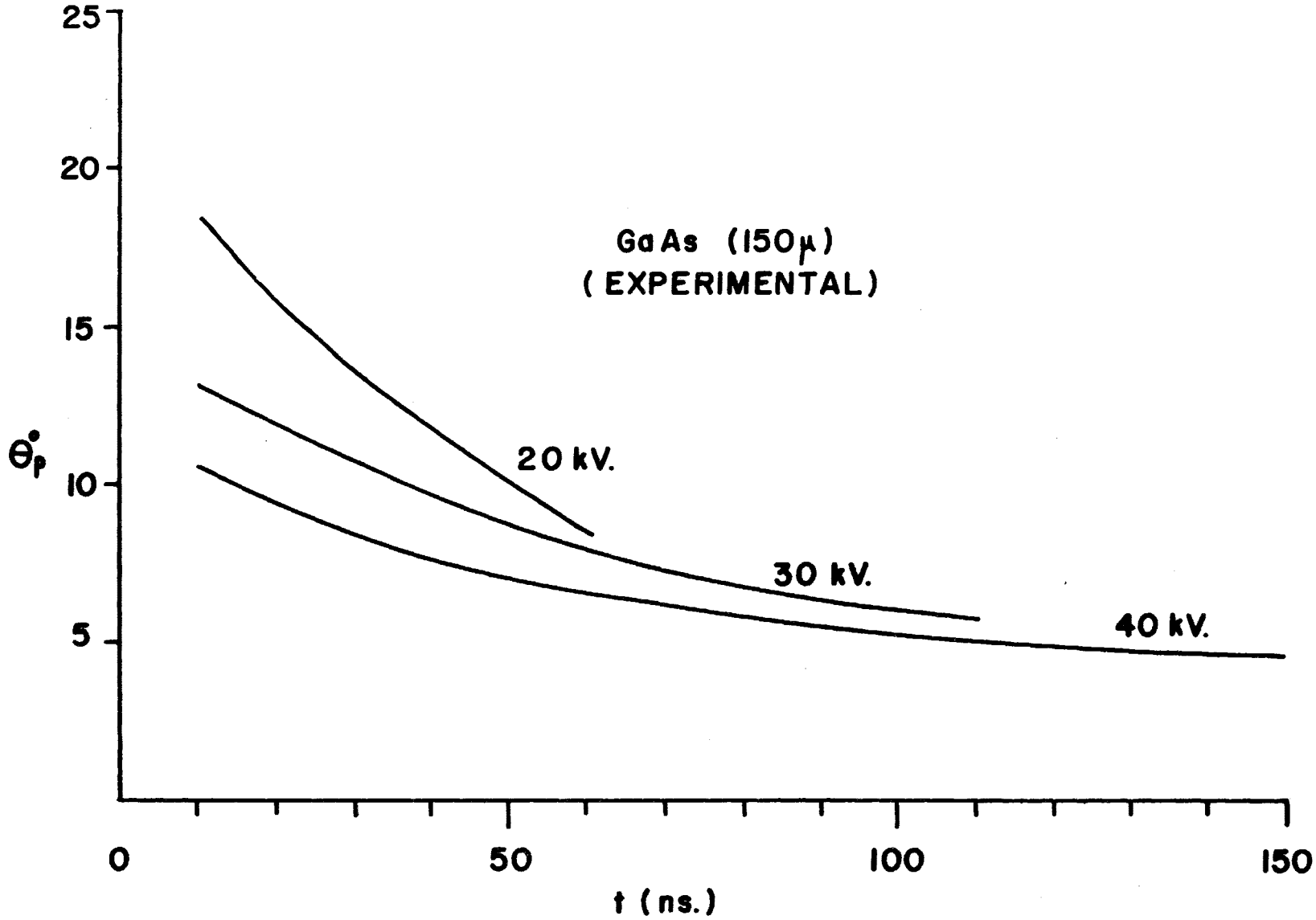

Fig. 19. Measured rates of tuning of θ_p from GaAs at three values of pump voltage. The curve at each voltage is an average over several values of pump current density. Holder temperature is 77°K.

occurred at approximately 1.8 A/cm^2. The general trend of the deviation angle is from an initial off-axis position toward the cavity axis. Within experimental error there is no clear dependence of the time variation of θ_p on beam current density. There is, however, a definite trend as beam voltage is changed. Figure 19 shows the results of measurements, averaged over different current densities, taken for three beam voltages. The initial deviation angle and subsequent time variation of θ_p are evidently functions of beam voltage. The laser output pulse duration decreased with decreasing beam voltage. The maximum deviation angle observable was limited to approximately 25° by the aperture of the sample-housing vacuum chamber.

(ii) Cadmium Selenide

For CdSe the angular tuning is generally similar in form to that observed for GaAs. Figure 20 shows a typical set of far-field radiation patterns from electron-beam-pumped CdSe measured at several times following the start of the pump cycle, using a beam voltage of 40 kV and a current density of 10 A/cm^2. As with GaAs there is a trend of the peak of the radiation pattern from an off-axis position toward the cavity axis. In GaAs the rate of angular tuning was practically independent of beam current density.

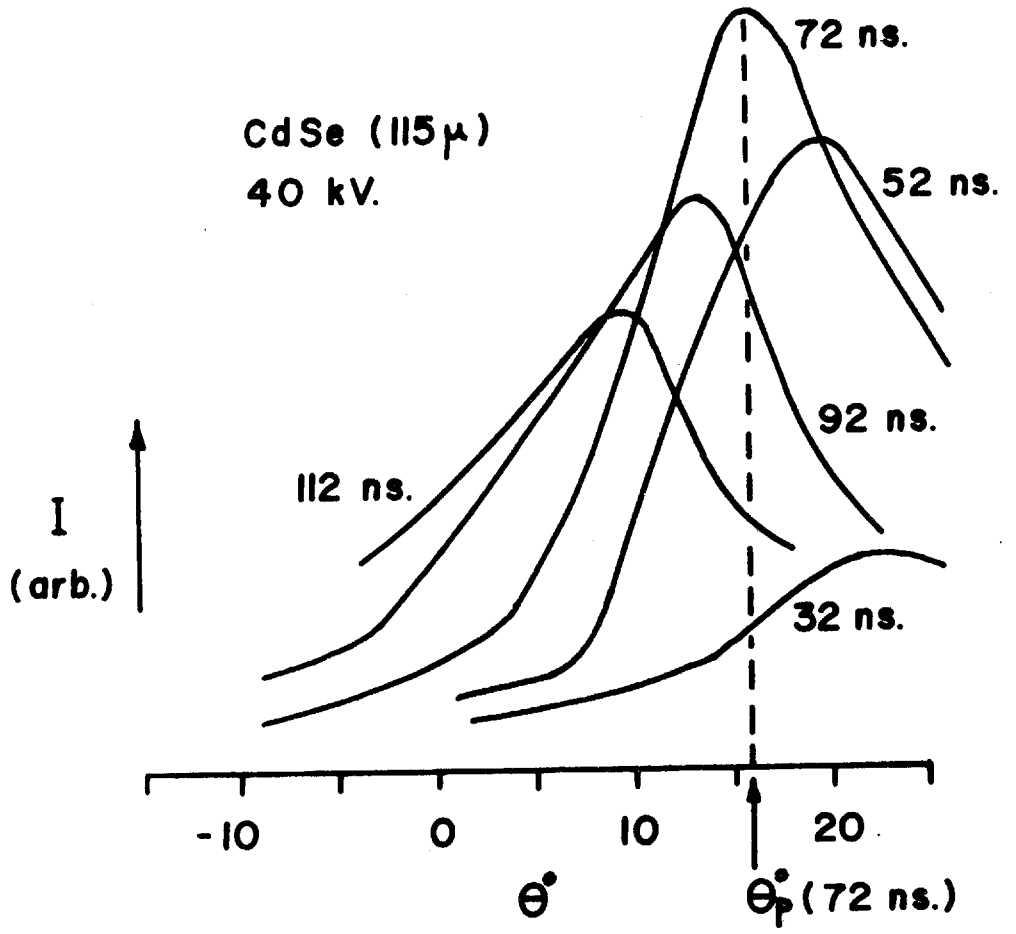

Fig. 20. Experimental observations of far-field radiation pattern from CdSe at a beam voltage of 40kV, a current density of 10 A/cm^2 and a holder temperature of 77°K. The observations are made at several times following the start of the pump cycle.

However, in CdSe there is a clear relationship between the two - the rate of angular tuning increases with beam current density (Fig. 21). This difference between GaAs and CdSe can be related to different origins for the index change in the two materials, in agreement with the theory.

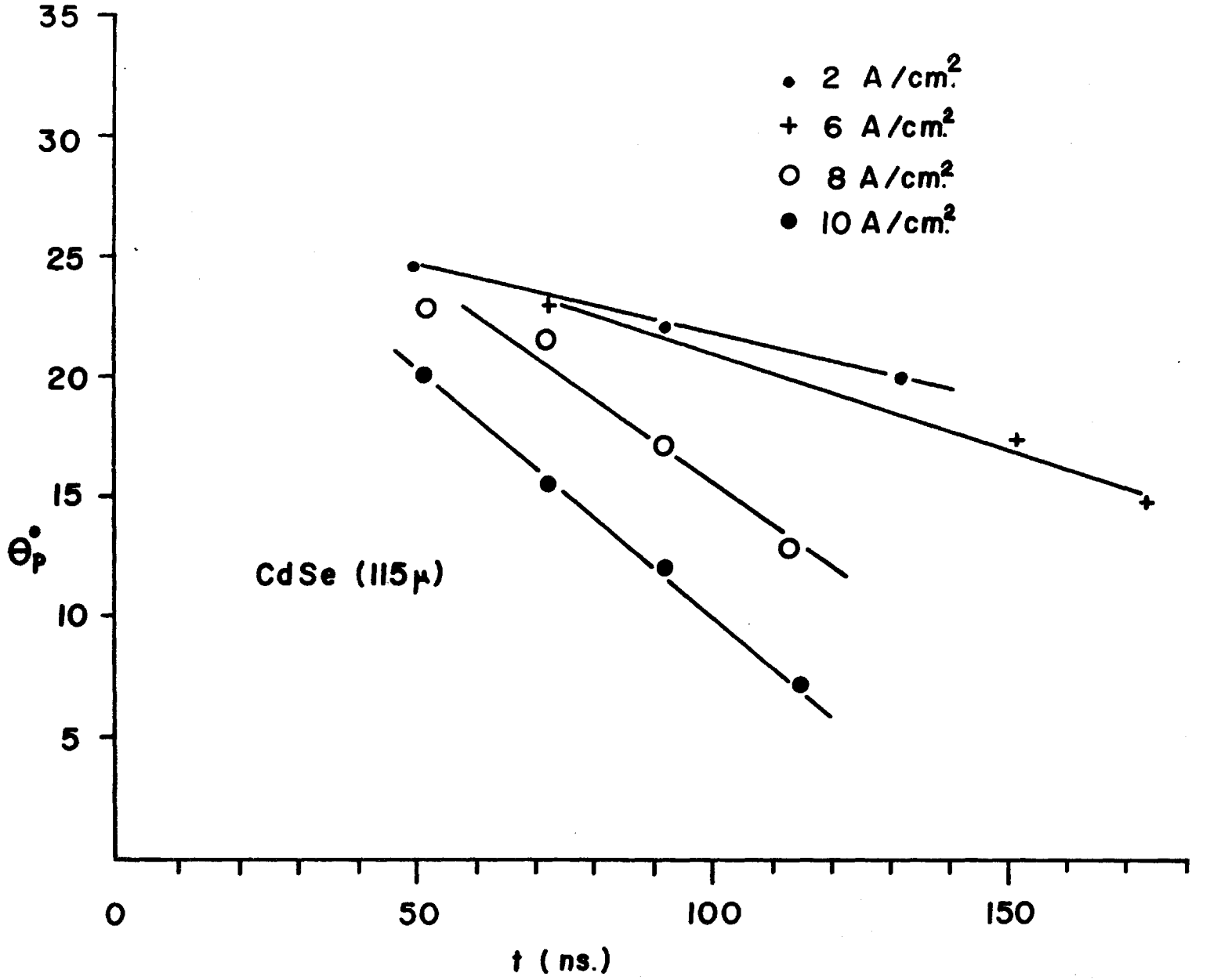

Fig. 21. Experimental rates of tuning of θ_p for CdSe at a beam voltage of 40kV and several values of beam current density. The holder temperature is 77°K.

CHAPTER IV

ANALYSIS OF EXPERIMENTAL DATA

1. General

In the experimental work, two apparently independent "tuning" effects were observed in both GaAs and CdSe - wavelength tuning toward lower energies and angular tuning of the spatial radiation mode. We have applied the cavity theory to an analysis of these experimental observations with varying degrees of success. The observed angular tuning of the far-field modes in both GaAs and CdSe is well explained by the analysis and these results are presented in the next section.

It was shown in a previous chapter that diffraction losses can be very large in this type of laser system and are determined to a large extent by the difference in refractive index between the pumped and unpumped regions of the cavity for a given pump voltage. The index difference is, in turn, a function of both wavelength and temperature in the gain region. This behaviour generates a loss which varies with both wavelength and temperature (or time). A sufficiently large effect of this nature has evident implications for wavelength tuning. In section 3 we investigate the impact of this wavelength and temperature

dependent loss on the dynamical variations of lasing wavelength in both GaAs and CdSe. It is found that a proper account of this loss (subject to limited knowledge of material parameters) generates a wavelength shift of the lasing output which is a good deal faster than the tuning of the bandgap. This tuning rate is sufficient to generate wavelength tuning of the magnitude observed experimentally. However, this model does not account in any obvious way for the observed saturation in the wavelength tuning rate for pump current densities above threshold.

2. Application of the Theoretical Model to the Analysis of Angular Tuning

Before proceeding with this analysis it seems appropriate to give a physical picture of angular tuning to facilitate the understanding of the subsequent calculations. In Fig. 22 the radiation intensity pattern of an idealized laser mode (the portion that is travelling in one direction) is shown on the scale of the crystal gain region width, d. The amplitude of the mode is zero at the crystal surface, reaches a maximum in the gain region, and tails off towards zero in the unpumped, lossy region further into the crystal. During propagation part of the mode (A) exists in the gain region and part (B) in the loss region. Now, by its very nature a mode cannot change its relative shape during propagation. It follows that, to maintain the shape, a net flow of energy must occur from A to B. Thus, if we consider the overall picture, the main energy flow is along the direction of propagation of the laser mode, but there is an additional component of energy flow directed into the crystal which is necessary to maintain the relative mode shape. This situation causes the laser mode to be emitted at an angle deviated with respect to the cavity axis. The loss associated with energy flow into the bulk crystal will hereafter

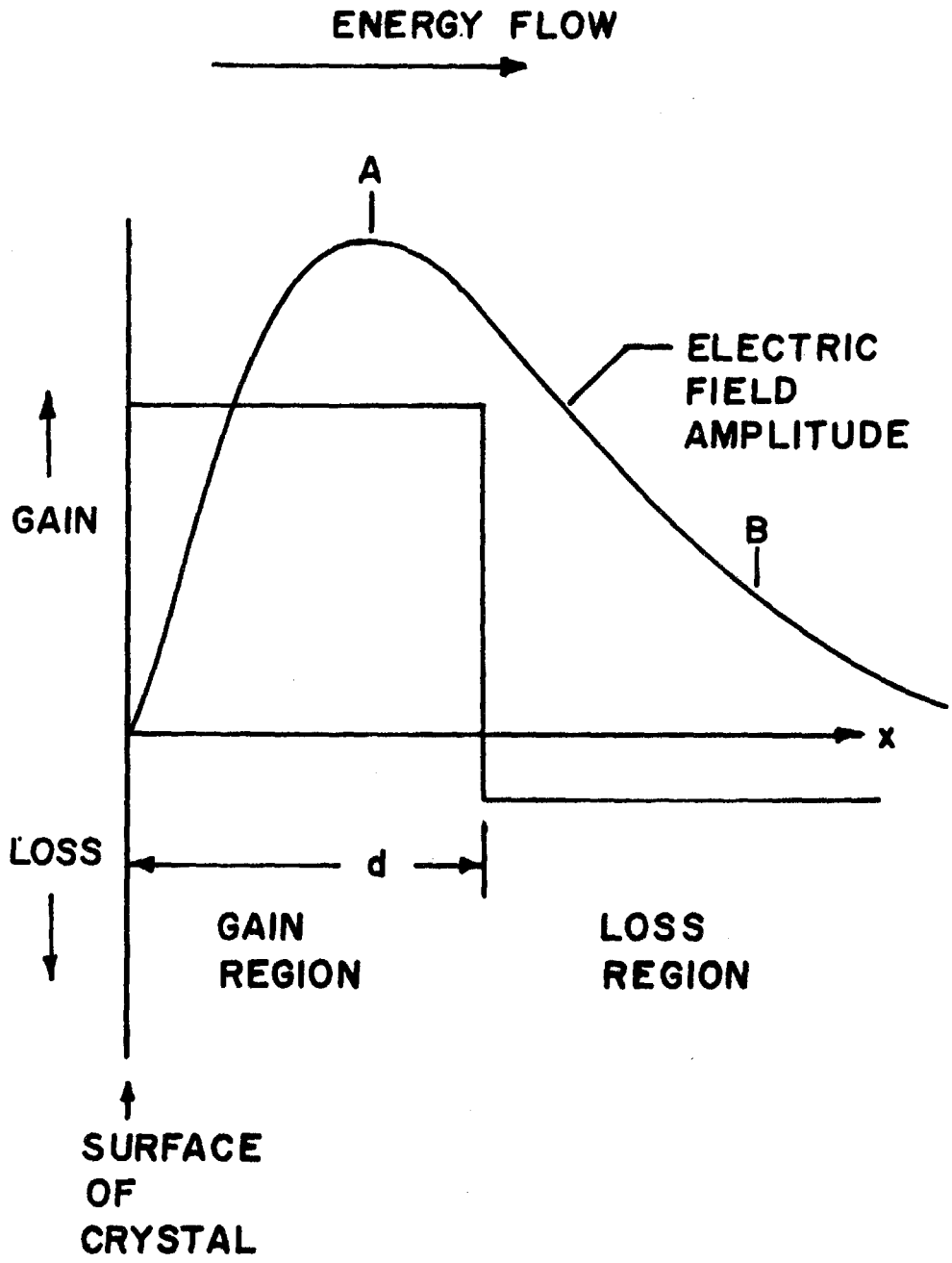

Fig. 22. Diagram of a near field mode profile relative to pumped region.

be referred to as diffraction loss. This diffraction loss can be many times larger than the losses due to imperfect reflection from the cavity ends. It, therefore, becomes apparent that the degree of deviation of the laser beam from the cavity axis will be determined by the amount of energy flow directed into the crystal relative to the main energy flow.

In Chapter 2 it was stated that the deviation of the peak of the far-field laser mode, θ_p, from the cavity axis was the most suitable parameter for comparing theoretical and experimental results. Consideration of the angular width of the far-field mode shows this to be an unsuitable parameter for analysis. Results predicted by the two models for angular width of the spatial modes were similar for values of α_s above 100 cm^{-1}. For lower values of α_s, however, the stepped index model predicted near-field modes extending further into the unpumped region than for the "$sech^2$" model and correspondingly narrower far-field modes. Moreover, both theories predict large changes in far-field mode width as a function of α_s. This makes the angular width of the far-field mode a particularly unsuitable parameter because of its sensitivity to the uncertainty in experimental knowledge of α_s.

On the other hand, predicted results for the deviation angle of the peak of the spatial mode, θ_p, from the cavity axis, show a relatively small theory dependence.

The two theories are essentially in agreement when the value of d, the width of the gain region, is adjusted to allow for carrier diffusion. Also both models indicate that the dependence of θ_p upon α_s is slight over large ranges of α_s. For these reasons θ_p was chosen as the most suitable parameter in the analysis of the far-field mode experimental results.

The theoretical models considered for the electron-beam-pumped system predict variations in the far-field mode width and deviation angle as a result of a time-varying index of refraction step. The magnitude of the index changes required to significantly affect the far-field pattern restrict the effects of potential significance to heating by the electron beam and index changes related to the presence of gain. Calculation of the magnitude of these effects in CdSe and GaAs [Appendix E] indicates that heating is the dominant mechanism in CdSe and gain dependence of the index in GaAs. This has the consequence that angular tuning should be dependent on pump current density in CdSe and relatively independent of that quantity in GaAs. This prediction is borne out well by experiment. Details of the fit between theory and experiment for the two materials is described below.

(a) Cadmium Selenide

In this material, index changes due to heating of the crystal by the electron beam are large in comparison with those due to differences in gain. In CdSe, optical loss in the unpumped region for the range of wavelengths over which we observe lasing (6900 Å to 7000 Å) can be taken to be between 5 cm^{-1} and 50 cm^{-1} [34]. The effective gain region width is small because of the small penetration depth of the electrons [20] and the short diffusion length of the excitons - of the order of or less than 0.1 microns [31]. On this basis, average values of the gain region depth in our calculations for CdSe were taken to be 0.45 and 1.3 microns at 20 and 40 kV respectively.

Figure 23 shows the angular tuning predicted by the model for an electron beam voltage of 20 kV and the experimental measurements. The important features to note here are that both the deviation angles and the rate of angular tuning are accounted for at each current density.

In CdSe at 40 kV, the angular tuning is similar in overall behaviour to the 20 kV case, but the observed angular deviations are too large to be accounted for by the first order mode hitherto employed. However, as can be seen in Fig. 24 the use of a second order mode calculation

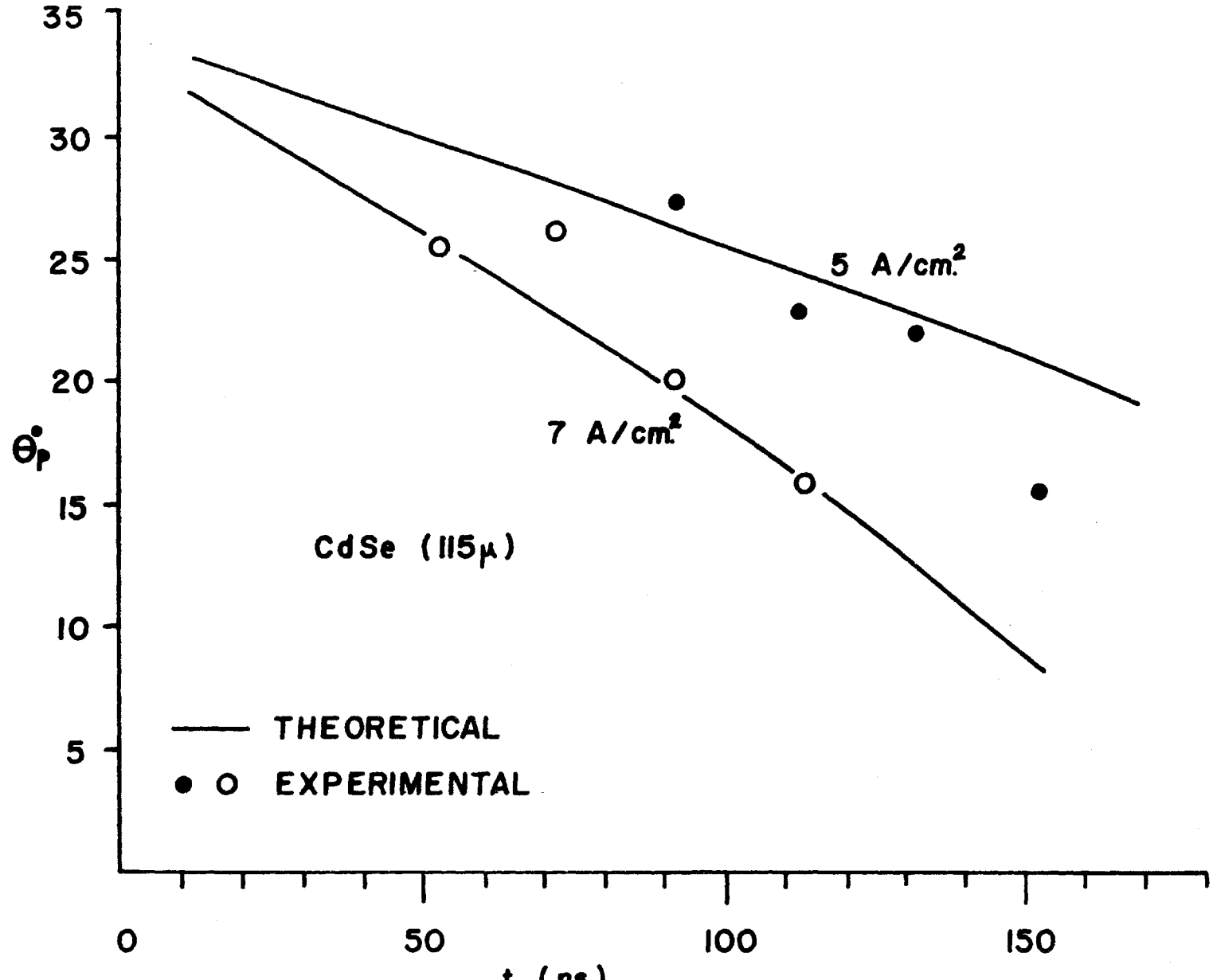

Fig. 23. Comparison between theoretical tuning of θ_p and experimental observation in CdSe at a beam voltage of 20kV and two values of beam current density. The holder temperature is 77°K.

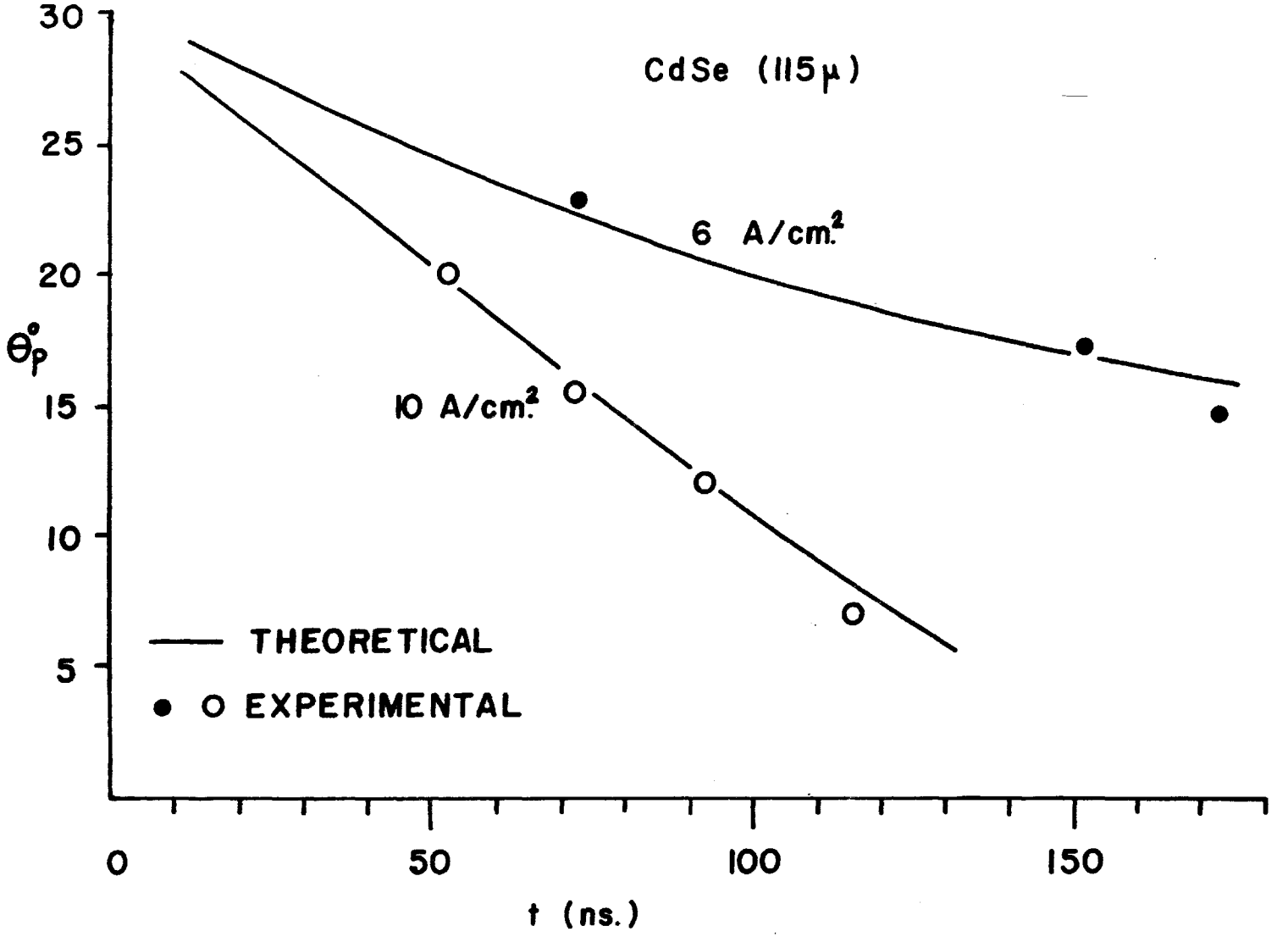

Fig. 24. Comparison between theoretical tuning of θ_p and experimental observation for CdSe at a beam voltage of 40kV and two values of beam current density. The holder temperature is 77°K.

provides an excellent fit to the observations. As the beam voltage is increased, the increased width of the gain region allows a second order mode to be supported more readily. Also the exciton diffusion length in CdSe is very short, thus permitting spatial hole-burning and the possible predominance of the second order mode. This apparently does not occur at 20 kV beam voltage because the narrow gain region causes the diffraction losses for the second order mode to be excessively high (approximately 10^4 cm^{-1}).

Observations with a beam voltage of 30 kV were inconclusive. The spatial modes observed were ill-defined, possibly suggesting a transition zone between the two orders of operation.

(b) Gallium Arsenide

In GaAs the dominant contribution to index differences between pumped and unpumped regions results from variations in gain and not temperature. Since this index change is dependent on wavelength, the wavelength tuning noted in the previous chapter will produce index changes with time, thereby causing an angular tuning of the laser beam. It was shown in Chapter 3 that the wavelength of the laser output from GaAs tunes toward longer wavelengths during each output pulse at a constant rate independent of pump current density, for

currents above lasing threshold. The saturated tuning rate is, however, a function of beam voltage [54]. The wavelength tuning for the crystal used in angular tuning measurements was:

beam voltage	20 kV	30 kV	40 kV
saturated tuning rate:	2.0 A/nsec	1.0 A/nsec.	0.7 A/nsec

Using these values for wavelength tuning and the previously described method for determining the wavelength dependence of the index step, the far-field modes can be generated as a function of time. The calculation becomes self-consistent once values of α_s, gain region depth d, and cavity end losses have been chosen. The diffraction losses (g in the model) can be calculated for a given value of index step. These, together with the cavity end losses, determine the gain required to maintain lasing, and the gain in turn determines the density of carriers present necessary to produce the index step. The value for α_s was taken to be 170 cm^{-1} [55,56] and the average values of gain region depth (allowing for a diffusion length of approximately 1.5 microns [29]) were estimated from Klein's data [20] to be 2.5, 3.2 and 4.5 microns at 20, 30 and 40 kV respectively.

Figure 25 shows the theoretically-generated rates of angular tuning for the far-field radiation peak for beam-

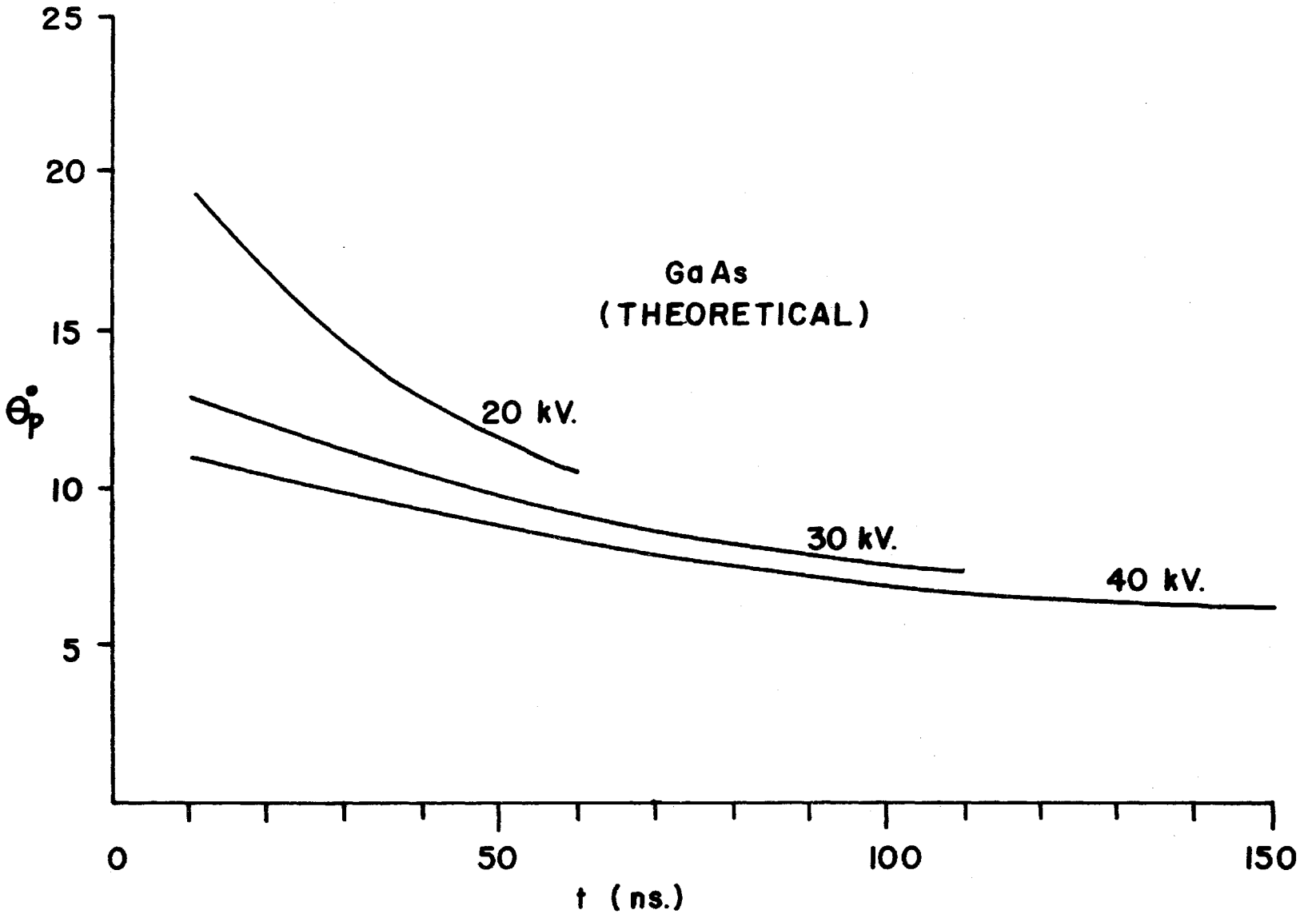

Fig. 25. Theoretically generated rates of tuning of the peak of far-field radiation pattern from GaAs at three beam voltages and holder temperature of 77°K.

pumped GaAs. These curves are in good agreement with the corresponding experimental observations of Fig. 19. The rate of angular tuning at a given beam voltage is independent of pump current density because the wavelength tuning is constant for pump current densities above threshold. The experimental observation that the angular tuning has a shorter duration and a greater rate at lower voltages results from the fact that the wavelength tuning occurs over approximately the same range of wavelengths at all voltages but at a greater rate at lower voltages. That there should be no significant dependence of the rate of angular tuning upon beam current density is a result of the constant wavelength tuning rate for beam current densities above threshold. The larger initial angular deviation at lower beam voltages results from the smaller gain region widths and the higher initial index variations. In this calculation we have omitted the refractive index changes due to heating in GaAs. For sizeable delay times, at sufficiently high pumping, this contribution can become significant as will be evident in the subsequent section. However, the inclusion of this effect in our present calculation would make relatively minor modifications to the fit between theory and experiment. It was judged that the changes so produced would not justify the greatly increased complexity of the calculation.

From the accuracy of the qualitative and quantitative fit of the deviation angle variation, we conclude that index variations due to gain, driven by the wavelength tuning of the laser output, are the major cause of angular tuning in GaAs.

(c) Discussion of Angular Tuning

Detailed observations of the far-field radiation patterns from electron-beam-pumped GaAs and CdSe have been presented. In the case of both materials, the far-field mode patterns are generally observed to be deviated by a substantial amount from the laser cavity axis. Moreover investigation of the temporal behaviour of the modes reveals that this angular deviation decreases monotonically as a function of time during each pump cycle.

The gross features of the angular deviations of the far-field spatial modes have been explained by use of a simple model for the laser cavity modes. In addition, the "angular tuning" of the spatial modes has been accounted for in terms of a time-varying refractive index difference between the pumped and unpumped regions of the cavity. In a quantitative analysis of this effect, two sources of index-variations which can produce effects of a magnitude sufficient to account for the experimental observations have been considered. The first effect arises through the

electron-beam heating of the pumped region of the laser cavity. This heating produces a spatial variation in the temperature of the crystal. Since the refractive index is a fairly sensitive function of temperature in semiconductors at wavelengths in the region of the band-edge, such temperature variations can produce sizeable spatial variations in the refractive index. If this source of index variation is dominant, then the effects it produces depend on the crystal temperature variation and hence on the pump current density of the electron beam. Calculations indicate that this is the dominant source of spatial and temporal index variation in CdSe, and indeed, the angular tuning is observed to be dependent on the electron beam current at a given voltage.

The other source of spatial index variations results from the well-known dispersion relations between the real and imaginary parts of the complex dielectric constant. It is a consequence of this relationship that the existence of differences in the "absorption" between the two regions results in differences in refractive index. Since this refractive index difference is also a function of wavelength, variations in laser wavelength with time result in changes in this difference. Such wavelength tuning has previously been observed and found to be independent of pump current density for above threshold operation. Therefore, the refractive index variation and the resultant angular tuning

is predicted to be approximately independent of pumping current, as was observed for GaAs.

Spatial variations in the refractive index have consequences other than the angular tuning of the far-field spatial mode patterns. In particular, the effect on the diffraction losses in CdSe is considerable for moderate beam voltages. Figure 26 shows a normalized plot of diffraction loss as a function of the size of a positive index step. For a given d, the diffraction loss starts at a very high value and rapidly decreases as the index difference builds up. For parameters appropriate to CdSe at moderate beam voltages, large changes of diffraction loss can occur during the pumping pulse. Such effects have a great impact on laser dynamics - i.e., time to onset of lasing, value of lasing threshold, etc. Moreover, the index variations are wavelength-dependent, leading to the presence of a wavelength-dependent diffraction loss. Such a loss is evidently a potentially important feature in an analysis of time variations of the laser wavelength. In the next section it is shown how the incorporation of this diffraction loss in the dynamics of the laser system leads directly to faster-than-bandgap wavelength tuning.

Fig. 26. Normalized plot of diffraction loss as a function of size of the positive index step.

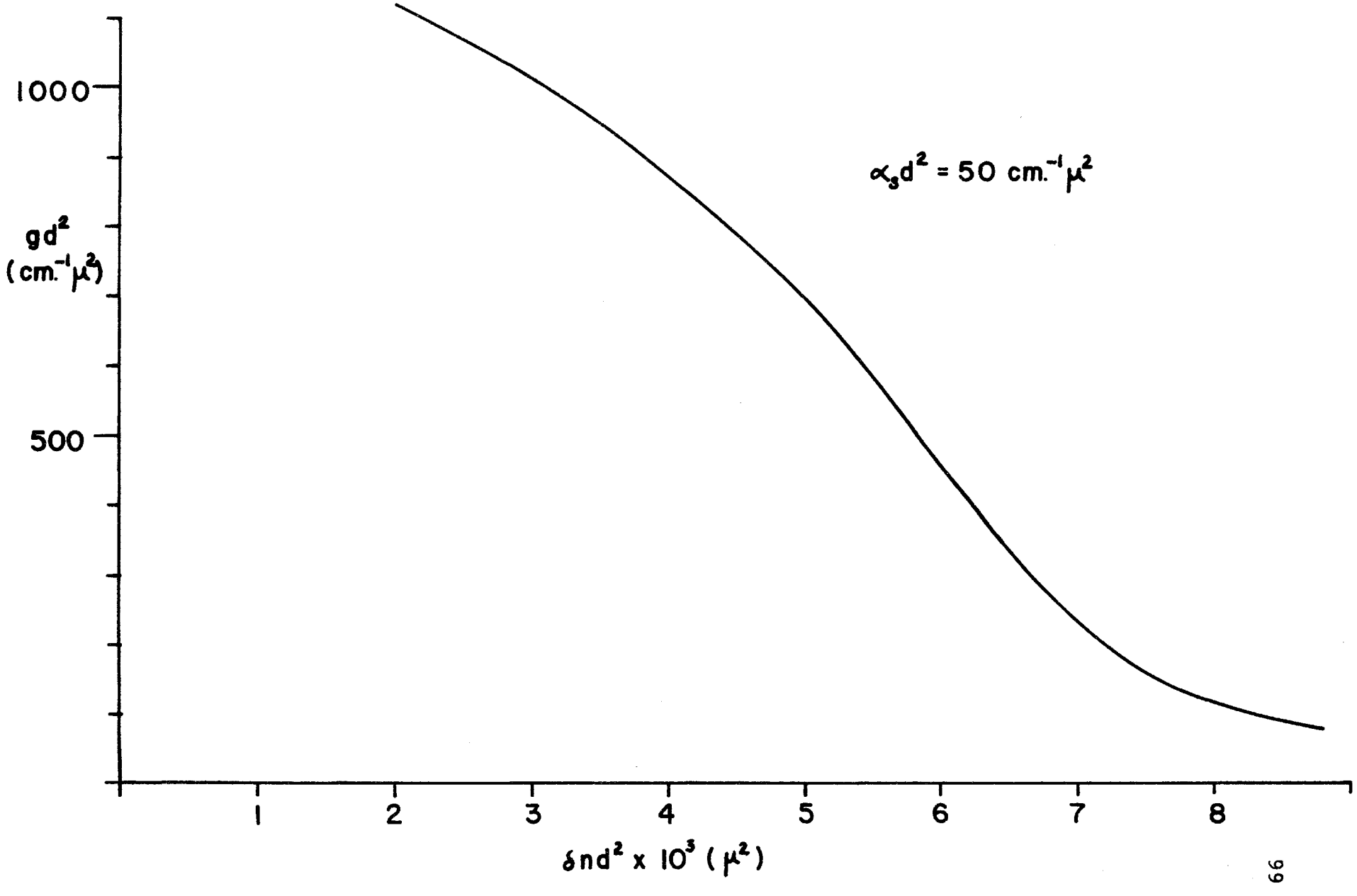
1000
500
gd² (cm.⁻¹μ²)
α₃d² = 50 cm.⁻¹μ²
1
2
3
4
5
6
7
8
δnd² x 10³ (μ²)

3. Dynamic Loss Variations with Particular Application to Wavelength Tuning Effects

(a) General Dynamics:

Calculations of the gain required to attain lasing threshold in electron-beam and optically pumped semiconductor lasers [32,55,57] generally incorporate some allowance for cavity diffraction losses. In general, such losses have been lumped with various absorption effects such as free-electron absorption. Frequently, the resulting effective absorption loss has been taken to be of a size similar to, or less than, that due to cavity end reflectivity losses. It was shown in the previous analysis of angular tuning that these diffraction losses can, however, vastly outweigh the totality of other sources of loss.

The previously discussed (Appendix E) refractive index difference between the pumped and unpumped regions of the laser cavity is very important for the determination of diffraction losses. A sufficiently large index difference between the pumped and unpumped regions of the laser cavity produces very large changes in cavity diffraction losses. This is to be expected since, if the pumped region of the cavity has the relatively larger index, it will tend to act as an optical wave-guide. The cavity mode tends to be more

confined to the pumped region and the diffraction losses reduced. Conversely a relatively smaller index in the pumped region of the cavity tends to increase the diffraction losses.

Since the refractive index step is a function of both wavelength and temperature, then so is the associated diffraction loss. Figure 27 shows the variation of diffraction loss plus cavity end loss (taken to be 110 cm^{-1}) with wavelength for several values of the temperature of the pumped region of a CdSe cavity. The wavelength dependence of this loss is due in part to the wavelength dependence of the optical loss in the unpumped region of the cavity [34] and partly to the wavelength dependence of dn/dT [41]. The depth of the pumped region was taken to be 1 micron which corresponds to a beam voltage of approximately 30 kV. The index step between the pumped and unpumped regions of the laser cavity was that due to heating. The index data of Parsons et al. [41] was used in the calculation of diffraction losses. As in the calculation for angular tuning, the index step due to gain in CdSe was negligible after the first few nanoseconds of the pump.

Figure 28 shows the variation of the sum of the diffraction loss, Urbach-type loss [62] in the gain region, and cavity end loss as a function of the temperature of the gain region. The pump conditions are the same as for Fig. 27. The incorporation of the Urbach loss causes the total

Fig. 27. Diffraction loss plus cavity end losses for CdSe laser. Gain region depth is 1 micron. Initial crystal temperature is 77°K.

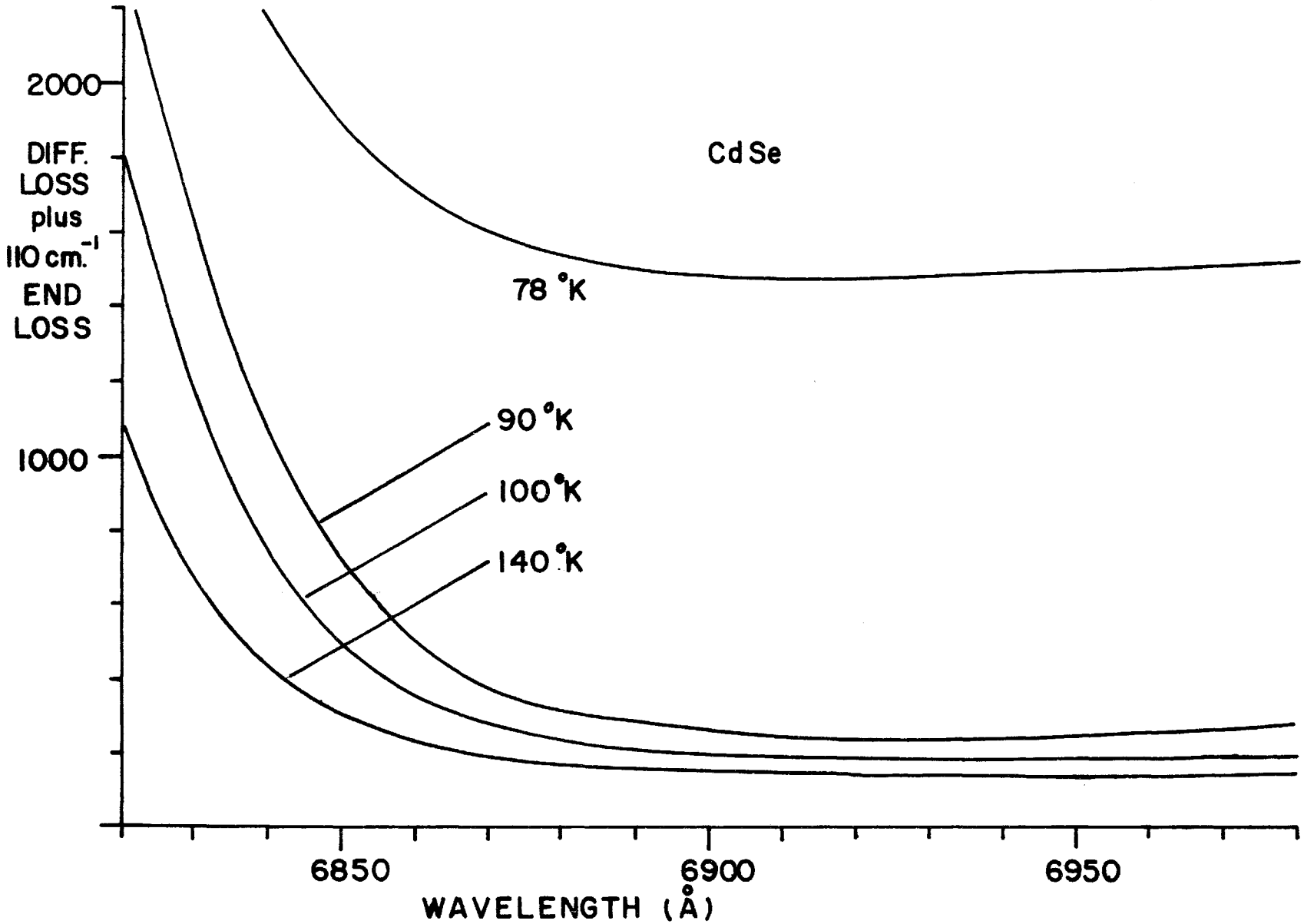
2000
DIFF.
LOSS
plus
110 cm.⁻¹
END
LOSS
1000
CdSe
78 °K
90 °K
100 °K
140 °K
6850
6900
6950
WAVELENGTH (Å)

loss to increase with temperature for a given wavelength as the diffraction losses decrease. The result is a distinct minimum in the total loss.

The losses in CdSe vary rapidly with both wavelength and temperature and will certainly have to be incorporated in any model of laser dynamics. In this description of the losses involved in the semiconductor laser, we have employed experimental parameters appropriate to CdSe. Basically similar behaviour is found for GaAs, except for the absence of an Urbach-type loss in the gain region.

Some general observations concerning the significance of these results for the dynamics of electron-beam-pumped lasers is appropriate. From Fig. 28, it is evident that if we knew the available laser gain then we could determine the range of wavelengths over which lasing would occur. In particular, the starting (shortest occurring) wavelength of the laser could be determined. Earlier theoretical work [61,62] indicates that the maximum allowed density of excitons before break-up is approximately 10^{18} cm^{-3} in CdSe. This information, together with a calculation by B. à la Guillaume [63] implies that gains above 400 cm^{-1} are not likely and thus laser wavelengths less than 6900 Å would not be expected to occur with our pump conditions. It also follows from Fig. 28, that considerable heating (ten or more °K) of the gain region must occur before the loss falls to values commensurate with the available gain for any wavelength. Now, the

Fig. 28. Variation of sum of diffraction loss, Urbach-type loss, and cavity end loss as a function of temperature of the gain region of CdSe laser. The gain region width is 1 micron and the initial crystal temperature is 77°K.

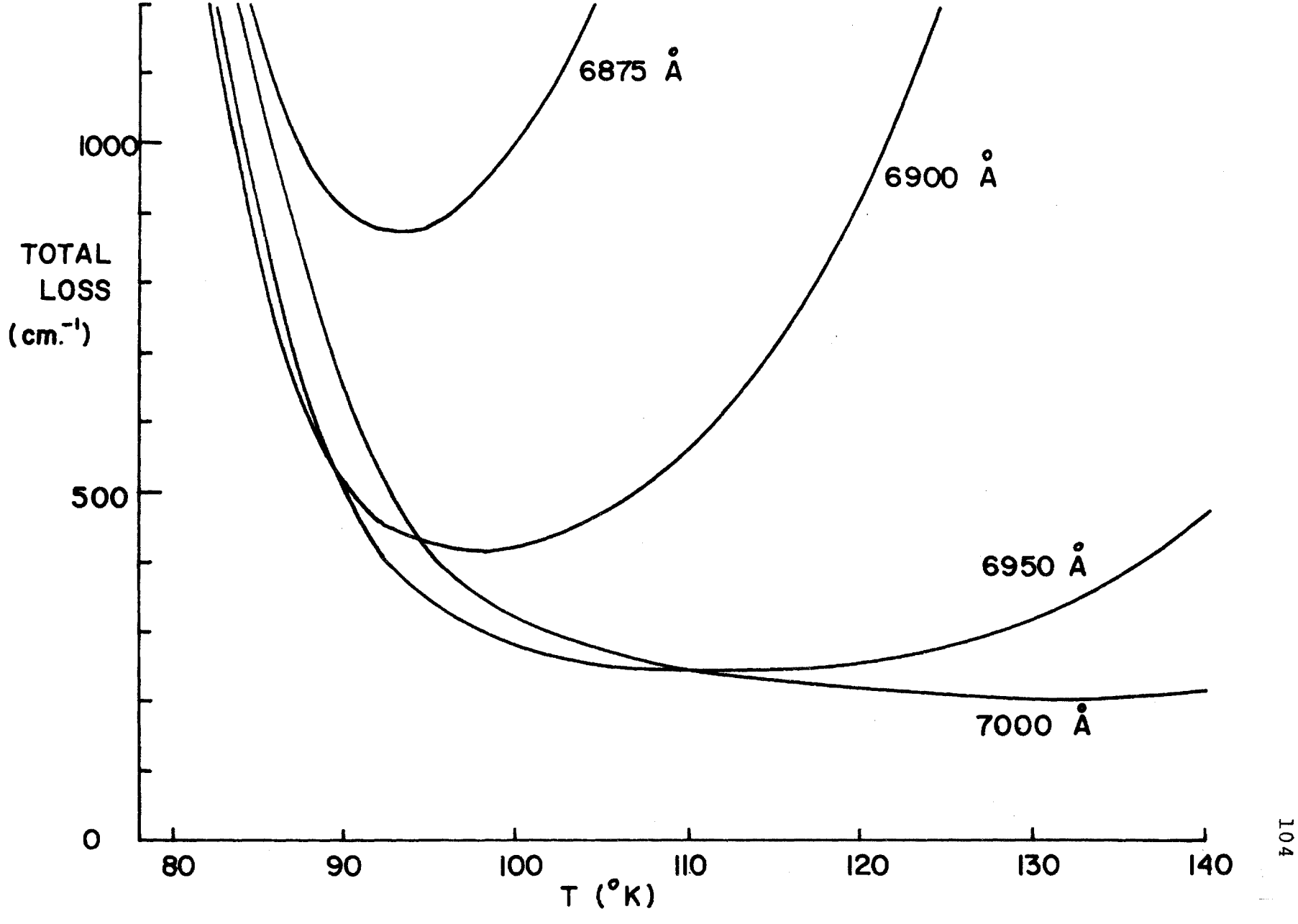
6875 Å
6900 Å
6950 Å
7000 Å
1000
500
0
TOTAL LOSS (cm.⁻¹)
80
90
100
110
120
130
140
T (°K)

temperature difference and time after the start of the pump pulse are directly related for given electron beam parameters. As a consequence, the cavity model presented here can account in a straight-forward fashion for unexpectedly long delay times observed between the start of the pumping pulse and the onset of lasing [48]. This is true for both GaAs and CdSe laser systems. The comparable figure to 28 for GaAs (Fig. 29) also explains the behaviour of lasing threshold as a function of time after the start of the pump pulse (illustrated in Fig. 8). Lasing threshold can be reached by pumping very hard for a short time or by reducing the pump intensity and waiting a longer period of time. We have not attempted to pursue these aspects of the analysis in detail and attention has been restricted to wavelength tuning.

We have chosen to analyse the importance of these time-varying and wavelength-dependent losses on the lasing wavelength in the following fashion. If the gain is denoted by $g(\lambda)$ and the loss by $L(\lambda)$, then the lasing wavelength, λ_m, occurs where the gain equals the loss, and the difference between the gain and loss is maximal. This may be expressed analytically by:

$$g(\lambda_m) - L(\lambda_m) = 0$$

$$d/d\lambda(g(\lambda) - L(\lambda))\Big|_{\lambda=\lambda_m} = 0 \quad .$$

Fig. 29. Sum of diffraction loss plus cavity end reflectivity losses (70 cm^{-1}) vs. temperature of the gain region of GaAs laser. The gain region width is taken to be three microns and the crystal holder temperature is 77°K.

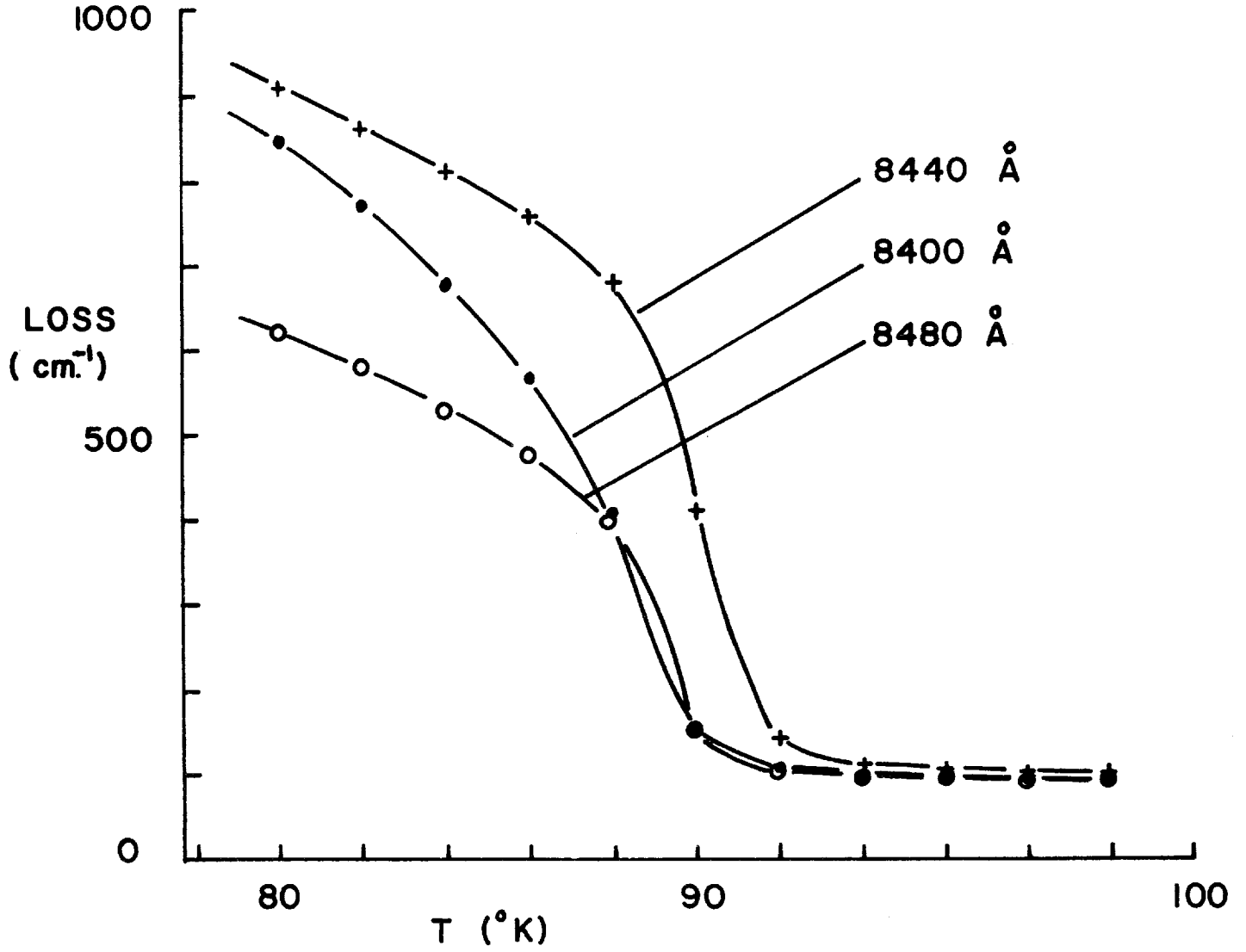
1000
500
0
LOSS
(cm.⁻¹)
8440 Å
8400 Å
8480 Å
80
90
100
T (°K)

This prescription allows the determination of the tuning rate (time variation of λ_m) in the region of the lasing threshold provided $g(\lambda)$ is a known function. For each material we have chosen a very simple model for gain with the intent of elucidating the impact of the wavelength and temperature dependence of loss on the lasing wavelength. Consequently, no account is taken of potentially more complex gain behaviour of which further mention will be made subsequently. Since no explicit account is taken of laser mode dynamics, this model is, in essence, restricted to the threshold region of laser operation. It is consequently not expected to account for the behaviour of λ_m in above-threshold operation.

Analysis of the variation of λ_m as indicated above is sufficiently different in GaAs and CdSe to merit separate consideration.

(b) GaAs

Figure 29 shows the variation of the sum of the diffraction loss and cavity end loss as a function of temperature in the pumped region of the GaAs crystal for several wavelengths. For the sake of definiteness, we employed the model for the gain and loss due to Lasher and Stern [32] which utilizes parabolic bands. The choice of

bandgap at 78°K is arbitrary in this calculation. It was chosen to set the gain peak roughly in the region in which we observed lasing. As a result, the absolute values on the wavelength scale are of no great significance. The depth of the pumped region was taken to be 3 microns which corresponds approximately to a beam voltage of 30 kV. The index contribution due to heating can be calculated directly from the time of pumping and the pumping current. For this, the experimental data of Sturge [36] was used. The negative index contribution, however, is not quite so simple. First the profile of gain is determined using the Lasher and Stern calculation. The refractive index contribution as a function of wavelength can then be calculated employing the Kramers-Kronig relations (Appendix E). Temperature is taken to be the independent variable. The gain peak was determined from the condition that the maximum of the gain minus the cavity reflection loss equals the diffraction loss. This must be done self-consistently since the diffraction loss is, in part, dependent on the value of the gain peak. The temperature range over which the plots are made in Fig. 29 is typically covered during a pumping pulse at moderately high current. Evidently the losses in the cavity are wavelength dependent as well as varying drastically with heating (or time).

The wavelength dependence of the gain and the loss can be calculated according to the methods indicated above. The lasing wavelength is then determined by the prescription described in the previous section. Figure 30 shows the variation of λ_m with crystal surface temperature (which can be related to time for given electron beam parameters). For comparison purposes, the rate of tuning of the bandgap is shown on the same figure. Evidently, the tuning rate of λ_m is a good deal faster than that due to the bandgap. For typical values of heating (0.2°K/nsec. at 6 A/cm^2 pump current density) the tuning rate to longer wavelengths is approximately 1 Å/nsec., of the same magnitude as was observed experimentally.

The rapidity of the shift of λ_m to long wavelengths is mainly due to the reduction of the value for the peak gain as the temperature increases occasioned by the decrease in cavity loss. This, in turn, leads to reduced values for the effective Fermi levels and a concomitant shift of the stimulated emission peak to longer wavelengths. This effect is akin to a dynamic Burstein shift [58], but occurring in the direction opposite to that usually considered [59]. Furthermore, it is relatively independent of the particular bandshape emploted in the gain calculation, as tests with other bandshapes indicated. For example, the use of triangular shaped bands, fitted to match the density of states of the parabolic bands at the Fermi levels, gave approximately the same results.

Fig. 30. Variation of lasing wavelength with gain region temperature for GaAs laser. The gain region width is taken to be 3 microns and the crystal holder temperature is 77°K. The variation of the bandgap with temperature is shown for comparison.

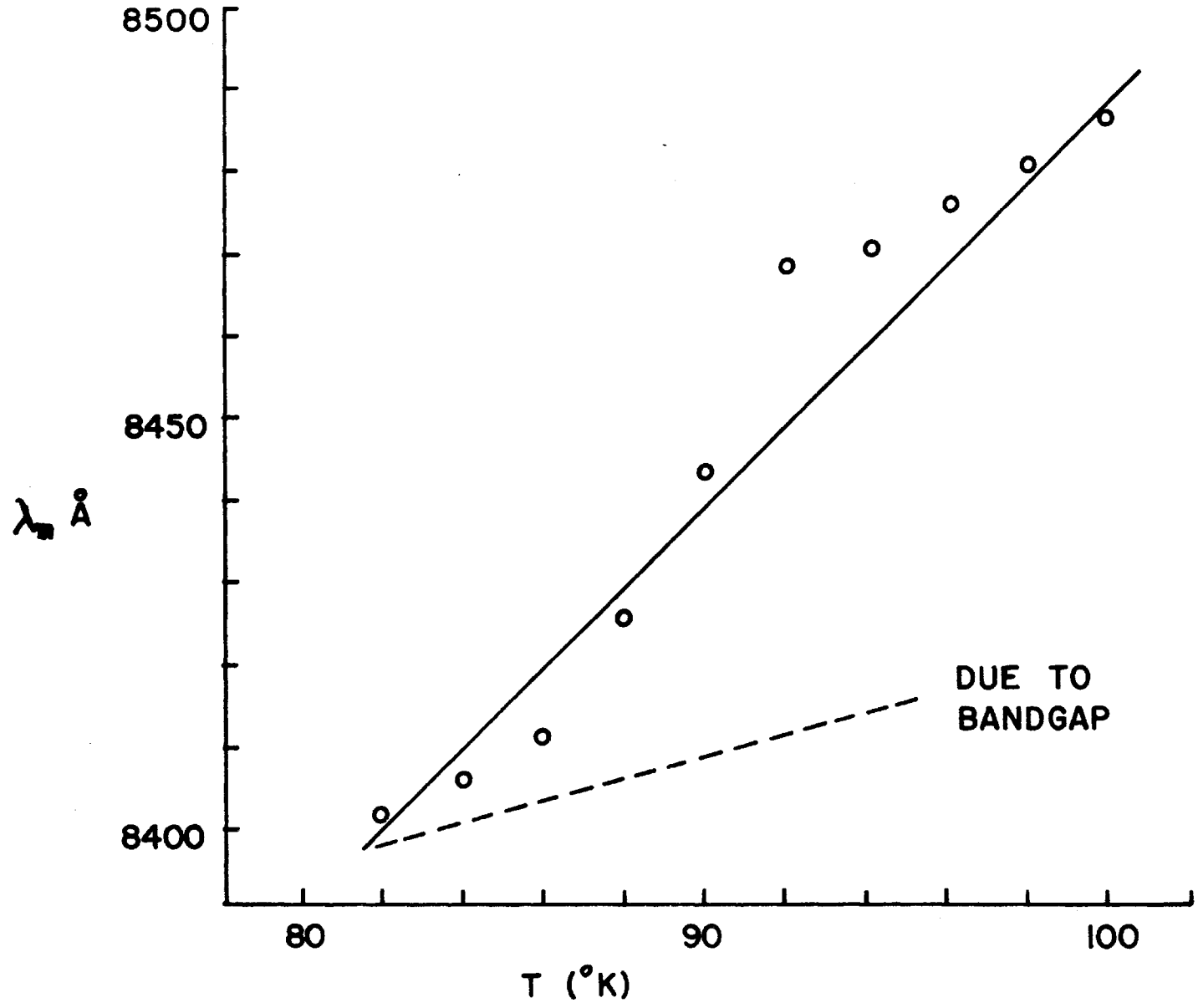
8500
8450
8400
λ_m Å
80
90
100
T (°K)
DUE TO
BANDGAP

(c) CdSe

In CdSe the gain mechanism in the temperature range we consider is the recombination of free excitons rather than the band-to-band recombination dominant in GaAs. Thus in CdSe the gain peak will essentially be fixed with respect to the band edge. For the simple gain model we use, any tuning of the lasing wavelength with respect to the band edge must result from the wavelength and temperature dependence of the loss mechanism alone.

The parameters used to generate the wavelength and temperature dependent loss for CdSe described in part (a) of this section were derived from reported [34,64] experimental measurements. We likewise use a gain profile for CdSe derived from experimental measurements. The data of Hvam [64] give the distributions for the spontaneous emission from electron-beam-pumped CdSe and we take these to represent the gain profiles. This data together with the prescription for determining lasing wavelengths is used to generate a tuning rate for λ_m as a function of the gain region temperature (which can be related to time for given pumping beam parameters). This is shown in Fig. 31, along with the tuning of the bandgap due to heating.

The tuning rate so calculated is faster than the bandgap tuning. However, with the particular parameters

Fig. 31. Variation of lasing wavelength with gain region temperature for CdSe laser. The gain region width is taken to be 1 micron, and the crystal holder temperature is 77°K. The variation of the bandgap with temperature is shown for comparison.

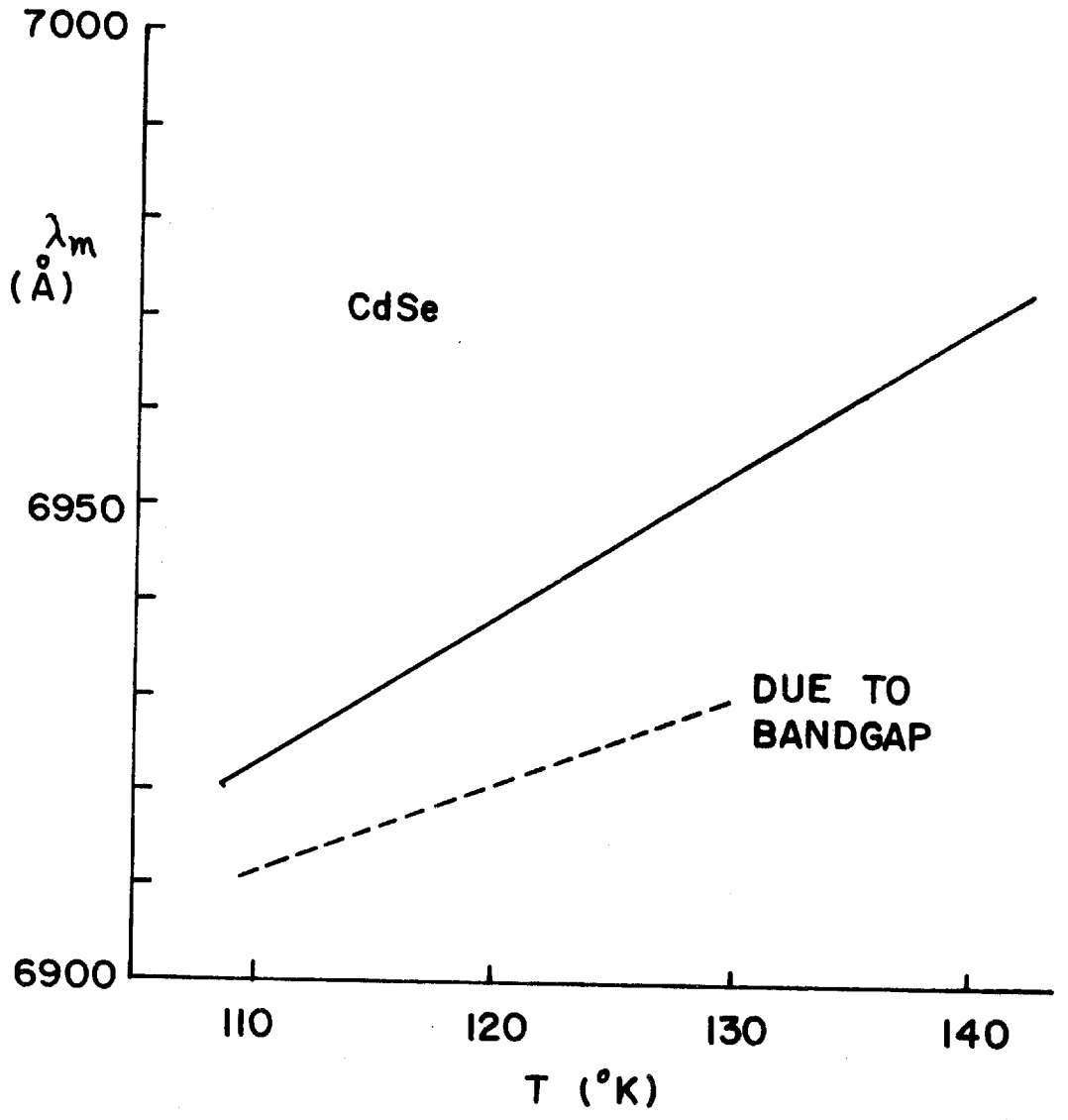
7000
λm
(Å)
CdSe
6950
DUE TO
BANDGAP
6900
110
120
130
140
T (°K)

employed, the tuning rates calculated are somewhat low compared with typical experimental values. This may reflect nothing more than deviations between our crystal parameters and those reported for CdSe in the literature.

Leheny et al. [39] have employed an Urbach loss representation in the gain region to explain an averaged lasing wavelength shift in an optically pumped laser. If we apply their model to the present situation, tuning rates of a generally similar magnitude to those we calculate using diffraction losses are found.

It should be emphasized that, as indicated above, we have based our calculations here on published data for crystals which in all likelihood have significantly different parameters from the material we used in the experimental work. These calculations, furthermore, are very sensitive to certain of the crystalline parameters. For example, a small adjustment of the temperature dependence of the optical loss in the unpumped region produces dramatic changes in the diffraction loss profile in the wavelength range of interest. These considerations indicate the potential value of a study of these effects in which all necessary parameters are measured on the actual laser crystal material.

(d) Discussion of Wavelength Tuning Model

We have analyzed the behaviour of wavelength tuning in GaAs and CdSe when simple models for gain are used and allowance is made for the wavelength and temperature variation of diffraction losses. Tuning of λ_m at faster-than-bandgap rates was found to occur. Furthermore, the actual values of tuning are in fair agreement with observed rates.

This simple model for wavelength tuning does not, however, lead in any obvious manner to the saturation of the rate of wavelength tuning with pump current density which is observed experimentally. This is not particularly surprising since no account has been taken of laser mode or gain dynamics beyond the limits of our simple approximations. The calculations of B. à la Guillaume et al. [63] indicate that lasers operating at the levels of gain suggested by our loss calculations (i.e., hundreds of cm^{-1}), show strong carrier interaction effects. These effects can lead to dramatic changes in the gain. For example, it has been suggested by B. à la Guillaume et al. [63] that, in CdS, the incorporation of electron-exciton interactions at high pump current densities will lead to rapid shifts of the gain peak with time. The same authors have reported observations, by an indirect method, of very rapid shifts (approximately

3 Å/ns.) of the gain to longer wavelengths as a function of time during the pump pulse.

Similarly, strong carrier interaction effects could occur in III-V materials such as GaAs. Indeed, such effects have been proposed by Keune et al. [48] to explain wavelength shifts. It is entirely possible that proper incorporation of gain dynamics, together with the wavelength dependent losses we have calculated, could lead to a satisfactory account for wavelength tuning, including saturation effects. As mentioned before, certain aspects of gain dynamics have been analysed for CdS, but the quantitative application of those results to our situation is not a simple undertaking. No equivalent theory for III-V materials is available. Furthermore, there is a great lack of detailed knowledge of physical parameters on which to base the theories. These reasons render such calculations inappropriate at the present time.

CHAPTER V

CONCLUSIONS

In this thesis some major aspects of the dynamics of electron-beam-pumped lasers have been investigated both experimentally and theoretically.

The experimentally observed effects divide naturally into two parts. The first part relates to the tuning of the peak of the stimulated emission to longer wavelengths during the excitation pulse (wavelength tuning) in both CdSe and GaAs. This tuning is observed to occur at rates faster than the tuning of the bandgap (induced by heating), and to be approximately constant for pump current densities above threshold. This saturated tuning rate is a function of beam voltage for a given sample.

The second part of the experimental data relates to a deviation of the far-field laser modes from the cavity axis and the subsequent angular tuning of these modes during the excitation pulse. Both wavelength and angular tuning are found to occur in a basically similar form in both the III-V and II-VI materials investigated.

In parallel with the experimental investigation, a theoretical model of this laser system has been developed to

account for the observed effects in terms of laser parameters. It was found that a relatively simple model of the laser including spatial variations of the gain and refractive index in the laser medium was sufficient to account for the observed angular tuning rates.

The calculations indicate that much larger refractive index changes (up to a few percent) occur between the pumped and unpumped regions of the laser cavity than have previously been considered. These index changes are caused by heating of the crystal and the presence of gain (related to index by Kramers-Kronig relations), and are functions of both time and wavelength. The calculations also show that diffraction losses, which are strongly dependent on the refractive index difference between pumped and unpumped regions of the laser cavity, are the major cause of the angular deviation behaviour observed. The theoretical analysis, including both first and second order transverse cavity modes, permitted an excellent fit to the experimental observations in GaAs and CdSe lasers. A particularly interesting feature of the angular tuning calculation is that, though the rates in both GaAs and CdSe are dependent on pump beam voltage, only in CdSe should there by a significant dependence on pump current density. This prediction agreed with experiment.

Diffraction losses can be the dominant source of loss in these lasers. The impact of the large wavelength and temperature dependence of diffraction losses on wavelength

tuning has been investigated using simple gain models for these materials. In GaAs, the diffraction losses lead to a faster-than-bandgap tuning of the lasing wavelength mainly through an effect akin to a dynamic Burstein shift [58], but occurring in the direction opposite to that usually considered. The decreased gain requirement for lasing as the crystal heats leads to reduced values for the effective Fermi levels and a concomitant shift of the stimulated emission peak to longer wavelengths. In CdSe, the incorporation of diffraction losses together with a simple gain model leads directly to faster-than-bandgap tuning in a manner similar to the model previously proposed by Leheny et al. [39] using Urbach-type losses.

This treatment of wavelength tuning is basically a threshold model and cannot be expected to explain above-threshold effects such as the experimentally observed saturation of the wavelength tuning rates. The implications and limitations of the incorporation of gain dynamics into a treatment of wavelength tuning are discussed in Chapter 4.

Both the behaviour and magnitude of the diffraction losses have several other important consequences for electron-beam-pumped and, under certain circumstances, light pumped lasers. It is generally accepted that lasing in II-VI materials occurs by an exciton-1LO phonon mechanism. Theories employing this mechanism predict [65,66] a rapid increase in threshold pump current density as a function of

initial sample temperature. This is in contrast with experimental measurements [9,39]. Typical measurements show that the threshold current changes by approximately two for a temperature increase of 100°K whereas theories predict changes of more than an order of magnitude. These theoretical predictions are based on a fixed, temperature-independent cavity loss. The relative pumping required to maintain this fixed loss as temperature rises is then calculated. However, the present work has demonstrated that the assumption of fixed cavity loss as a function of temperature is inappropriate. Indeed, the cavity loss can fall by as much as an order of magnitude during a pump pulse (or equivalently as the cavity gain region heats some tens of degrees with respect to the cold finger temperature). Evidently, incorporation of a total cavity loss which falls rapidly as a function of time during a pump pulse will produce a much slower increase in the required threshold current since the necessary gain to attain threshold falls during the pump pulse. This is the more so, the larger the value of the pump current density. It seems probable that proper allowance for variations in cavity loss can reconcile the results of theoretical calculation and experimental observation.

Previous observations [48,63] have shown unexpectedly long time delays between start of the excitation pulse and onset of lasing in semiconductor lasers. The analysis of diffraction loss indicates a previously unsuspected mechanism

for producing such long delays. Since considerable heating (ten or more °K) may have to occur before total cavity loss falls to values commensurate with available gain, delay times (between pump pulse start and the onset of lasing) of the order of 100 nanoseconds or more can occur.

The above effects are naturally dependent on system conditions, in particular the gain region width. For electron-beam-pumping, diffraction loss and related effects decrease with increasing beam voltage. Our analysis does not apply directly to light pumped systems, particularly when very narrow gain region widths occur, as is frequently the case [4]. Nevertheless, the spatially-varying refractive index due to both heating and the presence of gain will certainly occur in these systems. A complete analysis of these devices will consequently require appropriate allowance for these effects.

Diffraction loss will be greatly reduced for platelet lasers. However, it should be observed that, in II-VI compounds this will only occur for extremely thin platelets of a width commensurate with the penetration depth of the pump electrons. For typical electron-beam-pumped systems this corresponds to thicknesses of the order of or less than 1 micron. This situation basically reflects the wave-guide nature of the pumped region which tends to confine the electric field strongly to this region. Effects of a

similar nature will occur in light pumped systems and must be properly taken into account.

APPENDIX A

THEORETICAL MODEL

Maxwell's equations to be solved for the electron-beam-pumped system are:

$$\text{curl } \underline{H} = \underline{j} + \frac{\partial \underline{D}}{\partial t} \tag{A1}$$

$$\text{curl } \underline{E} = -\frac{\partial \underline{B}}{\partial t} \tag{A2}$$

$$\text{div } \underline{D} = 0 \quad \text{(no net charge)} \tag{A3}$$

$$\text{div } \underline{B} = 0 \tag{A4}$$

$$\text{also} \quad \underline{D} = \varepsilon_o \underline{E} + \underline{P} = \varepsilon_o \varepsilon \underline{E} \quad \text{and} \quad \underline{B} = \mu_o \underline{H} \tag{A5}$$

$$\text{from (2)} \quad \text{curl}(\text{curl } \underline{E}) = -\text{curl}\left(\frac{\partial \underline{B}}{\partial t}\right) = -\frac{\partial}{\partial t}(\text{curl } \underline{B})$$

$$= -\mu_o \frac{\partial}{\partial t}(\text{curl } \underline{H}) \quad \text{(non-magnetic medium)}$$

$$= -\mu_o \frac{\partial}{\partial t}\left(\sigma \underline{E} + \varepsilon_o \frac{\partial}{\partial t}(\varepsilon \underline{E})\right) \quad (\varepsilon = 1 \text{ for free space}) \tag{A6}$$

$$\text{grad div } \underline{E} - \nabla^2 \underline{E} = -\mu_o \sigma \frac{\partial \underline{E}}{\partial t} - \mu \varepsilon_o \frac{\partial^2}{\partial t^2} (\underline{E}) \quad . \tag{A7}$$

Now since div $\underline{D} = 0 = \varepsilon_o \text{ div}(\varepsilon \underline{E})$

$$\text{grad div } \underline{E} = -\text{grad}(\underline{E} \cdot \text{grad log } \varepsilon) \quad . \tag{A8}$$

Substituting this into (3)

$$\mu_o \sigma \frac{\partial \underline{E}}{\partial t} + \frac{1}{c^2} \frac{\partial^2}{\partial t^2} (\varepsilon \underline{E}) - \nabla^2 \underline{E} - \text{grad}(\underline{E} \cdot \text{grad log } \varepsilon) = 0 \quad . \tag{A9}$$

The last term is negligible for the small index changes encountered in this work even when $\underline{E}$ not $\perp$ grad log ε, and for a lossless dielectric the first term is zero.

Thus

$$\nabla^2 \underline{E} = \frac{1}{c^2} \left(\frac{\partial^2 \varepsilon}{\partial t^2} \cdot \underline{E} + 2 \frac{\partial \varepsilon}{\partial t} \cdot \frac{\partial \underline{E}}{\partial t} + \varepsilon \cdot \frac{\partial^2 \underline{E}}{\partial t^2} \right) \quad . \tag{A10}$$

We now represent ε in the form:

$$\varepsilon(x,t) = \varepsilon_o' + \delta\varepsilon_o''(x,t) - i\varepsilon''(x,t) + i\varepsilon_o'' \quad . \tag{A11}$$

The time derivatives of ε are taken to be small compared to the derivatives of E.

We look for solutions in the form:

$$\underline{E} = A(x,t)\sin\frac{\pi n z}{\ell}\, e^{i\omega_o t} \qquad \text{(A12)}$$

where ℓ is the laser cavity length and n is an integer. A(x,t) is complex and slowly varying. We obtain

$$\frac{\partial A}{\partial t} = \frac{c^2}{2i\omega_o\varepsilon}\left[-\frac{\partial A^2}{\partial x^2} + k^2 A - \frac{\omega_o^2\varepsilon}{c^2} A\right] \quad . \qquad \text{(A13)}$$

The eigenmodes of the laser will have amplitudes stable in time and, therefore, the solutions must fulfil the condition $\partial A/\partial t = 0$. The boundary conditions which must be fulfilled are:

1. $A = 0$ at $x = 0$
2. $A \to 0$ as $x \to \infty$
3. the field and its derivative must be continuous at x=d (A14)

Substituting for the index, the general wave equations in the two regions are:

$$\frac{\partial^2 A}{\partial x^2} = \left(k^2 - \frac{\omega_o^2}{c^2}(\varepsilon' + i\varepsilon_o'')\right)A - \frac{i\omega_o^2\varepsilon_g''}{c^2} A - \frac{\omega_o^2\delta\varepsilon_o''}{c^2} A \quad (0,d) \qquad \text{(A15)}$$

$$\frac{\partial^2 A}{\partial x^2} = (k^2 - \frac{\omega_o^2}{c^2}(\varepsilon' + i\varepsilon_o''))A + \frac{i\omega_o^2 \varepsilon_\ell''}{c^2} A \qquad (d,\infty) \qquad \text{(A16)}$$

where

$$\varepsilon_\ell \ , \ \varepsilon_g > 0 \ .$$

We assume solutions of the general form:

$$A = \sin px \quad \text{in} \quad (0,d)$$

$$A = A_o \exp(-qx) \quad \text{in} \quad (d,\infty) \ . \qquad \text{(A17)}$$

Substitution into the wave equations gives

$$p^2 + q^2 = i(\alpha+\beta) + \frac{\omega_o^2}{c^2} \varepsilon_o''$$

with $$\qquad \text{(A18)}$$

$$\alpha = \frac{\omega_o^2}{c^2} \varepsilon_g \ , \quad \beta = \frac{\omega_o^2}{c^2} \varepsilon_\ell$$

$$p/q = -\tan pd \quad \text{(Boundary condition 3.)}$$

$$p^2 = [\frac{\omega_o^2 \delta \varepsilon_o''}{c^2} + i(\alpha+\beta)] \sin^2 pd$$

$$\qquad \text{(A19)}$$

$$q^2 = [\frac{\omega_o^2 \delta \varepsilon_o''}{c^2} + i(\alpha+\beta)] \cos^2 pd$$

(19) together with the identity $-2ip^2 = [(p'+p")-i(p'-p")]^2$ gives

$$(p'+p") - i(p'-p") = \sqrt{2}\ (\gamma'+i\gamma")\sin pd \tag{A20}$$

where

$$p = p'+ip" \ , \ \gamma'^2-\gamma"^2 = (\alpha+\beta)$$

and (A21)

$$\gamma'\gamma" = \frac{-\omega_o^2\delta\varepsilon"_o}{2c^2} \ .$$

Expanding (20) and separating real and imaginary parts,

$$\frac{1-k}{1+k} = - \frac{\cot u \tanh (ku)-E_p}{1+E_p \cot u \tanh ku} \tag{A22}$$

where

$$u = p'd \ , \ ku = p"d \quad \text{and} \quad E_p = \frac{-\gamma'}{\gamma"} \tag{A23}$$

is a measure of the index step, $\delta n = \delta\varepsilon"_o/2n$.

Lemma 1. Relation of Parameters to Gain and Loss

From Appendix A,

$$\nabla^2 E = \frac{\varepsilon}{c^2} \frac{\partial^2 E}{\partial t^2} \quad .$$

If $\varepsilon = \varepsilon_o' + i\varepsilon_o''$, $\sqrt{\varepsilon} = n + ik$

then $\varepsilon_o' = n^2 - k^2$, $\varepsilon_o'' = 2nk$.

Assume a solution of the form:

$$E = E_o \exp i(\omega t - kz) \qquad \text{(plane wave)}$$

and substitute for k to give

$$E = E_o \exp i(\omega t - \frac{\omega n}{c} z) \exp(\frac{\omega k}{c} z) \quad .$$

There is thus gain for $k > 0$ with the intensity gain being:

$$g = \frac{2\omega k}{c} = \frac{2\omega}{c} \frac{\varepsilon_o''}{2n} = \frac{\omega \varepsilon_o''}{cn}$$

$$\therefore \quad \alpha = \frac{\omega^2}{c^2} \varepsilon_g'' = \frac{\omega n}{c} g$$

$$\beta = \frac{\omega^2}{c^2} \varepsilon_\ell'' = \frac{\omega n}{c} \alpha_s$$

also

$$\alpha+\beta = \frac{n\omega}{c} (g+\alpha_s) \quad .$$

APPENDIX B

NEAR AND FAR FIELD RELATIONS

If we consider Fig. 32 relating the aperture (cavity boundary) and far-field planes:

$$r_o = \sqrt{x^2 + z^2}$$

$$r = \sqrt{(x-\eta)^2 + z^2} \sim r_o \left(1 - \frac{\eta x}{r_o^2}\right) \quad . \tag{B1}$$

If the distribution of the field over the aperture is $E(\eta)$, then in the "Huygens" formulation:

$$E(x) = \int_{\text{aperture}} \frac{1}{r} \cdot E(\eta) \exp(ik \cdot r) d\eta$$

$$= \int_{\text{aperture}} \frac{1}{r_o\left(1 - \frac{\eta x}{r_o^2}\right)} E(\eta) \exp\left[ikr_o\left(1 + \frac{\eta x}{r_o^2}\right)\right] d\eta$$

$$= \frac{\exp(ikr_o)}{r_o} \int_{\text{aperture}} \left(1 - \frac{\eta x}{r_o^2}\right) E(\eta) \exp\left(\frac{ik\eta x}{r_o}\right) d\eta \tag{B2}$$

which, for sufficiently large r_o is equal to:

$$E(x) = \frac{\exp(ikr_o)}{r_o} \int_{\text{aperture}} E(\eta) \exp\left(\frac{ik\eta x}{r_o}\right) d\eta \tag{B3}$$

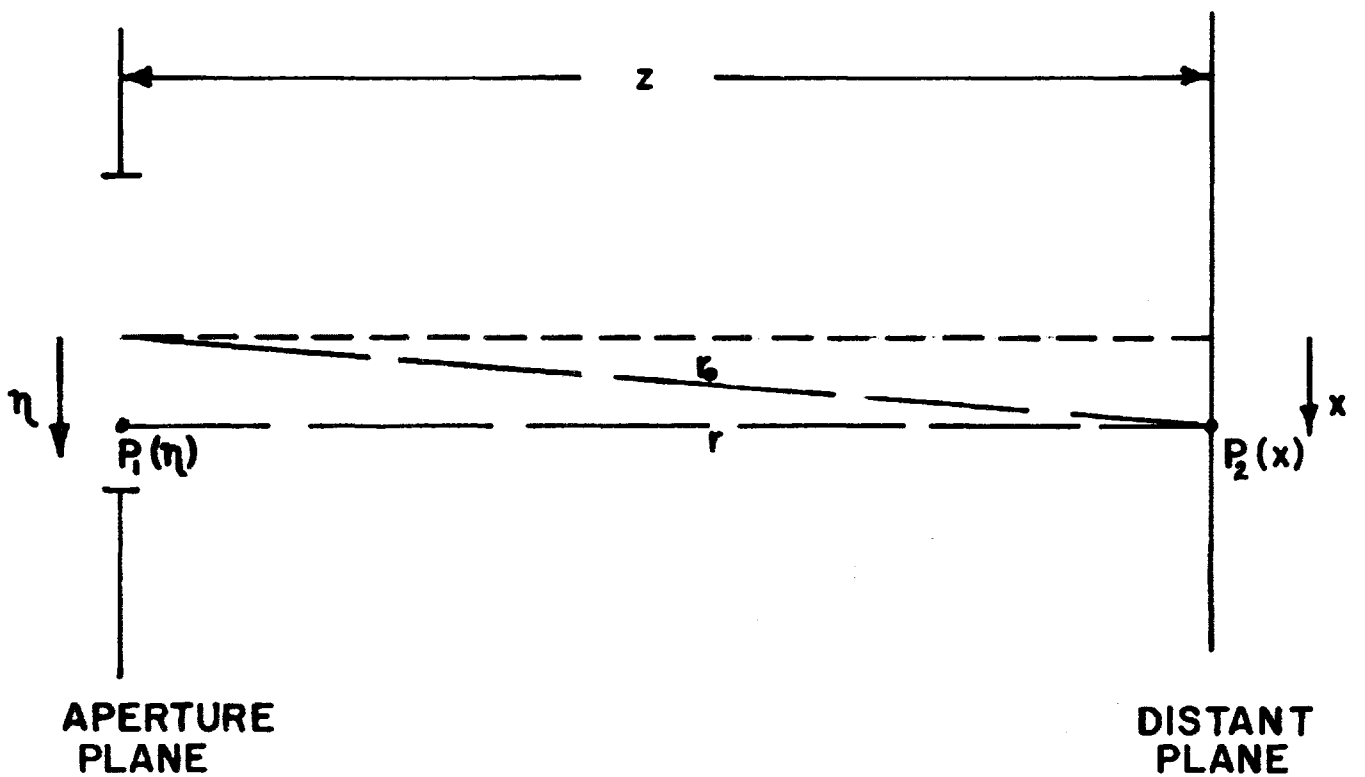

Fig. 32. Near- and far-field model.

which shows that, to within multiplicative factors, $E(x)$ is given by the Fourier transform of $E(\eta)$.

APPENDIX C

SOLUTION FOR THAT PORTION OF THE FAR FIELD RELATING TO THE NEAR FIELD REGION (d,∞)

$$E'(\nu) = \int_0^\infty |E(\alpha)| \exp[i\phi(\alpha)] \exp[i\nu\alpha] d\alpha \qquad (C1)$$

where $\nu = k\theta$

$$|E(\alpha)| = [\sin^2 ku + \sin^2 u]^{1/2} \exp[\tfrac{\sigma}{2}(\alpha-1)] \qquad (C2)$$

$$= b \exp[\tfrac{\sigma}{2}(\alpha-1)]$$

$$\sigma = u \left[\frac{\sin 2u + k \sinh 2ku}{\sin^2 u + \sinh^2 ku}\right]$$

$$\phi(\alpha) = \tan^{-1} [\cot u \tanh ku] - (\alpha-1)\xi \qquad (C3)$$

$$\xi = \frac{u}{2} \left[\frac{\sinh 2ku - k \sin 2u}{\sinh^2 ku + \sin^2 u}\right] .$$

Also let $\alpha - 1 = \beta$

$$\therefore \quad E'(\nu) = b \int_0^\infty \exp(i\nu) \exp(\tfrac{\sigma}{2}\beta) \exp[-i(\xi - \tan^{-1}\{\cot u \tanh ku\} - \nu)\beta] d\beta$$

$$= b \int_0^\infty \exp(i\nu) \exp(\tfrac{\sigma}{2}\beta) \exp[-i(\xi - Q - \nu)\beta] d\beta \qquad (C4)$$

where $Q = \tan^{-1}[\cot u \tanh ku]$

$$E'(\nu) = b \exp[i(\nu+Q)] \int_0^\infty \exp[\beta\{\frac{\sigma}{2} - i(\xi-\nu)\}]d\beta$$

$$= \frac{-b \exp[i(\nu+Q)}{\frac{\sigma}{2} - i(\xi-\nu)}$$

$$= \frac{-b \exp[+i(\nu+Q)][\frac{\sigma}{2} + i(\xi-\nu)]}{(\frac{\sigma}{2})^2 + (\xi-\nu)^2}$$

$$= \frac{-b[\cos(\nu+Q) + i \sin(\nu+Q)][\frac{\sigma}{2} + i(\xi-\nu)]}{(\frac{\sigma}{2})^2 + (\xi-\nu)^2} \qquad \text{(C5)}$$

This is the form which is put into the computer program.

APPENDIX D

MECHANISMS PRODUCING VARIATIONS IN d

Since d is determined at least initially by the penetration of the beam electrons into the semiconductor, d will depend upon beam voltage and material type [20]. Assuming that we hold beam voltage, material type and pumping current density constant, the ways in which d, the gain region width, can change with time are limited to:

1. diffusion of electrons (assumed to diffuse faster than holes)
2. creation of electron-hole pairs further into the pumped region of the crystal by the spontaneous and stimulated photon fields.

1. We will consider first the diffusion of electrons. Boltzmann's equation for the diffusion of excess electrons is:

$$D\nabla^2 n + g - \frac{n}{\tau} = \frac{\partial n}{\partial t} \qquad \text{(D1)}$$

if we assume no electric field present. Where:

D = electron diffusion coefficient

n = number of excess electrons

τ = recombination lifetime of electrons

g = rate of production of electrons .

A general solution [27] for this equation is:

$$\delta n(x,t) = \iint \frac{g(x',t')}{\sqrt{4\pi D(t-t')}} \exp\left[\frac{-(x-x')^2}{4D(t-t')} - \frac{(t-t')}{\tau}\right] dx'dt'. \tag{D2}$$

The boundary conditions for the pump g(x',t') are as shown in Fig. 33(a). The pump is uniform in time and space over a depth d from the crystal surface. Since we do not wish to lose electrons through the crystal surface, we can set up an equilibrium condition of electron transfer at the surface of the crystal by letting the pump condition be shown in Fig. 33(b) and considering the solution for $x \geq 0$. The pump will be permitted to operate from time t' = 0 to t' = t at which time the excess carrier distribution will be observed. The distribution at time t will be given by:

$$\delta n = \int_0^t \int_{-d}^{d} \frac{g}{\sqrt{4\pi D(t-t')}} \exp[-(t-t')/\tau] \exp\left[\frac{-(x-x')^2}{4D(t-t')}\right] dx'dt' \tag{D3}$$

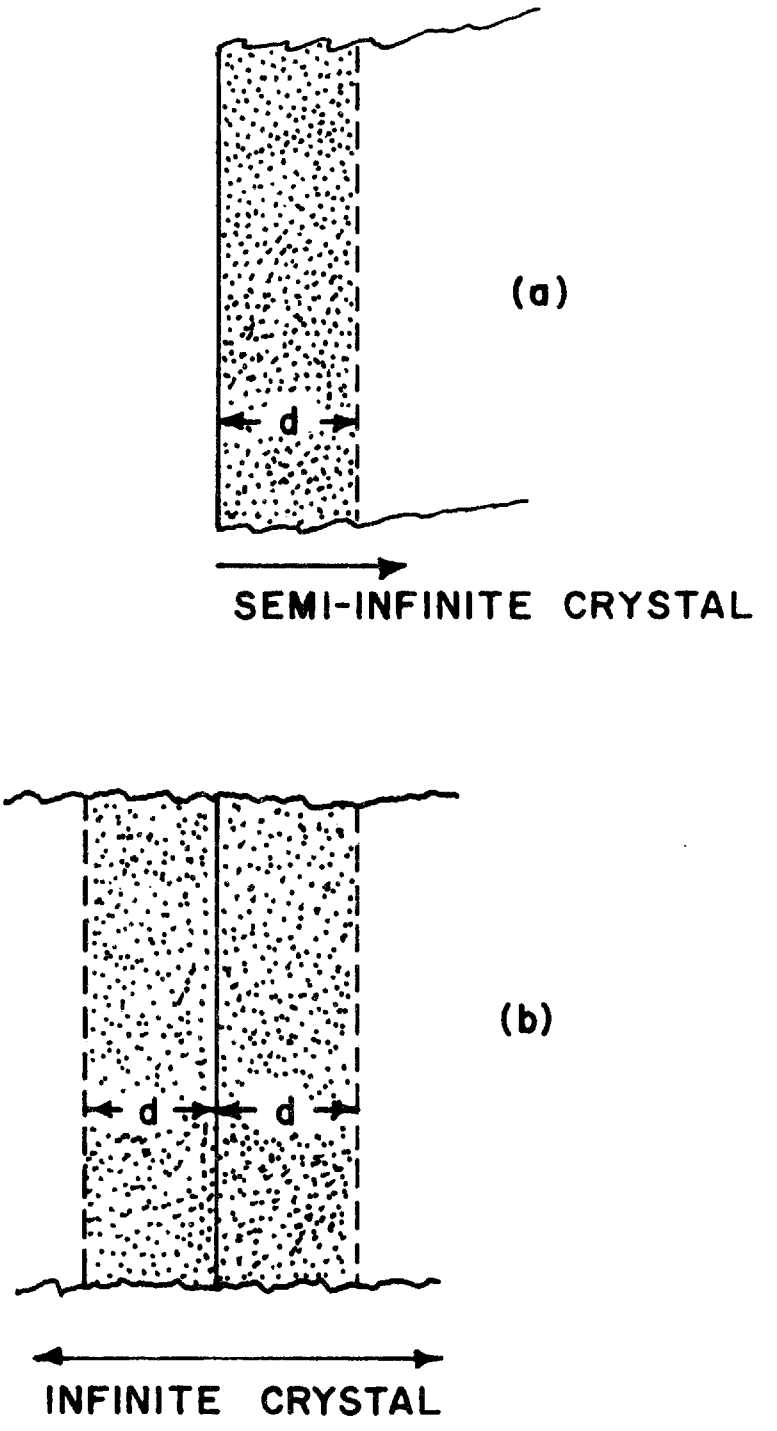

Fig. 33. Actual crystal model (a) and analyzed crystal model (b) of pumped region for carrier diffusion consideration.

transform

$$y = \frac{x-x'}{\sqrt{4D(t-t')}} \qquad \therefore \quad dy = \frac{-dx'}{\sqrt{4D(t-t')}}$$

$$\therefore \quad \delta n = \frac{-g}{\sqrt{\pi}} \int_0^t \int_{\frac{x+d}{\sqrt{4D(t-t')}}}^{\frac{x-d}{\sqrt{4D(t-t')}}} \exp[-\frac{(t-t')}{\tau}]\exp(-y^2)\,dy\,dt'$$

$$= \frac{-g}{2} \int_0^t \exp[-\frac{(t-t')}{\tau}][\frac{2}{\sqrt{\pi}} \int_{\frac{x+d}{\sqrt{4D(t-t')}}}^{\frac{x-d}{\sqrt{4D(t-t')}}} \exp(-y^2)\,dy]\,dt'$$

$$= \frac{-g}{2} \int_0^t \exp[\frac{-(t-t')}{\tau}]\left[\int_0^{\frac{x-d}{\sqrt{4D(t-t')}}} \exp(-y^2)\,dy\right.$$

$$\left. - \int_0^{\frac{x+d}{\sqrt{4D(t-t')}}} \exp(-y^2)\,dy\right]dt' \quad . \qquad \text{(D4)}$$

The two regions of x which must be solved are:

$$(1) \quad x-d > 0 \qquad (2) \quad x-d < 0 \quad .$$

In (1)

$$\delta n = \frac{-g}{2} \int_0^t \exp[\frac{-(t-t')}{\tau}][\mathrm{erf}(\frac{x-d}{\sqrt{4D(t-t')}}) - \mathrm{erf}(\frac{x+d}{\sqrt{4D(t-t')}})]\,dt' \qquad \text{(D5)}$$

In (2)

$$\delta n = \frac{-g}{2}\int_0^t \exp[\frac{-(t-t')}{\tau}][-\mathrm{erf}(\frac{d-x}{\sqrt{4D(t-t')}}) - \mathrm{erf}(\frac{x+d}{\sqrt{4D(t-t')}})]dt'. \tag{D6}$$

The limits of integration have been changed here so that the erf are positive and the identity

$$\mathrm{erf}(-x) = -\mathrm{erf}(x) \tag{D7}$$

has been invoked.

The integrals are now combinations of the form:

$$\frac{g}{2}\int_0^t \exp[\frac{-(t-t')}{\tau}]\mathrm{erf}(\frac{c}{\sqrt{t-t'}})dt' \quad .$$

The solution [28] of the above is:

$$\frac{-g\tau}{4}\{2\exp(\frac{t'}{\tau})\mathrm{erf}(c/t'^{1/2}) - \exp(\frac{2c}{\tau})\mathrm{erf}(\sqrt{\frac{t'}{\tau}} + \frac{c}{\sqrt{t'}})$$

$$-\exp(\frac{-2c}{\tau})\mathrm{erf}(\frac{c}{\sqrt{t'}} - \sqrt{\frac{t'}{\tau}})\}\Big|_0^t = \frac{-g\tau}{4}\{2\exp(\frac{-t}{\tau})\mathrm{erf}(\frac{c}{\sqrt{t}}) - 2$$

$$-\exp(\frac{-2c}{\sqrt{\tau}})[\mathrm{erf}(\frac{c}{\sqrt{t}} + \sqrt{\frac{t}{\tau}}) - 1] - \exp(\frac{-2c}{\sqrt{\tau}})[\mathrm{erf}(\frac{c}{\sqrt{t}} - \sqrt{\frac{t}{\tau}}) - 1]\} \tag{D8}$$

if we let, $c = \frac{x-d}{\sqrt{4D}}$, $d' = \frac{x+d}{\sqrt{4D}}$ and $c' = \frac{d-x}{\sqrt{4D}}$

the solutions for the two x regions are:

$$(1)\quad \delta n = \frac{g\tau}{4}\{2\exp(\frac{-t}{\tau})[\mathrm{erf}(\frac{c}{\sqrt{t}})-\mathrm{erf}(\frac{d'}{\sqrt{t}})]-\exp(\frac{-2c}{\sqrt{\tau}})[\mathrm{erf}(\frac{c}{\sqrt{t}}+\sqrt{\frac{t}{\tau}})-1]$$

$$+\exp(\frac{2d'}{\sqrt{\tau}})[\mathrm{erf}(\frac{d'}{\sqrt{t}}+\sqrt{\frac{t}{\tau}})-1]-\exp(\frac{-2c}{\sqrt{\tau}})[\mathrm{erf}(\frac{c}{\sqrt{t}}-\sqrt{\frac{t}{\tau}})-1]$$

$$+\exp(\frac{-2d'}{\sqrt{\tau}})[\mathrm{erf}(\frac{d}{\sqrt{t}}-\sqrt{\frac{t}{\tau}})-1]\} \qquad (D9)$$

$$(2)\quad \delta n = \frac{-g\tau}{4}\{2\exp(\frac{-t}{\tau})[\mathrm{erf}(\frac{c'}{\sqrt{t}})+\mathrm{erf}(\frac{d'}{\sqrt{t}})]-4$$

$$-\exp(\frac{2c'}{\sqrt{\tau}})[\mathrm{erf}(\frac{c'}{\sqrt{t}}+\sqrt{\frac{t}{\tau}})-1]-\exp(\frac{2d'}{\sqrt{\tau}})[\mathrm{erf}(\frac{c'}{\sqrt{t}}+\sqrt{\frac{t}{\tau}})-1]$$

$$-\exp(\frac{-2c'}{\sqrt{\tau}})[\mathrm{erf}(\frac{c'}{\sqrt{t}}-\sqrt{\frac{t}{\tau}})-1]-\exp(\frac{-2d'}{\sqrt{\tau}})[\mathrm{erf}(\frac{d'}{\sqrt{t}}-\sqrt{\frac{t}{\tau}})-1]\}. \qquad (D10)$$

The above solutions are plotted in Fig. 34 for values of lifetime, pump rate and diffusion constant typical to GaAs [29]. The excess carrier distribution reaches an equilibrium in a few times the spontaneous recombination lifetime τ, and, as expected, the 10% to 90% spread of the distribution at x=d is approximately the electron diffusion length $(D\tau)^{1/2}$.

The important feature to note here is that the excess carrier distributions reach equilibrium in a few carrier lifetimes. For GaAs a few nanoseconds is sufficient for d changes due to diffusion to stop. Also the diffusion length of the excess carriers will not change significantly with temperature [30] in the range of experimental interest

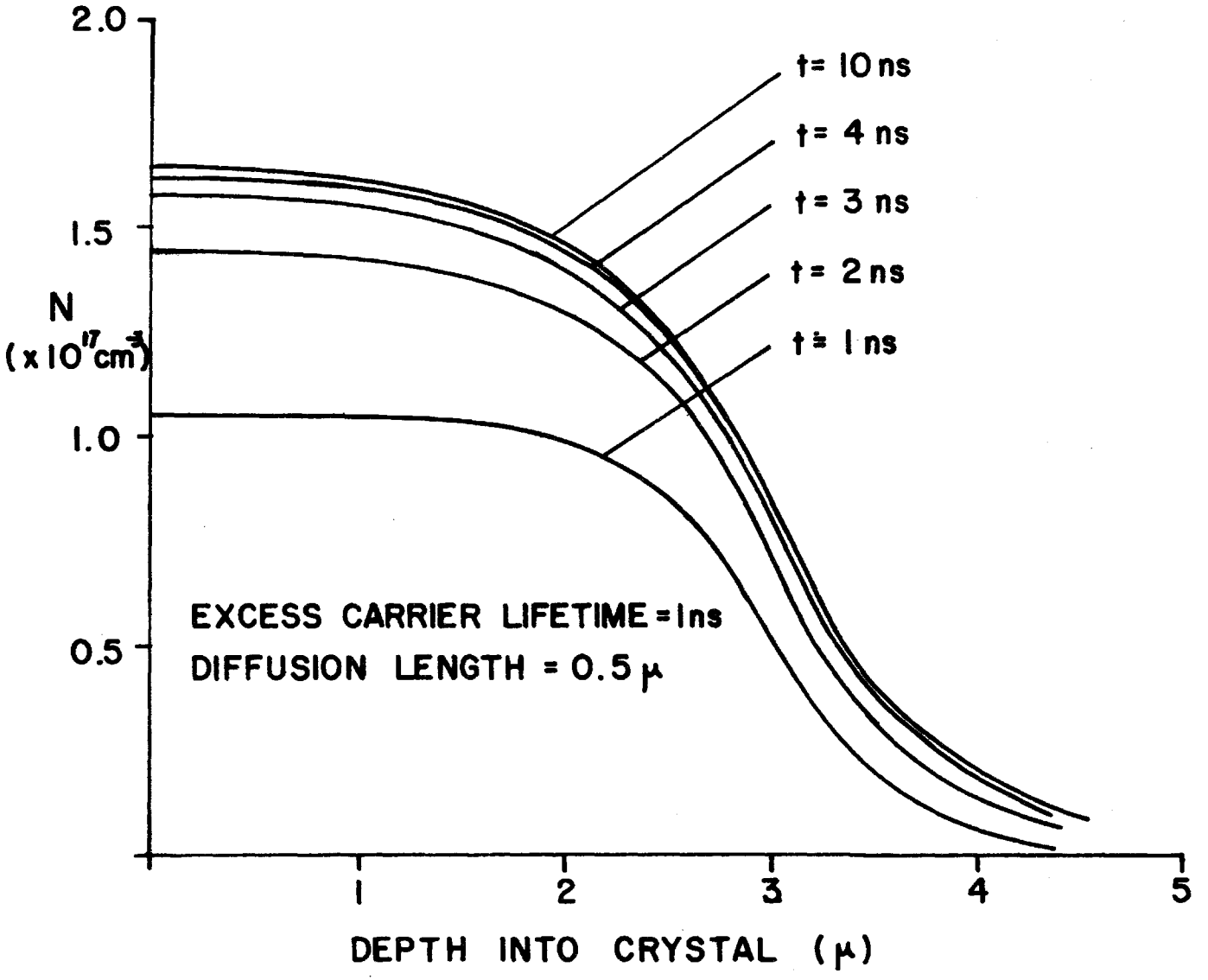

Fig. 34. Excess carrier density vs. depth into crystal for GaAs (EBP) showing rapid stabilization of carrier density after start of pumping cycle.

(77°K to 120°K). Since an explanation of the experimental results requires changes in d occurring over approximately 100 nanoseconds, d changes due to carrier diffusion cannot account for the observed angular tuning in GaAs.

In CdSe, angular tuning resulting from carrier diffusion can be discounted because of the small changes in d involved. In CdSe the carriers form excitons which have been shown by Billé [31] to have extremely short diffusion lengths - of the order of or less than 0.1 microns.

2. The generation of excess carriers further into the unpumped region (and a resultant larger effective d) can be caused by reabsorption of both spontaneous and stimulated radiation. The degree to which this occurs will depend on the intensity of the photon field and the effective optical loss of the semiconductor material. We expect more optical pumping to be done by the spontaneous light than the stimulated emission because of the much larger effective optical loss (approximately two orders of magnitude greater than for stimulated radiation) associated with the broad spectrum spontaneous emission. This results because a major portion of the spontaneous emission occurs in energy regions above the bandgap in which the optical loss is far greater than at the band-edge where stimulated radiation occurs.

In order to calculate effective optical loss, the spectrum of the spontaneous radiation and the energy shape

of the optical loss must be calculated. A method which can be used under certain circumstances to accomplish this for GaAs is outlined by Lasher and Stern [32]. Spontaneous and stimulated emission energy shapes are given by:

$$R_{spon}(E) = \int_0^{E-E_g} E'^{1/2}(E-E_g-E')^{1/2} f_u(1-f_\ell)dE' \quad (D11)$$

and

$$R_{stim}(E) = \int_0^{E-E_g} E'^{1/2}(E-E_g-E')^{1/2} (f_u-f_\ell)dE' \quad (D12)$$

where f_u and f_ℓ represent Fermi functions and E_g is the energy gap.

By assuming a given doping density, complete extrinsic behaviour of impurities, and a given carrier density due to electron beam pumping, the quasi-Fermi levels in each band are calculated by standard techniques [33]. Equations (D11) and (D12) are then used to calculate the spontaneous and stimulated emission energy profiles. Now the stimulated emission term is related to the optical absorption coefficient $\alpha(E)$ by:

$$\alpha(E) = - CR_{stim} \quad . \quad (D13)$$

C is a calculable constant for a given material and therefore, the average value of optical absorption coefficient can be calculated as follows:

$$\bar{\alpha} = \frac{\int \alpha(E) R_{spon}(E)\, dE}{\int R_{spon}(E)\, dE} \qquad \text{(D14)}$$

Figure 35 shows the results of this calculation using parameters typical for our experimental conditions. $\bar{\alpha}$ is calculated as a function of carrier density in the unpumped region.

The absorption coefficient will be of the order of a few thousand cm^{-1}. In other words, the effective pumping due to optical reabsorption will fall off in distances of the order of microns. For the pump voltages we use in the experimental work the "$sech^2$" gain distribution also falls off in distances of this order. It is difficult to estimate the actual magnitude of the effective pumping due to reabsorption because of the uncertainty of spontaneous lifetime and actual excess carrier profile as well as the fact that the effective absorption coefficient would decrease as the radiation propagated. The important thing to note is that in the most severe case, being when the reabsorption creates an effective pump of the same magnitude as the actual electron pump, its effect would be merely to alter the shape of the pump profile tail. Such a modification, we have already concluded will not affect our fitting of far-field angular tuning.

Fig. 35. Effective absorption coefficient for spontaneous light from GaAs in the unpumped regions of the crystal.

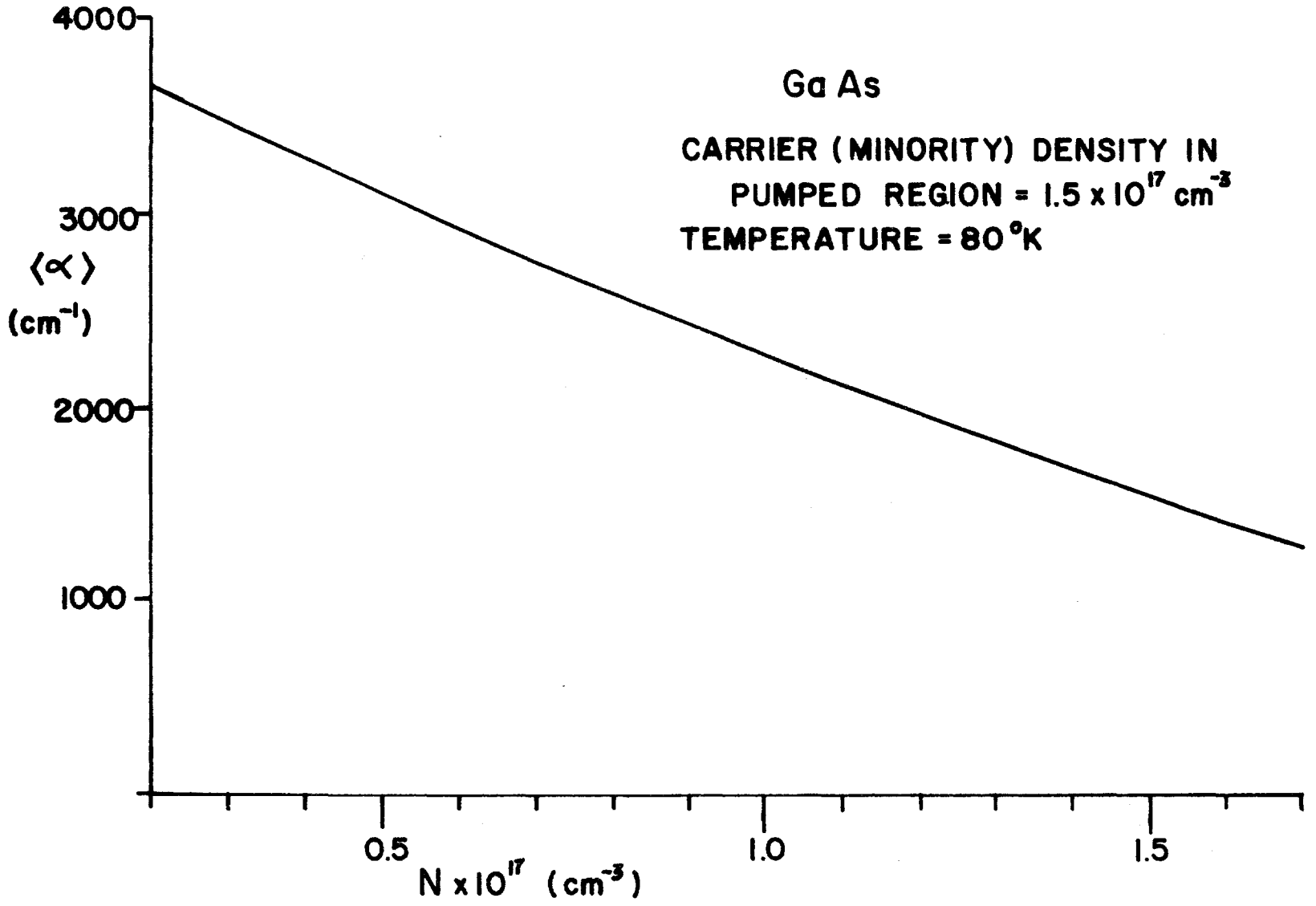
4000
3000
2000
1000
⟨∝⟩
(cm⁻¹)
Ga As
CARRIER (MINORITY) DENSITY IN
PUMPED REGION = 1.5 x 10¹⁷ cm⁻³
TEMPERATURE = 80 °K
0.5
1.0
1.5
N x 10¹⁷ (cm⁻³)

A similar explanation holds true for CdSe, though the generally lower absorption coefficients in this material [34] make spontaneous light reabsorption a smaller consideration.

APPENDIX E

(a) Effective Index Steps Due to Presence of a Gain Region

It has been shown by Stern [35] that an estimate of the contribution ($\Delta n(E)$) of the absorption edge region to the refractive index is given by:

$$\Delta n(E) = hc/\pi \int_{-\infty}^{E_s} \alpha(E') \; [E'^2 - E^2]^{-1} \; dE' \qquad (E1)$$

where $\alpha(E')$ is the optical loss and E_s is an "arbitrary" energy separating the region near the absorption edge from the high energy region. In GaAs, the optical absorption mechanism is taken to be band-to-band absorption near the band-edge, and then an approximation to $\alpha(E)$ can be obtained using the assumption of parabolic bands. A calculation of this type has been carried out by Lasher and Stern [32]. As $E_s \to \infty$, the assumption of parabolic bands permits infinitely high values of optical loss so it is necessary to modify $\alpha(E)$ in the form [35]:

$$\alpha'(E) = \alpha(E) \; (1 - E/E_s) \qquad (E2)$$

An estimate of band-tailing effects is made by the assumption of a constant loss of 10 cm^{-1} at photon energies less than but close to the band-gap.

The value of the index change between the pumped and unpumped regions is then given by:

$$\Delta\delta n(E) = (hc/\pi) \int_{-\infty}^{E_s} [\alpha_{pumped}(E') - \alpha_{unpumped}(E')] \times [1 - E'/E_s] \cdot [E'^2 - E^2]^{-1} \, dE' \quad . \qquad (E3)$$

The results of this calculation are sensitive to E_s, and careful consideration is needed in making this choice. An estimate can be made by deriving from this calculation a result which can be compared with a known numerical value. The temperature dependence of the index of refraction for GaAs can be determined from the experimental data of both Sturge [36] and Marple [37]. The temperature dependence of the index can also be determined from equation (E3) by the modification

$$\Delta n/\Delta T \sim (hc/\pi) \int_{-\infty}^{E_s} [\alpha_{pumped}(E') - \alpha_{unpumped}(E' + T \frac{\partial Eg}{\partial T})] \times [1 - E'/E_s] \cdot [E'^2 - E^2]^{-1} \, dE' \quad . \qquad (E4)$$

By fitting the results of this calculation to the experimentally based values, E_s was estimated to be 30 meV

measured from the band-edge. This result is consistent with Sturge's data on optical absorption in GaAs at liquid nitrogen temperatures.

In Fig. 36 the variation of the index step between pumped and unpumped p-type GaAs (2×10^{18} acceptors cm^{-3}) is displayed as a function of energy measured from the band-gap. In this calculation the band parameters used were the same as those used by Lasher and Stern. The parameter N indicates the density of minority carriers governing the gain in the pumped region. For energies near the band-gap the index change in the gain region, caused by the presence of excess minority carriers, is negative. For values of peak gain in the region 100 cm^{-1} to 1000 cm^{-1} (reasonable range for lasing electron-beam-pumped GaAs near liquid nitrogen temperatures), the index step is of the order 10^{-2}.

In CdSe it is generally accepted that the lasing transition involves an exciton interacting with other excitons or LO phonons [4,38,39]. The gain shape will, therefore, not reflect the parabolic bands but is here taken to be Lorentzian. For CdSe we can estimate from experimentally observed spectra that the half-width (FWHM) will be at least 40 Å. Using this gain shape in equation (E3) a maximum change in index is found to be 2×10^{-3} for a peak gain of 500 cm^{-1} (Fig. 37).

Fig. 36. Calculation of relation between refractive index change and energy from the band-gap (E-Eg) for GaAs at 77°K and various values of excess carrier population, N (cm^{-3}).

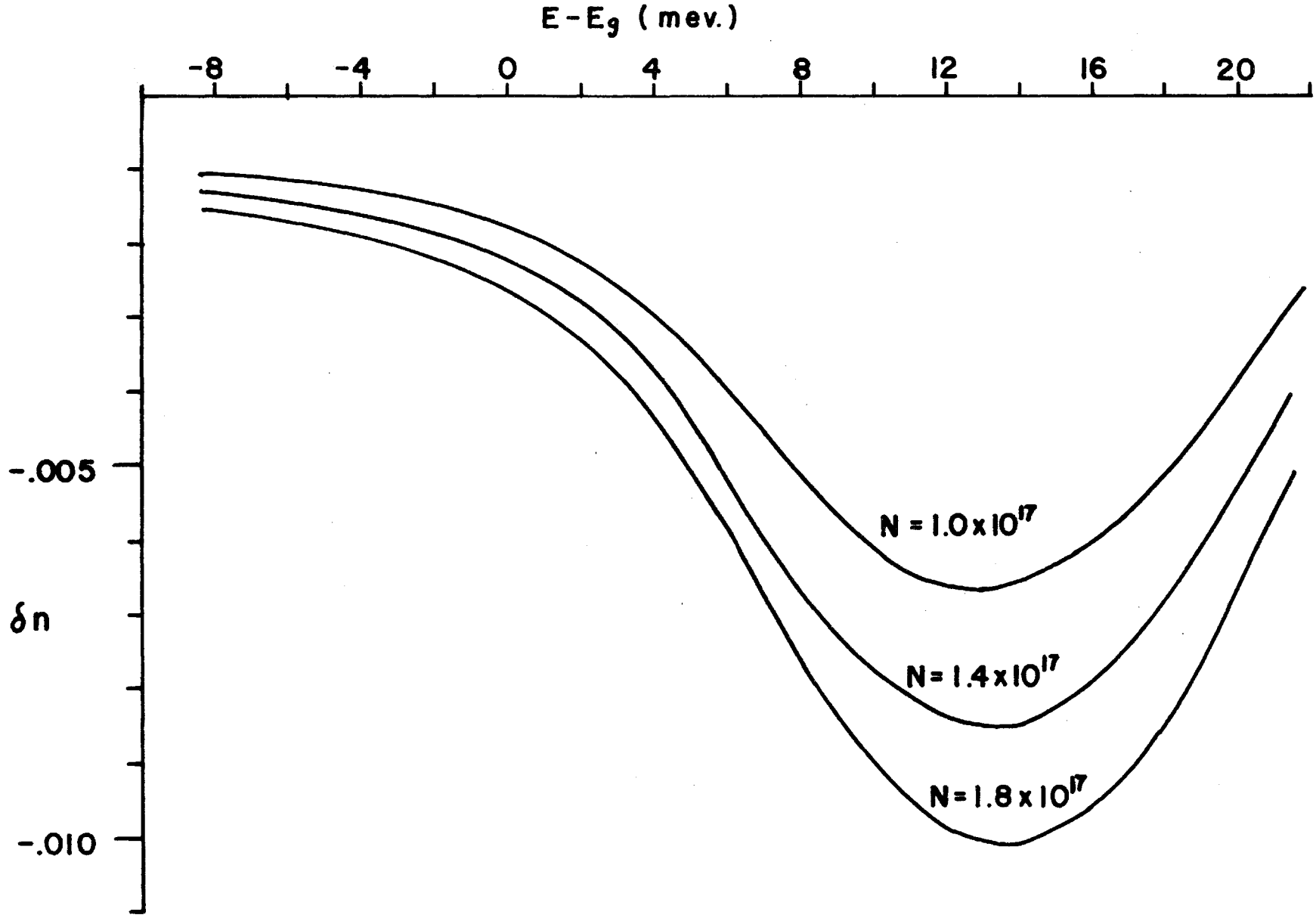
E - Eg (mev.)
-8
-4
0
4
8
12
16
20
-.005
δn
-.010
N = 1.0x10^17
N = 1.4x10^17
N = 1.8x10^17

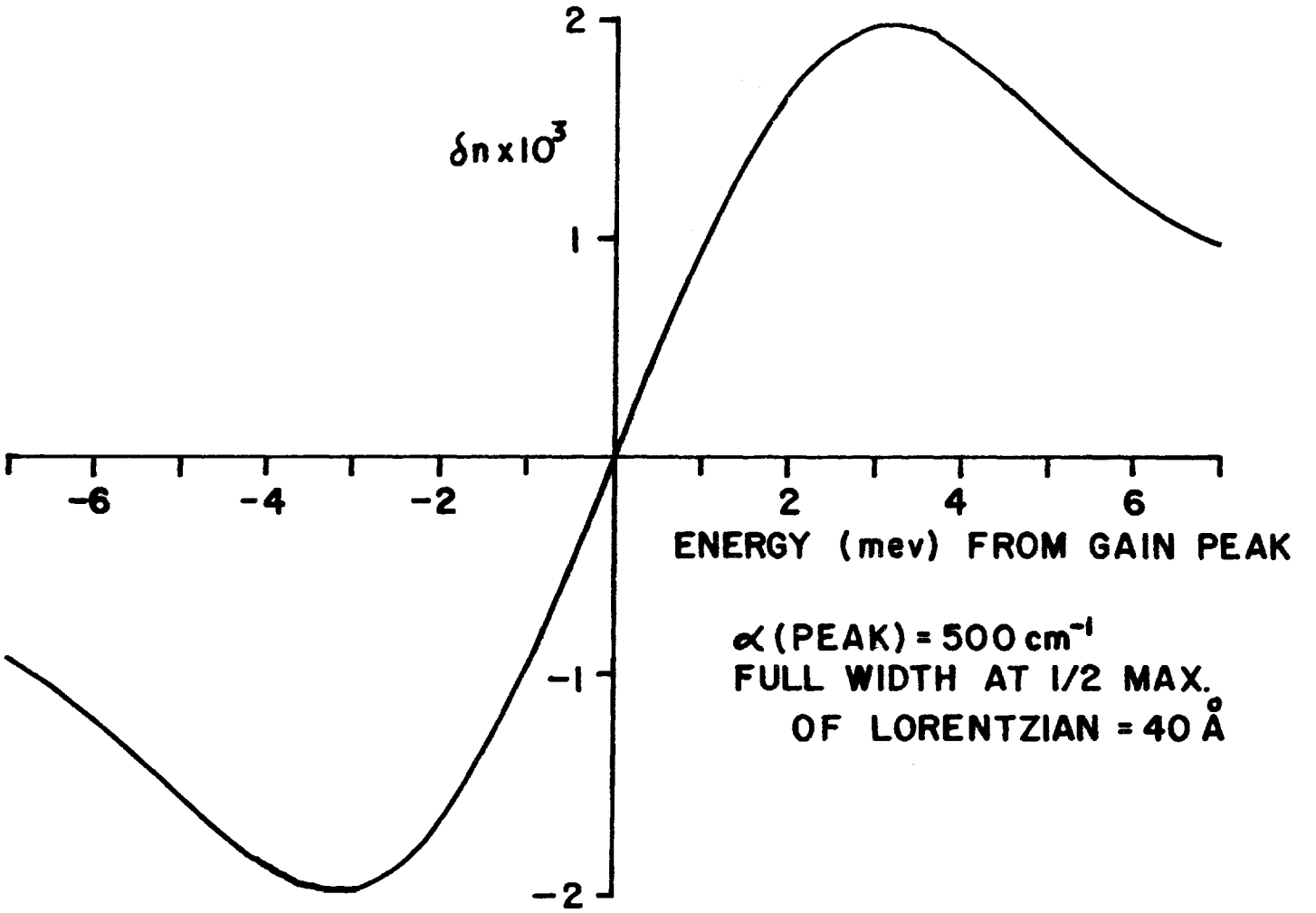

Fig. 37. Calculation of relation between refractive index change due to gain and energy for CdSe at 77°K.

(b) Effective Index Variations Due to Spatial Temperature Variations

This boundary value problem of heat conduction is given by [40]:

$$\frac{\partial^2 T}{\partial x^2} + \frac{g(x,t)}{k} = \frac{1}{\alpha}\frac{\partial T}{\partial x} \qquad 0 \leq x \leq \infty \ , \ t > 0$$

$$\frac{\partial T}{\partial x} = 0 \qquad x = 0 \ , \ t > 0 \qquad \text{(E5)}$$

$$T = F(x) \qquad 0 \leq x \leq \infty \ , \ t = 0$$

where

$\alpha = k/c$

k = thermal conductivity

c = specific heat .

The physical conditions are that a semi-infinite solid $0 \leq x \leq \infty$ is initially at a temperature $F(x)$. For times $t > 0$ heat is generated within the solid at a rate $g(x,t)$ while the boundary surface at $x = 0$ is kept insulated.

The solution of this problem is given by:

$$T(x,t) = \frac{1}{(4\pi\alpha t)^{1/2}} \int_0^\infty F(x') \cdot [e^{-\frac{(x-x')^2}{4\alpha t}} + e^{-\frac{(x+x')^2}{4\alpha t}}]dx'$$

$$+ \frac{\alpha}{k} \int_0^t \frac{dt'}{[4\pi\alpha(t-t')]^{1/2}} \int_0^\infty g(x',t')$$

$$\times [e^{-\frac{(x-x')^2}{4\alpha(t-t')}} + e^{-\frac{(x+x')^2}{4\alpha(t-t')}}]dx' \quad . \qquad \text{(E6)}$$

Additional simplifying assumptions used are that the initial temperature is a uniform 77°K and that heat is generated uniformly to a depth d by the electron beam. Backscattered energy from the electron beam is approximately 0.3 of the incident energy [20]. The main part of the remaining energy produces heat.

Profiles of temperature at given times after the start of pumping are shown in Fig. 38. Since $\delta n/\delta T$ is approximately constant for GaAs and CdSe over the range of refractive index change which we considered (i.e., up to 10^{-2}), the temperature profile approximates the profile of index difference. In the range of wavelengths over which we observe lasing the value of $\delta n/\delta T$ is approximately 1×10^{-3} in CdSe [41] and 2×10^{-4} in GaAs [37]. Thus for values of temperature rise of about 15°K (typical temperature rise during the 100 ns) the corresponding values of index change for CdSe and GaAs are 1.5×10^{-2} and 3×10^{-3} respectively.

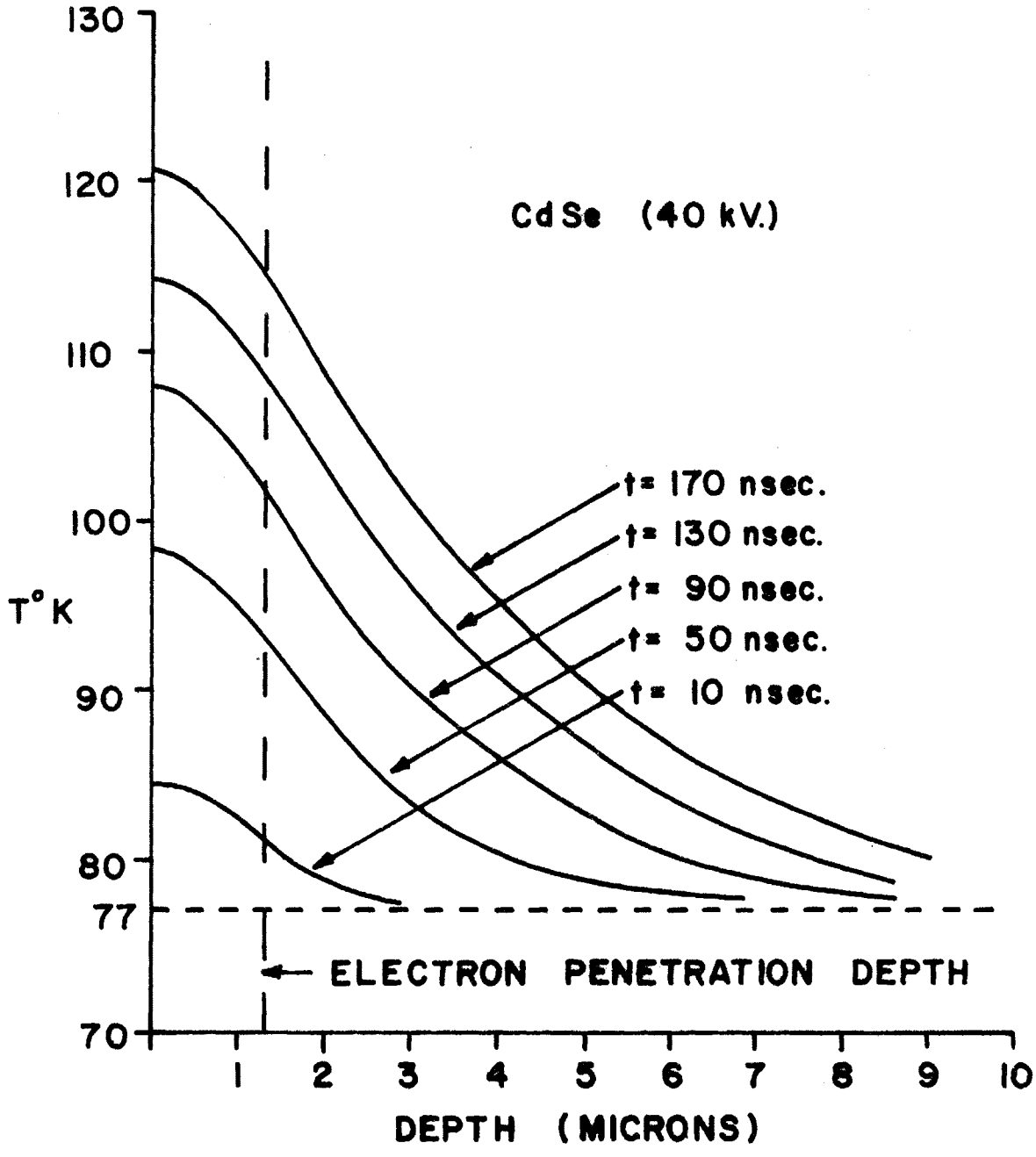

Fig. 38. Calculated temperature profiles of beam-pumped CdSe at 40kV beam voltage and initial temperature of 77°K.

The mathematical model for the electron-beam-pumped system has not been solved for the case of an arbitrary index profile in x; therefore, it is necessary to estimate an equivalent index step confined to the region x<d for any given temperature-generated index profile. A reasonable approximation of the index step in d is taken to be one-half of the peak of the temperature-generated index profile existing in the region of the laser cavity mode. With this or any other reasonable approximation, the index changes due to heating of the crystal are small in comparison to the Kramers-Kronig related index changes in GaAs and large for CdSe.

It is indicated above that only the major contribution to index change is needed to adequately explain the experimental observations of angular tuning in GaAs and CdSe. However, in the later analysis of wavelength tuning it is found that both effects must be considered to explain this somewhat more subtle effect. This situation occurs because the calculations must cover a wide range of wavelengths and temperatures and for some conditions of wavelength and temperature the two contributions to index change are of comparable magnitude.

REFERENCES

1. J. Shewchun, B.S. Kawasaki and B.K. Garside, I.E.E.E. J. Quantum Electron. QE-6, 133 (1970).
2. N. Holonyak, Jr., M.R. Johnson and J.A. Rossi, Appl. Phys. Lett. 12, 151 (1968).
3. J.R. Packard, W.C. Tait and D.A. Campbell, IEEE J. Quantum Electron. QE-5, 44 (1969).
4. W.D. Johnston, Jr., J. Appl. Phys. 42, 2731 (1970).
5. J.I. Pankove, IEEE J. Quantum Electron. QE-4, 161 (1968).
6. M.G. Craford, A.H. Herzog, N. Holonyak, Jr. and D.L. Keune, J. Appl. Phys. 41, 2648 (1970).
7. J.I. Pankove, IEEE J. Quantum Electron. QE-4, 427 (1968).
8. J. Nishizawa, IEEE J. Quantum Electron. QE-4, 143 (1968).
9. H. Aritome, K. Masuda and S. Namba, IEEE J. Quantum Electron. QE-7, 118 (1971).
10. G. Burns, F.H. Dill, Jr. and M.I. Nathan, Proc. IEEE 51, 947 (1963).
11. M. Pilkuhn, H. Rupprecht and J. Woodall, IEEE J. Quantum Electron. QE-1, 184 (1965).
12. M.I. Nathan, Proc. IEEE 54, 1276 (1966).

13. B. Lax, IEEE Spectrum, 61 (July 1965).

14. S.M. Sze, "Physics of Semiconductor Devices", Wiley-Interscience (1969).

15. C.H. Gooch, "Gallium Arsenide Lasers", Wiley-Interscience (1969).

16. O.N. Krokhin and Ju.M. Popov, Sov. Phys. JETP 11, 1144 (1960).

17. L.B. Griffiths, A.I. Mlavsky, G. Rupprecht, A.J. Rosenburg, P.H. Smakula and M.A. Wright, Proc. IEEE 51, 1374 (1963).

18. R.N. Hall, Proc. IEEE 52, 91 (1964).

19. P.R. Thornton, "The Physics of Electroluminescent Devices", E. and F.N. Spon Ltd. (1967).

20. C.A. Klein, Appl. Optics 5, 1922 (1966).

21. D.K. Wilson, Appl. Phys. Lett. 3, 127 (1963).

22. J. Melngailis, IEEE J. Quantum Electron. QE-1, 104 (1965).

23. O.V. Bogdankevich, V.S. Letokhov and A.F. Suchkov, Sov. Phys. Semi. 3, 566 (1969).

24. J.W. Cooley and J.W. Tukey, Math. of Comp. 19, 297 (1965).

25. L.D.Landau and E.M. Lifshitz, "Electrodynamics of Continuous Media", Addison-Wesley, 256 (1960).

26. A. Ashkin, B. Tell and J.M. Dziedzic, IEEE J. Quantum Electron. QE-3, 400 (1967).

27. J.P. McKelvey, "Solid State and Semiconductor Physics", Harper and Row, 341 (1966).

28. T. Harrett, Sol.-St. Electron. 13, 388 (1970).

29. C.J. Hwang, J. Appl. Phys. 42, 757 (1971).

30. H. Ehrenreich, Phys. Rev. 120, 1951 (1960).

31. J. Billé, Phys. Stat. Sol. 36, 775 (1969).

32. G. Lasher and F. Stern, Phys. Rev. 133, A553 (1964).

33. C. Kittel, "Introduction to Solid State Physics", Wiley, 304 (1956).

34. C. Kŏnak, J. Dillinger and V. Prŏsser, 1967 Int. Conf. on II-VI Semi. Comp., 850 (1967).

35. F. Stern, Phys. Rev. 133, A1653 (1964).

36. M.D. Sturge, Phys. Rev. 127, 768 (1962).

37. D.T.F. Marple, J. Appl. Phys. 35, 1241 (1964).

38. J.R. Packard, D.A. Campbell and W.C. Tait, J. Appl. Phys. 38, 5255 (1967).

39. R.F. Leheny, K.L. Shaklee, R.P. Ippen, R.E. Nahory and J.L. Shay, Appl. Phys. Lett. 17, 494 (1970).

40. M.N. Ozisik, "Boundary Value Problems of Heat Conduction", International, 75 (1968).

41. R.B. Parsons, W. Wardzynski and A.D. Yoffe, Proc. Roy. Soc. (London) 262, 120 (1961).

42. C.E. Hurwitz, Appl. Phys. Lett. 8, 121 (1966), also IEEE J. Quantum Electron. QE-5, 44 (1969).

43. J.L. Brewster, Appl. Phys. Lett. 13, 385 (1968).

44. N.G. Basov and O.V. Bogdankevich, Sov. Phys-S.S. 8, 1221 (1966).

45. F.H. Nicoll, Appl. Phys. Lett. 10, 69 (1967).

46. F.H. Nicoll, Appl. Phys. Lett. 9, 13 (1966).

47. N. Holonyak, Jr., M.R. Johnson and D.L. Keune, IEEE J. Quantum Electron. QE-4, 199 (1968).

48 D.L. Keune, J.A. Rossi, N. Holonyak, Jr. and P.D. Dapkus, J. Appl. Phys. 40, 1934 (1969).

49. M.I. Nathan, A.B. Fowler and G. Burns, Phys. Rev. Lett. 11, 152 (1963).

50. O.V. Bogdankevich, V.A. Goncharov, B.M. Lavrushin, V.S. Letokhov and A.F. Suchkov, Sov. Phys.-Semi. 1, 4 (1967).

51. N.G. Basov, O.V. Bogdankevich and B.M. Lavrushin, Sov. Phys-S.S. 8, 15 (1966).

52. N. Holonyak, Jr., M.R. Johnson, J.A. Rossi and W.O. Groves, Appl. Phys. Lett. 12, 151 (1968).

53. J. Shewchun, B.S. Kawasaki and B.K. Garside, IEEE J. Quantum Electron. QE-6, 133 (1970).

54. B.S. Kawasaki, J. Shewchun and B.K. Garside, J. Appl. Phys. 42, 5877 (1971).

55. R. Hunsperger, Sol. St. Electron. 12, 215 (1969).

56. W.J. Turner and W.E. Reese, J. Appl. Phys. 35, 350 (1964).

57. J.A. Rossi, D.L. Keune, N. Holonyak, Jr., P.D. Dapkus and R.D. Burnham, J. Appl. Phys. 41, 312 (1970).

58. E. Burstein, Phys. Rev. 93, 632 (1954).

59. P.D. Dapkus, N. Holonyak, Jr., R.D. Burnham and D.L. Keune, Appl. Phys. Lett. 16, 93 (1970).

60. F. Urbach, Phys. Rev. 92, 1324 (1953).

61. L.V. Keldysh and A.N. Kozlov, JETP Lett. 5, 190 (1967).

62. R.C. Casella, J. Appl. Phys. 34, 1703 (1963).

63. C.B. à la Guillaume, J-M. Debever and F. Salvan, Phys. Rev. 177, 567 (1969).

64. J.M. Hvam, Phys. Rev. B 4, 4459 (1971).

65. M.S. Brodin, S.V. Zakrevskii, V.S. Mashkevich and V.Ya. Reznichenko, Sov. Phys.-Semi. 1, 495 (1967).

66. H. Haug, J. Appl. Phys. 39, 4687 (1968).